TURBULENCE, DIFFUSION AND THE DAYTIME MIXED LAYER DEPTH OVER A COASTAL CITY

by

DOUW GERBRAND STEYN

B.Sc., University of Cape Town, 1967
B.Sc. (Hons.), University of Cape Town, 1968
M.Sc., University of Cape Town, 1970

A THESIS SUBMITTED IN PARTIAL FULFILMENT OF

THE REQUIREMENTS FOR THE DEGREE OF

DOCTOR OF PHILOSOPHY

in

THE FACULTY OF GRADUATE STUDIES

Department of Geography

We accept this thesis as conforming

to the required standard

THE UNIVERSITY OF BRITISH COLUMBIA

May 1980

In presenting this thesis in partial fulfilment of the requirements for an advanced degree at the University of British Columbia, I agree that the Library shall make it freely available for reference and study. I further agree that permission for extensive copying of this thesis for scholarly purposes may be granted by the Head of my Department or by his representatives. It is understood that copying or publication of this thesis for financial gain shall not be allowed without my written permission.

Department of Geography

The University of British Columbia
2075 Wesbrook Place
Vancouver, Canada
V6T 1W5

Date 8 Sept 1980.

ABSTRACT

The rate of dispersion of atmospheric pollutants and the volume of atmosphere available for the dilution of pollutants are examined in an unstable suburban atmosphere at a coastal location.

Within the framework of the statistical theory of diffusion, it can be shown that the non-dimensional dispersion functions $\sigma_y/\sigma_v t$ and $\sigma_z/\sigma_w t$ can be determined by integration of the Eulerian spectral functions multiplied by appropriately scaled sampling functions. This scaling, which arises out of the Hay-Pasquill form for the Eulerian-Lagrangian transform and the use of a non-dimensional frequency, gives rise to a dispersion scaling time $t_s = z/\sigma_u$ which is simply related to the Lagrangian integral time scale. Applying this analysis to turbulent velocity spectra measured over a selected suburban surface results in the following forms for the crosswind and vertical dispersion functions respectively.

$$S_y(t^*) = (1.0 + 0.16\sqrt{t^*})^{-1}$$

$$S_z(t^*) = (1.0 + 1.21\sqrt{t^*})^{-1}$$

The spectra and integral turbulence statistics determined in this part of the study are shown to be in general agreement with those determined over much smoother surfaces.

The volume of atmosphere available for the dilution of pollutants is controlled primarily by the mean wind speed and mixed-layer depth. This latter variable can be modelled on the basis of a simple thermodynamic analysis of the mixed layer processes. The currently available models have been generalized to include advection and subsidence. The effects of

advection on the mixed-layer depth have been modelled by resetting the model equations in a Lagrangian frame, performing an approximate first integral in order to derive the spatial dependence of the model variables, and using these spatial forms to give a set of Eulerian equations. The effects of subsidence have been modelled by imposing a subsidence velocity on the top of the mixed layer as well as allowing subsidence-induced warming of the atmosphere above that layer. This subsidence is driven by atmospheric divergence at both synoptic- and meso-scales, the latter phenomenon being linked to thermally driven circulatory systems. The inclusion of these processes into the mixed-layer depth model allows its application to areas in which meso-scale phenomena may have a considerable effect on the diurnal behaviour of the mixed-layer depth.

The model thus derived consists of a system of non-linear differential equations which may be numerically solved to elucidate the temporal behaviour of the mixed-layer depth. The boundary conditions necessary for such a solution were provided by measurements made in the unstable surface layer over a coastal city. The resultant mixed-layer depth behaviour is in general in good agreement with determinations of this depth made with an acoustic sounder, but can be a poor reflection of reality in the presence of synoptic-scale non-stationarities. The input requirements of the model are hourly values of surface sensible heat flux, mean wind speed and upwind distance to the surface giving rise to the advected heat flux (usually a coastline or urban-rural boundary), and estimates of the intensity of the capping inversion and horizontal divergence. The model is sensitive to all input variables, the degree of sensitivity being indicated by the dependence of the maximum mixed-layer depth on the measured boundary conditions.

TABLE OF CONTENTS

	Page
Abstract	ii
Table of Contents	iv
List of Tables	vii
List of Figures	viii
Acknowledgements	xii
1. Preface	1
1.1 Rationale	1
1.2 Objectives	1
Part One: Turbulent Diffusion	3
2. Introduction	3
2.1 Specification of Diffusion Parameters	4
2.2 Gaussian Plume Model Parameters and the Statistical Theory of Diffusion	6
3. An Application of the Statistical Theory of Diffusion to Measured Flows	10
3.1 The Dispersion Functions from Measured Eulerian Spectra	10
3.1.1 Eulerian-Lagrangian Transformations	10
3.1.2 Transformation of the Dispersion Integral	12
3.2 Eulerian Turbulence Functions over a Suburban Surface in Unstable Conditions	13
3.2.1 Integral Statistics	13
3.2.2 Spectra	22
3.3 Computation of the Dispersion Functions	25
3.3.1 Computational Details	25

3.3.2 Crosswind Spread 26

3.3.3 Vertical Spread 33

4. Conclusion 36

Part Two: The Depth of the Daytime Mixed Layer

5. Introduction 39

5.1 Specification of the Mixed Layer Depth 39

5.2 Mathematical Modelling of the Mixed Layer Depth 41

6. A Model of Mixed Layer Depth 44

6.1 Characteristics of the Observed Mixed Layer 44

6.2 Advection and Subsidence in the Mixed Layer Model 48

6.3 Subsidence 51

6.3.1 Synoptic Scale Subsidence 51

6.3.2 Meso-Scale Subsidence 56

7. Implementation of the Mixed Layer Model 59

7.1 Computational Scheme and Input Data 59

7.2 Results of Mixed Layer Modelling 62

7.3 Sensitivity Analysis 76

8. Conclusion 82

9. Summary of Conclusions 84

List of Symbols 87

References 91

Appendices 105

A. The Observational Site 106

A.1 General Requirements 106

A.2 The Selected Site 107

A.3 Sectorial Roughness Length Analysis 113

A.4 Displacement Length 116

B. The Tower, Instrumentation and Data Logging Systems 117

B.1 The Tower 117

B.2 Instrumentation and Data Logging Systems 120

B.2.1 UVW Anemometer 120

B.2.2 Yaw Sphere - Thermometer Eddy Correlation System 121

B.2.3 Differential Psychrometer System 122

B.2.4 Microvane and Cup Anemometer 123

B.2.5 Net Pyrradiometer 123

B.2.6 Theodolite-tracked Mini-Sonde System 124

B.2.7 Acoustic Sounder 125

C. Synoptic Background to the Observational Period 126

D. The Data Set 128

E. Determination of the Surface Energy Budget 129

E.1 Budget Closure by Distribution of Residuals 129

E.2 Examples of Surface Energy Budgets 138

F. Spectral Analysis 140

G. Dispersion Function Program 146

H. Application of the Dispersion Functions 147

I. Theodolite-Tracked, Balloon-Borne Temperature Soundings 149

J. Comparison of Acoustic and Balloon Soundings 153

K. Subsidence Estimation from Potential Temperature Profiles 155

L. Mixed Layer Depth Program and Sample Data 158

LIST OF TABLES

		Page
Table 3.1a	ζ_i vs σ_i/u_*; i = u,v,w.	16
Table 3.1b	ζ vs σ_i/u_*: i = u,v,w.	16
Table 3.2	Relation Between z/L classes and Pasquill-Gifford Classes.	17
Table 3.3	Least Squares Fitted Parameters to Equation (3.7) For Three Components.	17
Table 3.4	Comparison of Measured Values of (near) Adiabatic Non-Dimensional Wind Velocity Standard Deviations.	18
Table 3.5	Positions of Spectral Features.	25
Table 7.1	Mixed Layer Model Sensitivity.	81
Table A.1	Sectorial Analysis of Roughness Length.	115

LIST OF FIGURES

		Page
Figure 3.1	Non-dimensional Integral Alongstream Turbulence Statistics as Functions of Surface Layer Similarity Variables	19
Figure 3.2	Non-dimensional Integral Crosswind Turbulence Statistics as Functions of Surface Layer Similarity Variables	20
Figure 3.3	Non-dimensional Integral Vertical Turbulence Statistics as Functions of Surface Layer Similarity Variables	21
Figure 3.4	Energy Density Spectra for the Vancouver Suburban Site	24
Figure 3.5	Crosswind Dispersion Function	27
Figure 3.6	Crosswind Dispersion Function	32
Figure 3.7	Vertical Dispersion Function	35
Figure 6.1	Acoustic Sounder Trace for August 1st	45
Figure 6.2	Potential Temperature Profiles for August 1st	46
Figure 6.3	Potential Temperature Profiles at Various Distances from the Upwind edge of a Thermal Internal Boundary-layer	46
Figure 6.4	Subsidence Warming	55
Figure 7.1	Inversion Rise Modelling for July 20th	63
Figure 7.2	Inversion Rise Modelling for July 22nd	64
Figure 7.3	Inversion Rise Modelling for July 23rd	65
Figure 7.4	Inversion Rise Modelling for July 28th	66
Figure 7.5	Inversion Rise Modelling for July 29th	67
Figure 7.6	Inversion Rise Modelling for July 30th	68
Figure 7.7	Inversion Rise Modelling for July 31st	69
Figure 7.8	Inversion Rise Modelling for August 1st	70
Figure 7.9	Inversion Rise Modelling for August 2nd	71

Figure 7.10	Inversion Rise Modelling for August 3rd	72
Figure 7.11	Inversion Rise Modelling for August 4th	73
Figure 7.12	Inversion Rise Modelling for August 5th	74
Figure 7.13	Inversion Rise Modelling for August 8th	75
Figure 7.14	Maximum Inversion Height vs Maximum Surface Sensible Heat Flux	78
Figure 7.15	Maximum Inversion Height vs Mean Wind Speed in Mixed Layer	78
Figure 7.16	Maximum Inversion Height vs Entrainment Parameter	79
Figure 7.17	Maximum Inversion Height vs Inversion Intensity	79
Figure 7.18	Maximum Inversion Height vs Horizontal Divergence	80
Figure A.1	General Environs of Study Area, Near-Site Topography and Land-Use	108
Figure A.2a	Photographic View from the Top of the Tower to the West	109
Figure A.2b	Photographic View from the Top of the Tower to the North	110
Figure A.2c	Photographic View from the Top of the Tower to the East	111
Figure A.2d	Photographic View from the Top of the Tower to the South	112
Figure B.1	The Tower and Embankments	118
Figure B.2	Upper Sections of the Tower Showing Surface Layer Instrumentation	119
Figure E.1	Decision Tree for Budget Determination	134
Figure E.2	Residual ε_1 vs Wind Direction	135
Figure E.3	Frequency Distribution of ε_1 and ε_2	136
Figure E.4	Suburban Surface Energy Budget	139
Figure F.1	Spectrum for Single Stability Class	142
Figure F.2 a,b,c	Construction of Composite Spectra	143

Figure I.1 Mean Wind from Tower and Balloon Sonde 152

Figure J.1 Inversion Height from Acoustic Sounder and Potential Temperature Profile 154

Figure K.1 Subsidence in Potential Temperature Profiles on August 8th 156

ACKNOWLEDGEMENTS

I am grateful to the academic community of The University of British Columbia and in particular my colleagues in the Geography Department of that institute for providing an eclectic and stimulating intellectual environment in which to conduct my studies. In particular, my supervisor, Dr. T.R. Oke, served beyond the call of duty as mentor, teacher and perceptive critic of my ideas. His efforts in the bowels of City Hall provided the permission necessary for the erection of the instrumentation tower.

My examining committee, Drs. J.E. Hay, S. Pond and I.S. Gartshore were always available with invaluable advice and guidance.

Field assistance was provided by Bill Broomfield in the preparatory stages, Joanne Pottier and Brian Guy during the often arduous data gathering phase. Their efforts with the tracking theodolites are especially appreciated. Sheila Loudon served ably as a computing assistant. Brian Kalanda provided valuable advice on the operation of the differential psychrometer system.

Research grants by the Natural Sciences and Engineering Research Council of Canada and a Scientific Subvention from the Atmospheric Environment Service of Environment Canada to Dr. T.R. Oke covered the considerable funding requirements of the field work. I was personally supported by teaching assistantships, a summer research fellowship and latterly by a Killam Predoctoral Fellowship, all from The University of British Columbia.

The British Columbia Hydro and Power Authority gave permission to use their Mainwaring Substation as a research site. The Pacific Region of the Atmospheric Environment Service kindly lent their mini-sonde system and made available the services of Ron McLaren who instructed

us in its operation. Don Faulkner of that service provided a computer program for determining the balloon position from the theodolite sightings. Dr. M. Church kindly lent an analogue magnetic tape recorder for the turbulence data and the Institute (now Department) of Oceanography at The University of British Columbia allowed free access to their analogue to digital convertor and mini-computer for the digitization of those data. Richard Leslie willingly built the bridge-amplifier and active filters and provided much guidance on matters electronic.

1. Preface

1.1 Rationale

The concentration of pollutants in the atmosphere and at the surface of the Earth is determined primarily (apart from source strength variability) by the rate of dispersion into the atmosphere and by the volume of atmosphere available for dilution. The first determining factor is governed by the turbulent diffusion process and the second by the depth of the mixed layer and the mean wind through that layer. Under certain atmospheric conditions turbulent diffusion may be effectively absent, or there may exist no bar to vertical mixing. This study will not cover those conditions, but will rather concentrate on a highly turbulent mixed layer capped by an elevated inversion. Since the largest effects (in human terms) of air pollutants generally occur in urban and suburban situations, where few data are available for estimating the governing factors, this study will concentrate on those factors in a suburban situation. The city from which the study will draw its data is Vancouver, British Columbia, Canada, which has a mid-latitude coastal location. The results will thus be characteristic of this situation, but are not expected to be specific to any particular feature of the chosen city. The methods used will be those of micro- and meso-meteorology, and the turbulent diffusion process will be inferred from turbulence measurements, rather than by measuring the spread of a tracer.

1.2 Objectives

The overall objectives of the study are not to present an integrated scheme for dispersion or pollutant concentration calculation, but to investigate in some depth the two determining factors already

mentioned in Section 1.1: Turbulent diffusion and the depth of the mixed layer.

The study will be approached in two quite separate parts, the first dealing with turbulent diffusion and the second with the daytime evolution of the mixed layer depth. Though treated independently, these two phenomena are in reality both complexes of interacting processes linked to each other and to higher order phenomena.

The first part will be directed towards providing estimates of turbulent diffusion parameters that can be used to determine pollutant concentrations within the suburban mixed layer via the Gaussian plume model. The statistical theory of diffusion will be applied to turbulence velocity spectra measured within the surface layer. The historical and theoretical background of this topic will be covered in the introduction to the first part of this study.

The objectives of the second part will be to develop a mathematical model for the depth of the daytime mixed layer which will be applicable to situations having similar physical characteristics to the chosen site. The model will be a generalization of existing models, and will have to account for advective heat transport and meso-scale subsidence associated with thermally-driven circulation systems. The historical and theoretical background of this topic will be covered in the introduction to the second part of this study. By its nature, this model will require considerable computing power, while the diffusion scheme of the first part will be easily applicable on a hand calculator.

In order to reduce the clutter of secondary and peripheral analyses and background information in the body of the text, much of this material is contained in the appendices.

Part One:

TURBULENT DIFFUSION

2. Introduction

2.1 Specification of Diffusion Parameters

Analysis of the diffusion of material in a turbulent flow has followed three distinct lines, each developed from a different theoretical base. The Gradient Transfer approach is really a first-order closure scheme which relates mass fluxes to mean velocity gradients by an eddy diffusivity. The approach has a comforting feel because of the similarity it bears to the classic Fickian (molecular) diffusion framework. The crippling flaw of this approach is that the eddy diffusivity is a property of the flow (not the fluid), and in geophysical flows is generally component-dependent. For these reasons the so-called "K-theory" has been largely ignored in the recent history of turbulent diffusion, even if its influence lingers strongly enough to prompt Scorer's (1976) warnings against its use. In operational terms the K-theory is attractive as it can easily be incorporated into input/output formulations of regional-scale box models of pollutant transport (Nunge, 1974), but the detailed specification of the three component K's remains a problem. A variety of more or less realistic forms for the K's have been proposed, some of which yield analytic solutions to the diffusion equations (Sutton, 1953 and Pasquill, 1974).

The Similarity Theory of turbulent diffusion is based on the K-theory but uses similarity arguments to derive forms of K based on non-dimensional functions of the Monin-Obukhov length scale. These functions are invariably empirical and require extensive measurements of diffusion such as those presented by Deardorff and Willis (1975). An alternative view of this approach is to treat the concentration distribution as a

function of the chosen non-dimensional groups (Gifford, 1975). However, this ability to short-circuit process is a property of the similarity theory, rather than the phenomenon.

Diffusion from a continuous source may be treated from a purely statistical viewpoint in what is known as the Taylor (1921) Statistical Theory. This approach resolves many of the difficulties of the other two possibilities, is amenable to fairly straightforward measurement and analysis and produces results which can conveniently be used to estimate pollutant concentrations using the so-called Gaussian plume model.

The Gaussian Plume model estimates mean concentrations of pollutants emitted into turbulent flow with a bivarate Gaussian distribution. The standard deviations in the vertical and horizontal crosswind directions are used as diffusion parameters that must be specified, and will be functions of the flow type and downwind distance. These parameters are usually specified as functions of downwind distance and atmospheric turbulence stability type. The six Pasquill turbulence types (Pasquill, 1961) form the most convenient operational scheme and can be related (Golder, 1972) to more basic stability measures. Under this scheme the standard deviations as functions of downwind distance are given as families of curves called the Pasquill-Gifford curves (Pasquill, 1961; Slade, 1968; and Turner, 1969). These curves have been compiled from diffusion observations over flat land for distances up to 1 km. It has been necessary to extrapolate (on the basis of solutions to the diffusion equation) these curves up to a distance of 100 km (Smith, 1972).

Since the flow within the surface layer reflects very strongly the nature of the underlying surface, it is reasonable to expect very different surfaces to be represented by different sets of Pasquill-Gifford curves. A set of curves to represent diffusion over urban surfaces has

been produced by McElroy and Pooler (1968) who performed measurements of tracer spread over St. Louis. Gifford (1976) presents a set of curves derived from their data and shows them to be quite different from the curves for much smoother surfaces. Briggs (1973) reviewed urban tracer data and their analysis up to that date and proposed sets of σ_y and σ_z curves in analytic form for diffusion over urban surfaces. Within this formulation, the need to derive diffusion parameters directly from observations of atmospheric diffusion makes their determination tedious, time consuming and subject to large statistical variability (all these factors being inherent drawbacks of that kind of observation). The Gaussian model itself remains (if properly used) a peerless mathematical tool for estimating diffusion because it is simple, flexible and in accord with most available diffusion theory. For this reason it has remained the core of the subject while the detailed specification of the standard deviations has been the subject of much uncertainty and some research.

2.2 Gaussian Plume Model Parameters and the Statistical Theory of Diffusion

Taylor (1921) in his statistical theory showed that an ensemble average of particle displacement under the influence of a stationary, homogeneous turbulent flow will have a variance given by:

$$\sigma_y^2 = 2\sigma_v^2 \int_0^t \int_0^{t'} R(\tau)d\tau dt' \qquad (2.1)$$

where $R(\tau)$ is the Lagrangian auto-correlation of the crosswind velocity component for a lag τ, and σ_v^2 is the variance of this velocity component. The limit of the outside integral is t, the travel time. It can be shown

(Pasquill, 1974) that with simple transformation equation (2.1) leads to

$$\sigma_y^2 = \sigma_v^2 t^2 \int_0^\infty \Phi_{v,L}(n)\{\sin(\pi nt)/(\pi nt)\}^2 dn \qquad (2.2)$$

where $\Phi_{v,L}(n)$ is the Lagrangian crosswind energy spectrum, and n the frequency. Under conditions of isotropic turbulence, a similar form holds for vertical diffusion, with the Lagrangian vertical energy spectrum replacing the crosswind function. Pasquill (1971) suggested expressing equation (2.2) as:

$$\sigma_y^2/\sigma_v^2 t^2 = S_y^2(t/t_L) \qquad (2.3)$$

where t_L, the Lagrangian integral time scale is given by:

$$t_L = \int_0^\infty R(\tau)d\tau.$$

The formulation of equation (2.3) has the convenience of the Gaussian plume model and the theoretical backing of the statistical theory, and has met with general approval among the research community active in this field (Hanna et al., 1977 and Randerson, 1979).

The detailed specification of S thus remains the major objective. Two limiting values of S are:

$S \to 1.0$ as $t \to 0$

$S \to (2t_L/t)^{1/2}$ as $t \to \infty$

the behaviour of S for intermediate values is entirely determined by the shape of the spectrum (or equivalently, the auto-correlation function), and may be approached in three quite distinct ways (Pasquill, 1975b).

- Closed mathematical forms for $\Phi_L(n)$ or $R(\tau)$ may be substituted into the integral in equation (2.2), which will then yield $S(t/t_L)$.

  This method has been illustrated by Pasquill (1975b) who uses a variety of forms suggested for $R(\tau)$ and tabulates $S(t/t_L)$.

- Direct observation of $\sigma_y/\sigma_v t$ over a range of values of t so that the large t limit can be used to find t_L. This method has been used by Draxler (1976) who compiled a large body of data from tracer diffusion observations over generally flat land. His compilation shows wide scatter but quite distinct trends from which he derives analytic forms for $S(t/t_L)$ for both vertical and crosswind spread. Irwin (1979) uses the same technique on vertical dispersion data under unstable conditions. His analysis uses a convective, rather than Lagrangian integral time scale.

- The Lagrangian energy spectra $\Phi_{v,L}(n)$ and $\Phi_{w,L}(n)$ (crosswind and vertical) can be estimated from measured Eulerian spectra, and the integration in equation (2.2) performed to give $S(t/t_L)$. It can be shown (Pasquill, 1974) that the integration for a particular travel time, t, is equivalent to computing variances with an averaging time equal to the travel time divided by the ratio of Lagrangian to Eulerian integral time scales. This method has been applied (Hay and Pasquill, 1959, and Haugen, 1966) in order to test the validity of a particular form of the Eulerian-Lagrangian transform, utilizing tracer diffusion

to determine σ_y. Sawford (1979) (whose work was concurrent with, but independent of this study) applies the same technique for determining $S_y(t/t_L)$ over flat grassland and shows that his results compare favourably with Draxler's (1976) analytic form of $S_y(t/t_L)$ for crosswind spread.

In this study, the crosswind and vertical dispersion functions will be derived by integrating the transformed Eulerian spectral functions that were observed in an unstable-to-highly unstable suburban atmosphere.

3. An Application of the Statistical Theory to Measured Flows

3.1 The Dispersion Functions from Measured Eulerian Spectra

3.1.1 Eulerian-Lagrangian Transformations

Turbulent diffusion is a strictly Lagrangian process, whereas virtually all atmospheric measurements are Eulerian in nature. This conflict of viewpoint would be easily resolved if some theoretical transformation existed for relating Eulerian and Lagrangian quantities. The lack of a theoretical basis for such a transformation is a reflection of our lack of understanding of the fundamental nature of turbulent flows. This rather formidable problem has been approached on the basis of a number of somewhat intuitive hypotheses, each having its own set of (often unclear) limitations. For the purposes of this study, the most convenient formulation of an Eulerian-Lagrangrian transform is one which addresses the ratio of the integral time scales from the two frames of reference.

The simplest approach to the integral time scale ratio is provided by the "frozen eddy" hypothesis which suggests (Pasquill, 1974) that:

$$t_L/t_E \simeq 1/i = \overline{u}/\sigma_u$$

where t_L/t_E is the ratio of the Lagrangian to Eulerian integral time scales, i is the turbulent intensity and is equal to the ratio of the longitudinal standard deviation of wind velocity (σ_u) to the mean wind speed ($\overline{u}$). A more detailed analysis may be based on Corrsin's (1959) conjecture that after sufficiently long migration times, particles may be considered to have velocities which are unbiased samples of the turbulent velocities

at their positions in an Eulerian frame. This hypothesis has led Saffman (1963) and Philip (1967) to the result:

$$t_L/t_E = \beta\bar{u}/\sigma_u \tag{3.1}$$

where $\beta = 0.80$ (Saffman)

$\beta = 0.35$ (Philip)

(note that Hay and Pasquill (1959) use a different β, viz; $\beta = t_L/t_E$). The different values for β are a result of minor differences in analytic forms chosen by the two authors. A similar treatment by Wandel and Kofoed-Hansen (1962) leads to a value of 0.44 for β. Identity of the similarity theory and statistical theory forms of eddy diffusivity require $\beta = 0.44$ (Pasquill, 1974).

The relation (3.1) has been experimentally investigated by Angell (1964) who performed "approximately - Lagrangian" measurements from radar-tracked tetroons. Haugen (1966) inferred Lagrangian functions from tracer diffusion experiments and so was able to test equation (3.1). Both these studies show clear inverse relationships between the scale ratios and turbulence intensity. The scatter in their data is large but the results indicate a value near 0.5 for β. A number of alternative approaches to this problem do exist and have been reviewed by Koper et al. (1978) who derive a powerful generalized transform for the autocorrelation functions, and show how equation (3.1) is a special case of their general form.

Brook (1974) uses a statistical approach introduced by Ariel and Buttener (1966) to determine the Lagrangian velocity autocorrelation function from Eulerian wind statistics gathered over an urban surface. From this function, he computes β but cannot confirm equation (3.1)

because his data cover only a very small range of turbulent intensity. They do, however, lead him to conclude that $\beta\bar{u}/\sigma_u$ is independent of stability, terrain and height.

In view of the foregoing evidence, it was decided to use equation (3.1) as the basis for an Eulerian-Lagrangian transform with $\beta = 0.5$.

3.1.2 Transformation of the Dispersion Integrals

From equation (2.2) we may write:

$$S_y^2(t) = \sigma_y^2/\sigma_v^2 t^2 = \int_0^\infty \Phi_{v,L}(n)\{\sin(\pi nt)/(\pi nt)\}^2 dn \qquad (3.2)$$

The Lagrangian-Eulerian transform takes the form (Pasquill, 1974)

$$\Phi_L(n) = r\Phi_E(rn)$$

where $\quad r = t_L/t_E = \bar{u}/2\sigma_u$

Applying this transform to (3.2) gives:

$$S_y^2(t) = \int_0^\infty \Phi_{v,E}(n)\{\sin(2\pi t\sigma_u n/\bar{u})/(2\pi t\sigma_u n/\bar{u}\}^2 dn \qquad (3.3)$$

where $\quad \Phi_{v,E}$ and $\Phi_{v,L}$ are respectively the Eulerian and Lagrangian forms of the transverse energy density spectra. Composite Eulerian spectra from a number of blocks of turbulence statistics are computed as functions of non-dimensional frequency $f = nz/\bar{u}$ (Appendix F). Transforming (3.3) to an integral over f gives:

$$S_y^2(t) = \int_0^\infty \Phi_{v,E}(f)\{\sin(2\pi t\sigma_u f/z)/(2\pi t\sigma_u f/z)\}^2 df$$

this may be rewritten as:

$$S_y^2(t^*) = \int_0^\infty \Phi_{v,E}(f)\{\sin(2\pi ft^*)/(2\pi ft^*)\}^2 df \qquad (3.4)$$

where $t^* = t/t_s = t\sigma_u/z$ is the non-dimensional travel time scaled by $t_s = z/\sigma_u$. This form of scaling arises naturally in the integral, and is operationally more convenient than t_L as suggested by Hanna et al. (1977) and Pasquill (1975). The scale t_s can be simply related to t_L (as shown in Section 3.3.2) and hence to Draxler's (1976) empirical surrogate t_i.

All that remains now is to determine the form of $\Phi_{v,E}(f)$ and $\Phi_{w,E}(f)$ and perform the integration to derive the form of $S(t^*)$ for cross-wind and vertical spread. Before this can be done, a brief detour will be taken through the integral turbulence statistics and the details of the turbulent velocity spectra that will be used in the calculations.

3.2 Eulerian Turbulence Functions over a Suburban Surface in Unstable Conditions

3.2.1 Integral Statistics

In accordance with the Monin-Obukhov similarity theory, the non-dimensional velocity standard deviations in the surface layer ($z \ll z_i$) should behave as (Lumley and Panofsky, 1964):

$$\sigma_i/u_* = \phi_i(\zeta), \; i = u,v,w \tag{3.5}$$

where u_* is the surface friction velocity, the ϕ_i are a set of non-dimensional functions and $\zeta = z/L$ where z is the height, L the Monin-Obukhov length and z_i is the depth of the mixed-layer. This scaling for the horizontal components appears to break down in unstable surface layers (Lumley and Panofsky, 1964) or at greater heights ($z \lesssim z_i$), and it has been suggested (Wyngaard and Coté, 1974 and Panofsky et al., 1977) that a more suitable form would be

$$\sigma_w/u_* = \phi_w(z/L) \tag{3.6a}$$

$$\sigma_{u,v}/u_* = \phi_{u,v}(z_i/L) \tag{3.6b}$$

where z_i is the height of the lowest inversion (taken to be the depth of the convectively mixed layer). Considerable work has been conducted on the adiabatic limit of the ratios σ_i/u_* and Counihan (1975) summarises the values as 2.5, 1.9 and 1.3 for u, v and w respectively. These ratios do not appear to depend on height. Binkowski (1979) develops a simple second-moment closure, Monin-Obukhov model for surface layer turbulence which predicts the form of $\phi_i(\zeta)$ in equation (3.5) for $-4.0<\zeta<4.0$, without explicit reference to the character of the underlying surface. His functions compare well with the data from two independent sets of field measurements which show wide scatter for the horizontal components in unstable cases (as pointed out above).

A fundamental bar to compilations and comparisons of integral statistics data from different experiments exists, and as a result these analyses should be treated with caution. The problem stems from different studies having different averaging bands (in non-dimensional frequency space) for the determination of the ratios σ_i/u_*. The most proper band is that covering the full range of micro-meteorologic fluctuations (i.e., from the centre of the spectral gap at $f \simeq 6\times10^{-5}$ (Smedman-Högstrom and Högstrom, 1975) to the high frequency end of the inertial subrange at $f \simeq 50$). In practice this range is seldom achieved, and so care should be taken to compare results only if the bands are of similar width and position.

Turbulence measurements in this study were made over a carefully selected suburban site, using a Gill UVW anemometer mounted on a free-standing steel tower at an effective height of $\sim$ 20 m into the surface

layer (see Appendices A and B). The integral statistics were calculated directly from 62 blocks of data each containing 8192 data points sampled at 2.5 Hz (see Appendix F for details of the analysis). These data yield a non-dimensional frequency range of $3.0 \times 10^{-3} < f < 50$. Surface layer turbulent sensible heat fluxes were determined by a variety of methods and the best estimate selected (see Appendices B.2.2, B.2.3 and E.1) so that the Monin-Obukhov stability length could be calculated. The depth of the mixed layer was determined by an acoustic sounder whose records were periodically verified with the temperature structure measured using twin theodolite-tracked minisondes (see Appendices B.2.6, B.2.7 and J). From these data the ratios σ_i/u_* could be plotted as functions of $\zeta = z/L$ and $\zeta_i = z_i/L$, these surface layer parameters having ranges (-0.02, -147.4) and (-0.0, -1211.8) respectively. The plots of the σ_i/u_* ratios against ζ and ζ_i show strong increasing trends with increasing instability with a great amount of scatter. This scatter is inherent in all atmospheric measurements of this type and is in part related to the use of finite length records. In order to reduce this scatter, the data were classified into eight classes, each represented by its mean ratio of σ_i/u_* and ζ, the analysis being repeated to give seven classes of ζ_i. This process of combining statistics from blocks of data is not strictly admissible since each block has a different mean wind ($\overline{u}$) and hence different range of f, all blocks being at the same height. However, since in this study the range of $\overline{u}$ was low (a mean of 2.5 m s^{-1} and a standard deviation of 1.1 m s^{-1} over all blocks), the range of f from block to block will be small enough to ignore. In general, the members of a ζ class do not correspond to those in the same (ranking) ζ_i class. These classes are shown in Tables 3.1a and 3.1b together with the corresponding means and standard deviations of the ratios σ_i/u_*.

Table 3.1a: ζ_i vs σ_i/u_*; i = u,v,w

Class	ζ_i	σ_u/u_*	σ_v/u_*	σ_w/u_*
1	-2.4±0.9	2.2±0.4	1.9±0.7	1.4±0.1
2	-5.2±1.5	3.1±1.1	2.6±1.3	1.7±0.8
3	-10.0±2.2	2.1±0.5	2.4±0.8	2.0±0.3
4	-16.9±2.2	2.8±1.0	3.4±1.1	2.3±0.6
5	-39±15	2.6±0.4	2.9±0.9	2.8±0.8
6	-122±58	4.0±0.8	4.2±0.7	3.9±0.8
7	-590±350	8.6±4.1	8.4±3.7	6.9±2.5

Table 3.1b: ζ vs σ_i/u_*; i = u,v,w.

Class	ζ	σ_u/u_*	σ_v/u_*	σ_w/u_*
1	-0.2±0.1	2.1±0.5	1.7±0.5	1.3±0.2
2	-0.4±0.1	2.2±0.4	2.1±0.5	1.7±0.2
3	-0.7±0.1	2.4±1.1	2.2±0.4	2.0±0.4
4	-1.2±0.7	2.6±0.8	2.7±1.2	2.1±0.6
5	-1.9±0.3	3.0±0.7	3.4±1.1	2.2±0.7
6	-4.5±1.2	3.2±0.9	3.5±0.7	3.2±0.8
7	-11.1±3.1	6.0±3.6	5.9±2.3	4.2±1.8
8	-70±53	8.6±4.0	8.3±3.7	6.1±3.2

These somewhat arbitrary classes can be related to more commonly used stability categories using Golder's (1972) relation between z/L and the Pasquill-Gifford classes, the correspondences are given in Table 3.2.

Table 3.2: Relation between z/L classes and Pasquill-Gifford classes.

z/L Class	P-G Class
1	C
2	B
3	B
4	A
5	A
6	A
7	A
8	A

Empirical functions of the form:

$$\sigma_i/u_* = (a - b\zeta)^c \tag{3.7}$$

can be fitted to these data (for both scaling variables) using least squares techniques. The results are shown in Figures 3.1 to 3.3, and the fitted parameters given in Table 3.3.

Table 3.3: Least Squares Fitted Parameters to Equation (3.7) for Three Components

		a	b	c
σ_u/u_*	ζ	5.57	17.94	0.30
	ζ_i	3.18	0.02	0.75
σ_v/u_*	ζ	0.00	36.81	0.27
	ζ_i	5.23	0.10	0.51
σ_w/u_*	ζ	0.00	19.05	0.25
	ζ_i	2.49	0.41	0.35

The adiabatic limits for the ratios σ_i/u_* are not explicit in the data since no truly neutral conditions were experienced. Clarke et al. (1978) investigated these ratios over an urban and suburban surface and found values in good agreement with those over homogenous terrain as reviewed by Counihan (1976). The work of Clarke et al. (1978) uses a non-dimensional frequency band of (1.15×10^{-3}, 15.0) (Clarke, pers. comm.) which is somewhat narrower than that of this study. Given the above reservations, the ratios for the nearest neutral class (represented by $\zeta = -0.2 \pm 0.1$) are in good agreement (see Table 3.4) with those presented by Clarke et al. (1978), those summarized by Counhian (1975), and those measured over a suburban surface by Coppin (1979).

Table 3.4: Comparison of Measured Values of (near) Adiabatic non-dimensional Wind Velocity Standard Deviations.

	This Study	Clarke et al. (1975)	Coppin (1979)	Counihan (1975)
σ_u/u_*	2.1±0.5	2.39	2.5	2.5
σ_v/u_*	1.7±0.5	1.79	-	1.88
σ_w/u_*	1.3±0.2	1.26	1.1	1.25

Given the wide scatter of the data (represented by the error bars in Figures 3.1 to 3.3) it is not possible to choose between the two scaling variables ζ and ζ_i, and neither can much weight be given to the actual values of the parameters in Table 3.3. The third of these parameters should, from scaling arguments (Panofsky et al., 1977), be equal to 0.33. This is neither supported nor contradicted by this study.

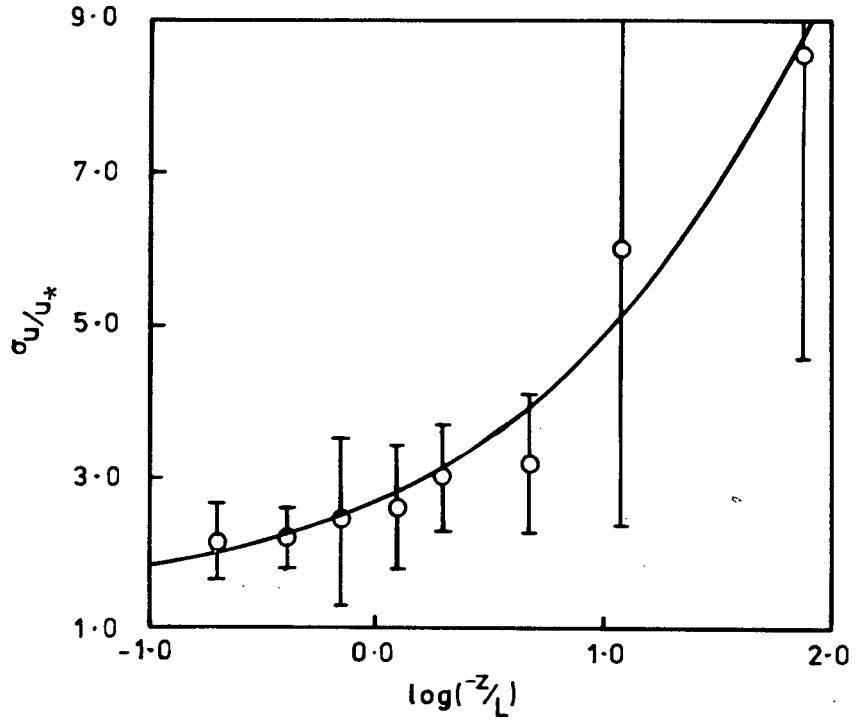

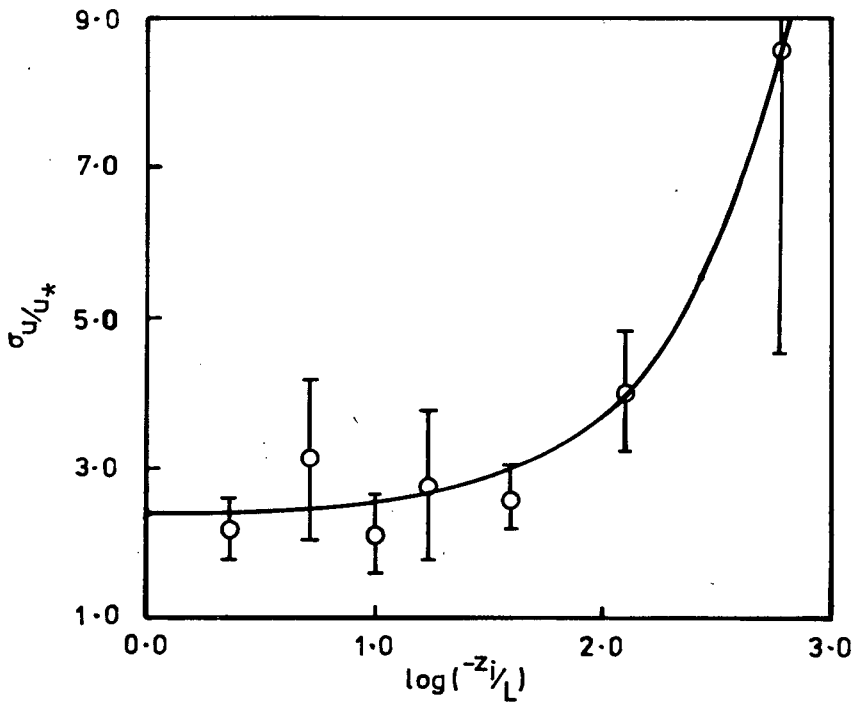

Figure 3.1: Non-dimensional Integral Alongstream Turbulence Statistics as Functions of Surface Layer Similarity Variables.

(solid lines are equation 3.7 with parameters given in Table 3.3)

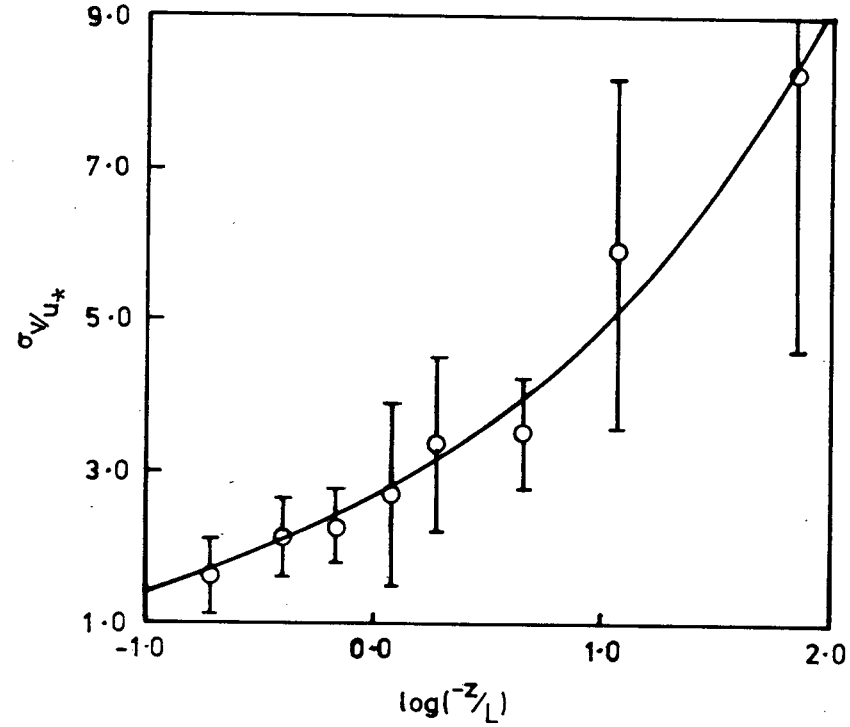

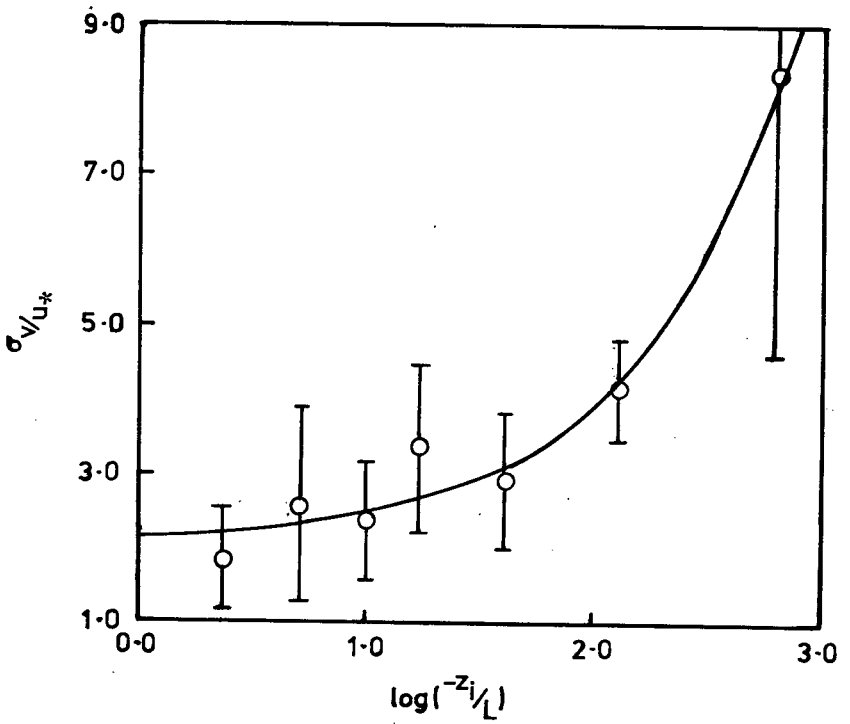

Figure 3.2: Non-dimensional Integral Crosswind Turbulence Statistics as Functions of Surface Layer Similarity Variables.

(solid lines are equation 3.7 with parameters given in Table 3.3)

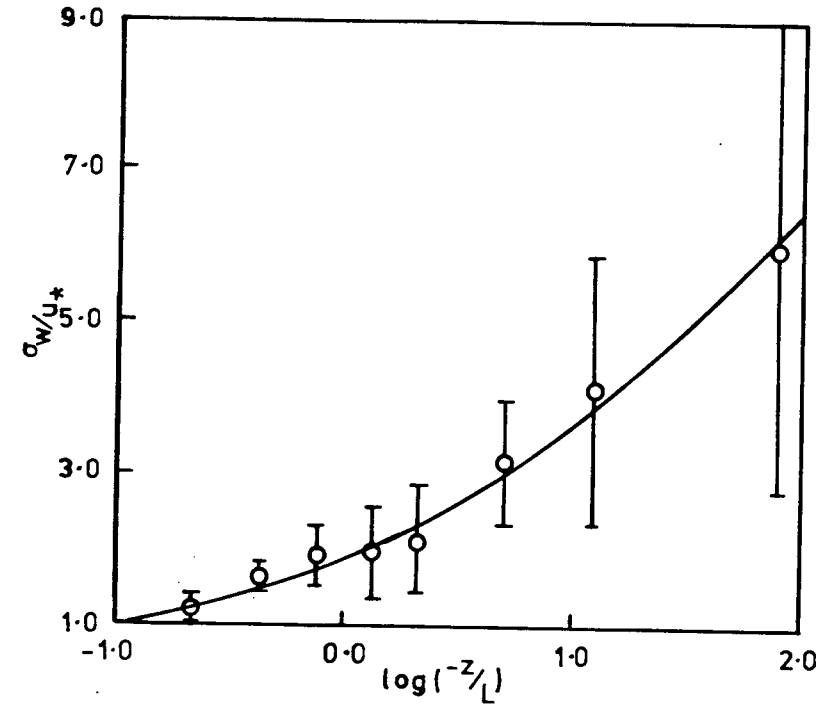

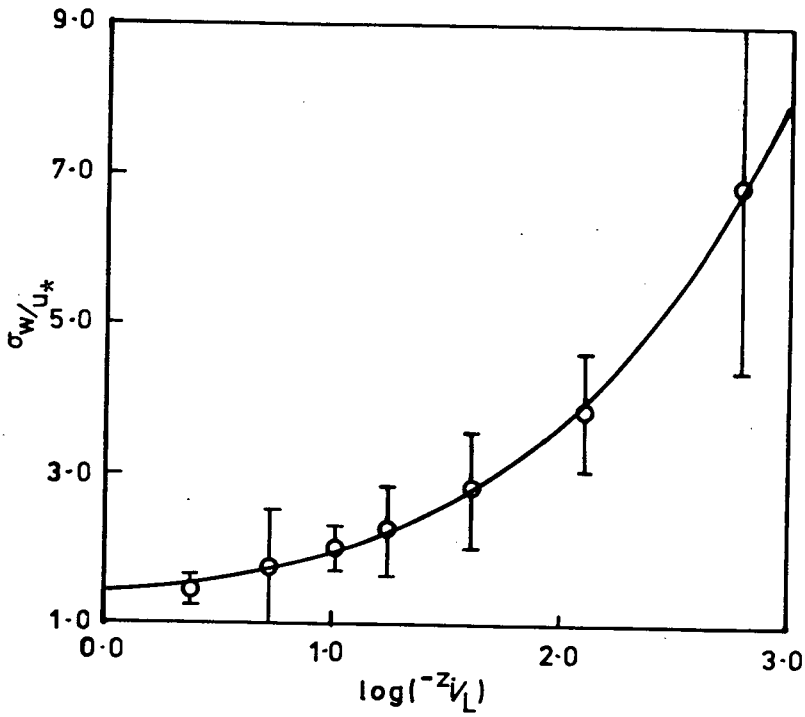

Figure 3.3: Non-dimensional Integral Vertical Turbulence Statistics as Functions of Surface Layer Similarity Variables.

(solid lines are equation 3.7 with parameters given in Table 3.3)

3.2.2 Spectra

Turbulent fields are conveniently and customarily analysed according to the theory of random functions (Monin and Yaglom, 1975). The application of this body of theory generally results in the representation of the fluctuations of some turbulence property (vector or scalar) in terms of its spectrum in frequency space via Taylor's hypothesis. The details of the derivation of the three energy density spectra are covered in Appendix F.

Apart from their use in deriving the dispersion functions in this study the spectra are powerful representations of the properties of turbulence, giving a frequency breakdown of energy content (variance) of the flow field. Surface layer similarity theory predicts that the normalized spectra will be functions of a dimensionless frequency $f = nz'/\overline{u}$ (where n is frequency and z' a length scale). Kaimal (1978) shows that the length scale is z (the height) for the vertical component and the horizontal components at high frequencies, and z_i (the depth of the mixed layer) for the horizontal components at low frequencies. His spectra are normalized by division by $u_*^2\phi_\varepsilon^{2/3}$ where u_* is the surface layer friction velocity and ϕ_ε is the non-dimensional dissipation rate, the data being collected over "flat featureless terrain". The spectral properties of the atmosphere over this type of surface have been thoroughly investigated and a review presented by Busch (1973). Similar investigations over urban or suburban surfaces have been carried out by Davenport (1967), Deland (1968), Bowne and Ball (1970), Steenbergen (1971), Brook (1974), Dûchene-Marullaz (1975) and Coppin (1979), all of whom report their spectra as being similar in general form to those reviewed by Busch (1973).

The three spectra (one for each velocity component) used to represent the atmospheric fluctuations are curves extracted from composite plots of spectra for each of the eight z/L classes of Table 3.1b. Appendix F details the time series analysis that produced the individual spectra and shows how they collapse onto three "universal" curves. The residual scatter (between spectra) is due to inherent uncertainty in the methods of analysis. The low frequency scatter for the horizontal components is partly due to using $f = nz/\overline{u}$ rather than $f_i = nz_i/\overline{u}$ as suggested by Kaimal (1978). These more proper scalings would produce more certain spectral estimates but are not appropriate in this context as the integral in equation (3.3) would not transform to the convenient form of equation (3.4). Figure 3.4 shows the "u", "v" and "w" spectra as functions of f, with the approximate boundaries of Kaimal's (1978) three scaling regions.

In spite of the uncertainty in the measurements made over this kind of surface, the spectra bear a strong resemblance to Kaimal's (1978) curves and represent the first confirmation that urban atmospheric fluctuations have similar details of structure as do those over flat (low roughness length) surfaces, the previously mentioned studies having somewhat limited ranges of f. The "w" spectrum is the simplest, having one simple maximum at $\lambda = 10z$ where $\lambda = \overline{u}/n$ is the characteristic wavelength, this being somewhat longer than the maximum position of $\lambda = 6z$ for the accepted empirical form for the unstable vertical spectrum (Kaimal, 1978). The two horizontal spectra ("u" and "v") exhibit a clear maximum at lower frequencies and a less prominent point of inflexion at higher frequencies shown by Kaimal (1978) to be characteristic of these components in an unstable surface layer. The positions of these two features and those found by Kaimal (1978) are shown in Table 3.5. For rough comparative purposes, in this study z_i ranged from 3z to 30z (see Part Two for more detail).

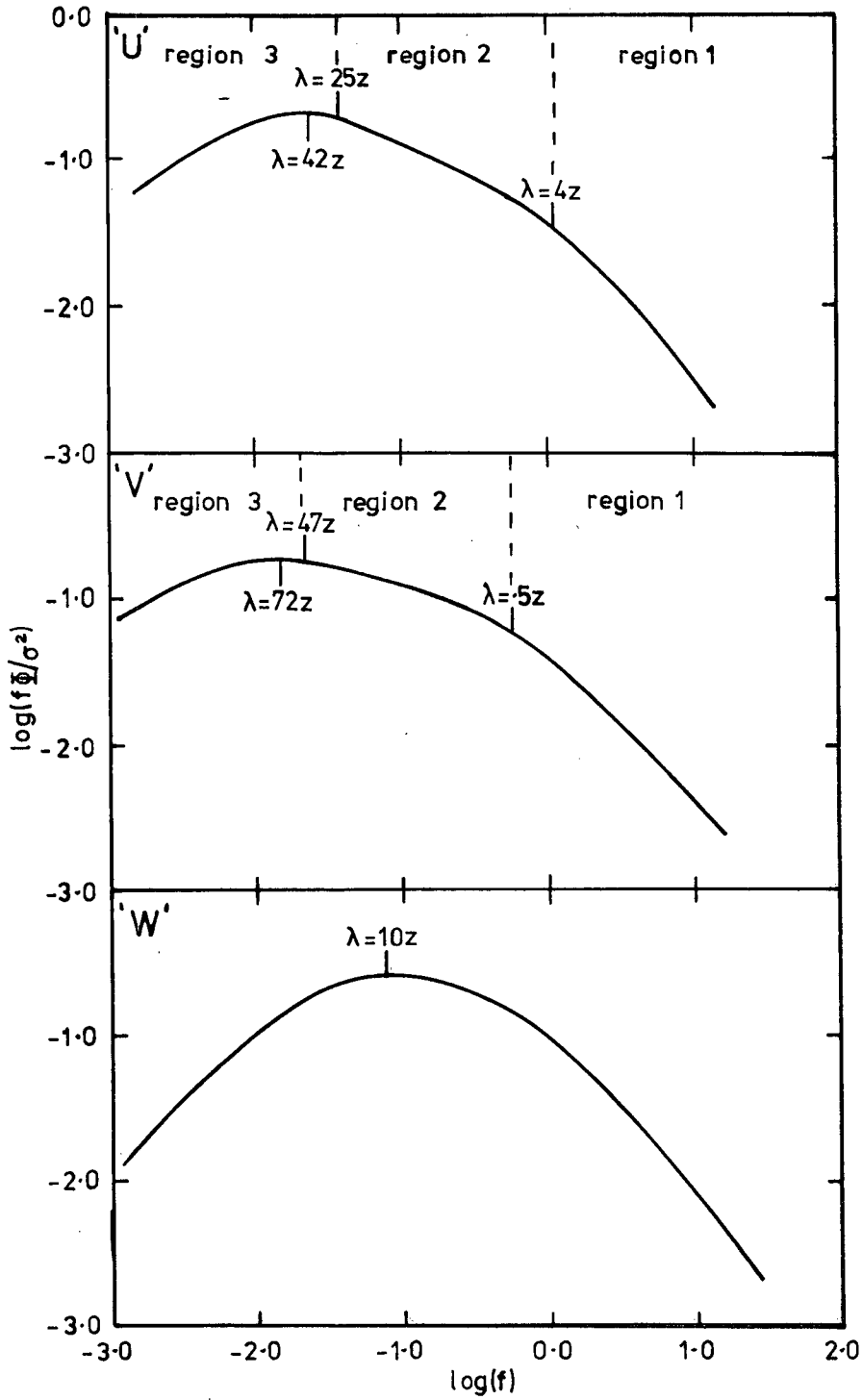

Figure 3.4: Energy Density Spectra for the Vancouver Suburban site.

Table 3.5: Positions of Spectral Features.

	Regional Boundaries in Spectra		
	1-2	2-3	Maxima
"u" This Study	4z	25z	42z
"u" Kaimal (1978)	2z	$0.67z_i$	$1.6z_i$
"v" This Study	0.5z	47z	72z
"v" Kaimal (1978)	1z	$0.25z_i$	$1.6z_i$
"w" This Study	-	-	10z
"w" Kaimal (1978)	-	-	6z

Given the uncertainty of the exact positions of the spectral features (especially when plotted in log frequency space), it is not possible to discern any differences between spectra measured over "rough" and "smooth" surfaces.

The "v" and "w" spectra of Figure 3.4 will be used to complete the integrand in equation (3.4) and so provide estimates of the crosswind and vertical dispersion functions which are the object of this part of the study.

3.3 Computation of the Dispersion Function

3.3.1 Computational Details

The integration of equation (3.4) with tabulated values for the spectral function is a straightforward exercise in numerical quadrature. The "v" and "w" spectra in Figure 3.4 were digitised at 50 uniformly spaced points in log space (thus providing higher resolution at lower frequencies); multiplied by the sampling function appropriate to the

travel time being considered; and the integration performed with a standard numerical quadrature package available as a library routine in The University of British Columbia's Computing Centre. This routine (called QINT4P) fits a fourth order polynomial to four consecutive data points and computes an analytic integral over the middle interval. This process is repeated for every interval except the first and last which are handled by forward- and backward-difference schemes (Madderom, 1978). The listing of a FORTRAN IV program which will perform this analysis is given in Appendix G.

The maximum non-dimensional travel time is 150, this corresponding to t = 54 min (the length of the turbulence data blocks) with a representative upper limit for σ_u of 0.8 m s^{-1} at z = 20 m. The dispersion function is computed every 3.0 units of t*.

The value of this integral for zero travel time should be exactly unity for a complete, well normalized spectrum. Since normalization by the total variance is proper, departure from unity will indicate an incomplete spectrum. This will be referred to later.

3.3.2 Crosswind Spread

The computed crosswind dispersion function is shown in Figure 3.5. The lower curve (marked a) is derived by applying the method of 3.3.1 to the "v" spectrum in Figure 3.4. The upper curve (marked b) is similarly derived but the low frequency end of the spectrum has been linearly extended (in log-log space) to an amplitude of -1.75 at a frequency of -4.00. The integral at zero travel time for the extended spectrum is 1.002 while that for the spectrum as calculated is 0.950, indicating a 5% loss of total variance, probably mostly in the low frequency end. As intuitively expected, the difference is most marked at long travel times. This low frequency extension of the spectrum is

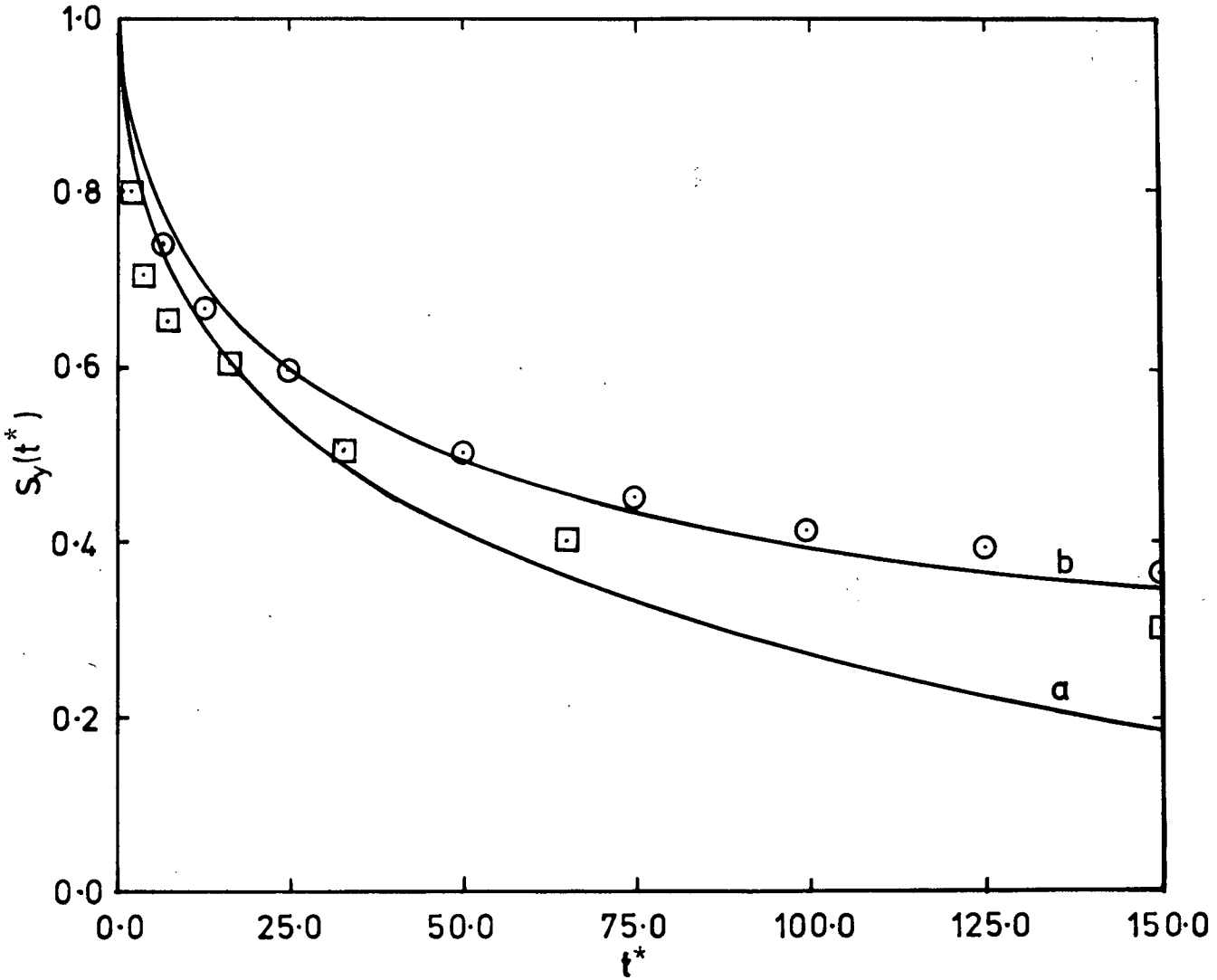

Figure 3.5: Crosswind Dispersion Function.

⊙ Draxler's (1976) function
a Measured urban spectrum
⊡ Hanna et al. (1977) values
b Measured urban spectrum with low frequency extension

somewhat arbitrary, and results derived from it should not be accorded too much deductive weight. The form of travel time scaling used here is operationally more convenient than the theoretically more proper Lagrangian scaling, and can be related to the latter in a simple manner. Hunt and Weber (1979) present the relation:

$$t_L = 0.33\ z/\sigma_w$$

Busch (1973) reports σ_w/σ_u to be constant at 0.52 for all unstable conditions. The data of this study show this ratio to scatter widely between 0.4 and 0.8. Taking the value of 0.52 leads to

$$t_s = 1.58 t_L \tag{3.7}$$

where $t_s = z/\sigma_u$, our scaling time. From this it can be seen that t_L (and t_s) is implicitly a function of stability as suggested in Section 3.2. Draxler (1976) scales his travel time with t_i, the time at which the dispersion function equals 0.5. From Figure 3.5, S(47.17) = 0.5000, which means that

$$t_i = 47.17\ t_s \tag{3.8}$$

or, using (3.7),

$$t_i = 74.53\ t_L \tag{3.9}$$

Equation (3.8) was used to transform Draxler's (1976) recommended function.

$$S(t/t_i) = (1.0 + 0.9(t/t_i)^{1/2})^{-1}$$

at selected points onto Figure 3.5. The agreement between these points and curve b is excellent, with only very slight relative skewing. Sawford's (1979) calculated points envelop Draxler's (1976) function and so are also in agreement with this study.

There remains, however, an inconsistency that must be addressed. Draxler (1976) uses the long-time limit of his function to relate t_i to t_L and shows that

$$t_i = 1.64 t_L \tag{3.10}$$

in conflict with (3.9). A possible reason for this disagreement is the uncertainty inherent in extrapolating an empirically fitted function to its limiting value at infinity. Draxler (1976) suggests t_i = 1000s, thus implying t_L = 610s by equation (3.10), or t_L = 13s by equation (3.9). While their constancy is an unrealistic simplification, the latter value is in good agreement with the prediction of equation (3.7), using a typical value of $\sigma_u = 0.75$ m s^{-1} (this corresponds to $\overline{u} = 2.5$ m s^{-1} and a turbulent intensity of 0.30), giving t_L = 12.7 s. Fichtl and McVehil (1969) suggest that t_L may be approximated by:

$$t_L' = \frac{\lambda_{max}}{2\pi\overline{u}}$$

where λ_{max} is the wavelength maximum of the Lagrangian "u" specturm. From the spectra of this study (Table 3.4), this leads to

$$t_L' = \frac{42z}{2\pi\overline{u}} \cdot \frac{2\sigma u}{\overline{u}} ,$$

using the Eulerian - Lagrangian transform of Section 3.1.1. The ratio of this time scale to that given by Equation (3.7) is:

$$t_L'/t_L = \frac{42 \times 1.58}{\pi} i^2$$

This ratio is unity for a turbulent intensity of 0.22, well within the range of 0.30 ± 0.15 for the present data set. Brook (1974) determines the Eulerian integral length scale over an urban surface to be 110 m at 18 m

height (an interpolation from his Figure 9.1), which is in agreement with the estimate of 120 m obtained from the Fichtl and McVehil (1969) formula with $\lambda_{max} = 42z$. This consistency is taken as further indication of the correctness of equation (3.8), and strengthens the use of t_s as a time scale. Sawford (1979) has t_i ranging from 30s to 230s, depending on the run chosen (see his Table 1). His non-dimensional frequency range is $1.2\times10^{-4}<f<0.2$, the same width (in log space) and extending to 2.5 decades lower than the data in this study. The lower frequency coverage explains why Draxler's (1976) and Sawford's (1979) determinations of $S(t^*)$ agree with curve b rather than a. The foregoing leads us to the conclusion that in general t_i is a poor surrogate for t_L, and will depend on the non-dimensional frequency band over which the analysis is performed. External time scales such as t_L or t_s are preferable to t_i, and in any case the averaging band is of vital importance.

Hanna et al. (1979) recommended a set of values for crosswind dispersion as a function of travel distance. Bearing in mind Pasquill's (1975a) reservations about a simple Galilean transformation from distance to time, travel distance can be related to the present non-dimensional travel time. We want $x = \overline{u}t$.

Since $$t^* = t\sigma_u/z,$$

we have $$x = \frac{z}{i}t^*$$

which for this study is equivalent to

$$x = 66.7\ t^* \tag{3.11}$$

if $z = 20.1$ m and $i = 0.30$.

Equation (3.11) is used to transform the Hanna et al. (1977) values for f(x) onto Figure 3.5. These agree well with curve b.

It has been asserted (Pasquill 1974; Sawford, 1979) that the form of S(t*) will not be sensitive to details of the autocorrelation function (and hence the spectral function). In order to test this assertion, Kaimal's (1978) "v" spectrum was extended to low frequencies by linear extrapolation, renormalised and integrated to produce a form of $S_y(t^*)$ appropriate to those surfaces. The results are shown in Figure 3.6. The almost inconsequential differences in these two curves is an indication that turbulent diffusion as represented by the statistical theory is not sensitive to the differences in spectral functions used to determine the two curves. Before the dispersion function given in Figure 3.5 can be ascribed any universality, this analysis must be repeated on spectra determined over a range of surface types using identical methods (viz identical de-trending, smoothing, band - averaging and convolution). At present, the similarity of the curves in Figure 3.6 is an indication that these curves may be universal (i.e., applicable to a range of surfaces).

The high frequency tail of the spectra shown in Figure 3.4 roll off as approximately $f^{-0.88}$, rather than the expected -2/3 behaviour of the inertial subrange. This is presumably due to the inability of the sensors to respond to high frequency fluctuations. In order to quantify this shortcoming, the "v" spectrum was extended linearly (in log-log space) with the appropriate slope, redigitized and the integration of Section 3.3.1 performed. This correction resulted in only a 0.5 percent increase in the total variance, and no significant change in $S_y(t^*)$.

The computed values of $S_y(t^*)$ were found (by least squares methods) to fit very closely the analytic form

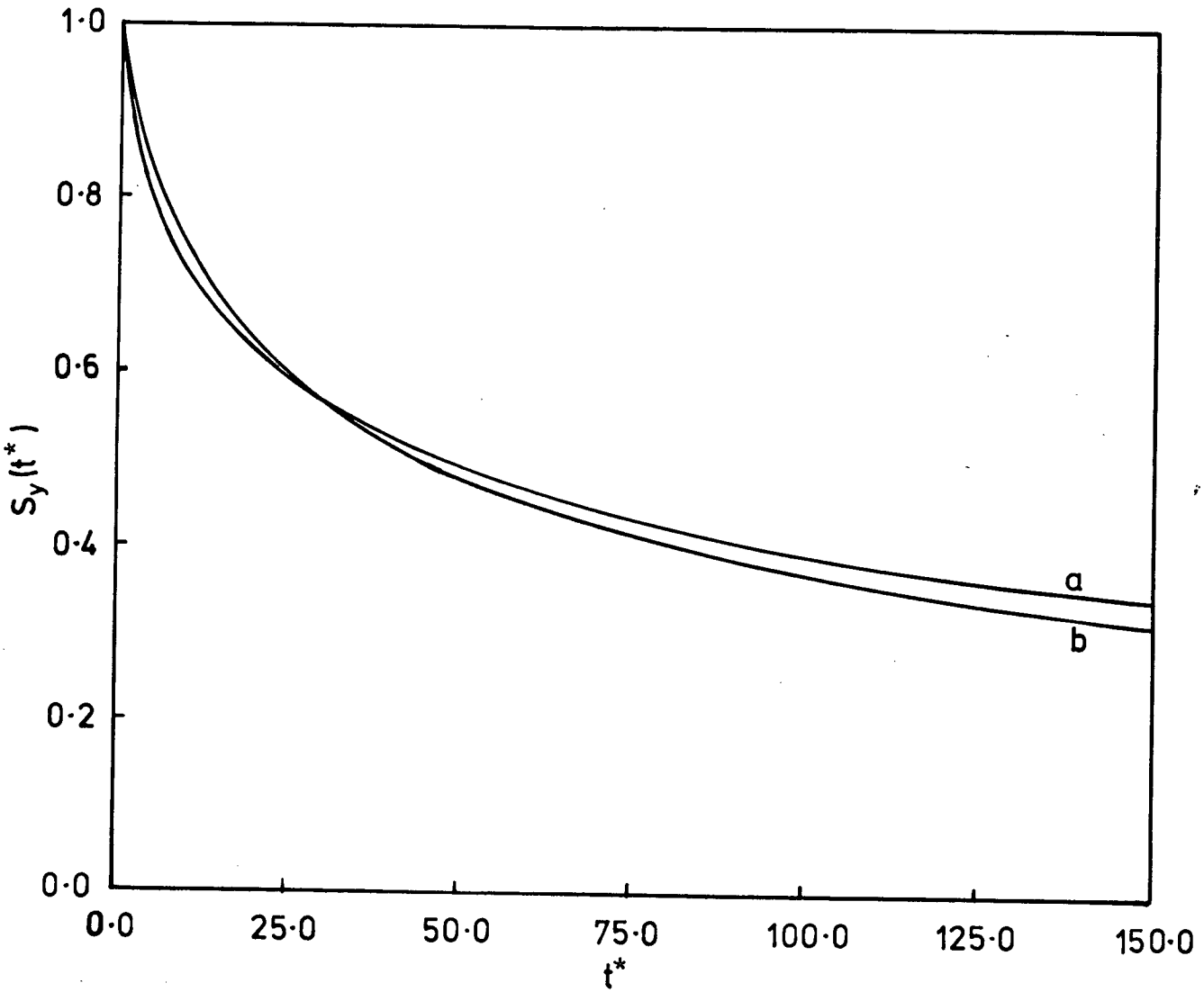

Figure 3.6: Crosswind Dispersion Function S(t*) for:

b - Kaimal's (1978) extended Spectral function
a - Extended spectral function from this study.

$$S_y(t^*) = (1.0 + 0.16\sqrt{t^*})^{-1}$$

This form may then be used to determine crosswind plume width (see Appendix H) for input into Gaussian plume model dispersion calculations.

3.3.3 Vertical Spread

The computational scheme of Section 3.3.1 can be applied to a measured vertical velocity spectrum to produce a vertical dispersion function $S_z(t^*) = \sigma_z/\sigma_w t$, analogous to the crosswind function of Section 3.3.2. The vertical dispersion function derived from the "w" spectrum of Figure 3.4 is shown in Figure 3.7. The use of this technique for determining σ_z is much less sound than its use for determining σ_y. The major problem lies in the vertical inhomogeneity of the atmosphere which reduces the results to approximations at best. These approximations are likely to be good for elevated releases in unstable atmospheres, and poor for ground-level releases in unstable atmospheres and elevated releases in stable atmospheres. A secondary problem lies in the choice of scaling time. Inherent in the method of this study is the scaling time t_s which can be easily related to a number of possible surface layer integral scaling times, including the Lagrangian integral time scale (see Section 3.3.2). The most rational scaling time for vertical diffusion in unstable conditions is $t_u = z_i/w_*$ (Deardorff and Willis (1975) and Hanna et al. (1977)) where z_i is the depth of the mixed layer, and $w_* = (\frac{g}{\bar{\theta}} \overline{w'\theta'} z_i)^{1/3}$ is the mixed layer convective velocity scale where g is the acceleration due to gravity, $\bar{\theta}$ the mean potential temperature of the mixed layer and $\overline{w'\theta'}$ the surface kinematic sensible heat flux. Irwin (1979) collects a body of data to relate σ_w/w_* to z/z_i in the form

$$\sigma_w/w_* = a(z/z_i)^b$$

where a and b are empirical coefficients varying with z/z_i.

Since $t_u/t_s = 1.92z_i/z \cdot \sigma_w/w_*$,

we find that

$$t_u/t_s = 1.92a\ (z/z_i)^{1-b}.$$

Our data are generally in the range $0.03<z/z_i<0.3$ (see Part Two),

where a = 0.72, b = 0.21, giving

$$t_u/t_s = 1.38(z/z_i)^{0.79}$$

yielding $0.1<t_u/t_s<0.5$

A statistical analysis of data from the 62 data blocks shows this ratio to be 0.12 with large scatter. In the absence of a single representative value of z/z_i for the entire data set, the time scale ratio of 0.12 was used to transfer Irwin's (1979) curve onto Figure 3.7 as a set of points. The results can be seen to agree substantially with the curve, in spite of the uncertainty about the analysis expressed before.

The curve on Figure 3.7 is well represented by

$$S_z(t^*) = (1.0 + 1.21\ \sqrt{t^*})^{-1}$$

which may be used to determine vertical plume dimensions for input into Gaussian plume model dispersion calculations.

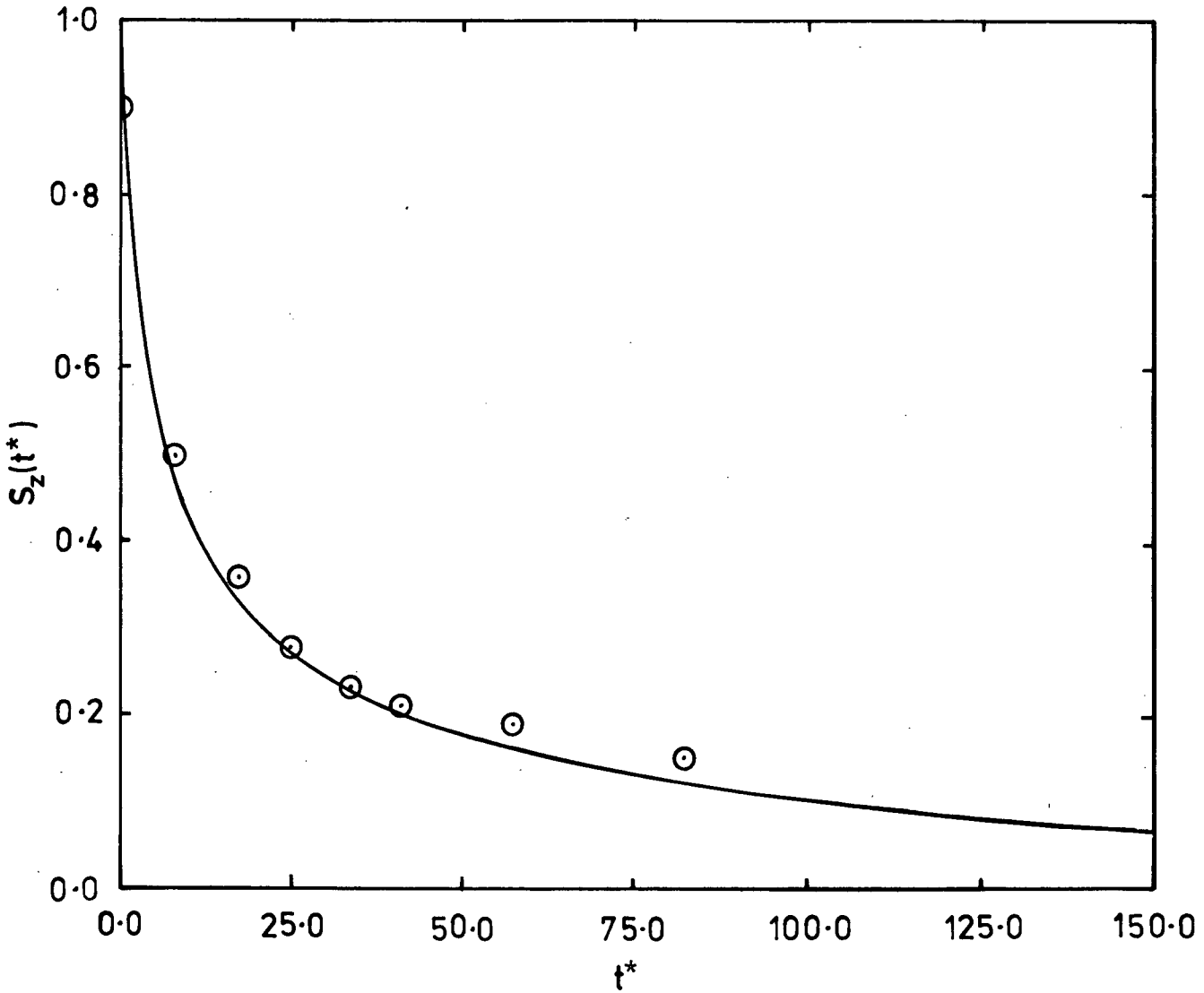

Figure 3.7: Vertical Dispersion Function.
⊙ - Irwin's (1979) values.

4. Conclusion

The results of this part of the study have shown that the Gill UVW anemometer can be successfully used to measure the turbulent structure of the unstable atmosphere over a very rough surface ($z_0 \sim 0.5$m). Its response shortcomings, particularly in the vertical sensor, are partly ameliorated by the relatively large vertical velocities encountered. In particular the non-dimensional velocity variances σ_i/u_* were shown to behave much as those over smoother surfaces. The details of their dependence on the stability parameters z/L and z_i/L were obscured by the scatter in the data, but their general behaviour was not in contradiction with previously published empirical functions. The spectral functions over this surface were found to be of the same general form as those observed over smoother surfaces.

Within the framework of the statistical theory of diffusion, it was shown that the non-dimensional dispersion functions $\sigma_y/\sigma_v t$ and $\sigma_z/\sigma_w t$ can be determined by integration of the Eulerian spectral functions multiplied by an appropriately scaled sampling function. This scaling, which arises out of the Hay-Pasquill form for the Eulerian-Lagrangian transform and the use of a non-dimensional frequency, gives rise to a scaling time $t_s = z/\sigma_u$ which is simply related to the Lagrangian integral time scale. This treatment of diffusion is strictly speaking only applicable to turbulent fields whose mean properties are uniform in both space and time, and does not take account of wind shear as a means of cross-wind diffusion. The dispersion functions so produced agree very well with previous forms and are:

$$S_y(t^*) = (1.0 + 0.16\sqrt{t^*})^{-1} \tag{4.1}$$

and

$$S_z(t^*) = (1.0 + 1.21\sqrt{t^*})^{-1} \tag{4.2}$$

The numerical coefficients being least squares fitted parameters. The success of this method is due partly to the weak dependence of diffusion on the exact form of the spectral function, and hence on the details of the Eulerian-Lagrangian transform. The scaling time is shown to be a much more appropriate one than the somewhat arbitrary and unrealistically constant empirical form used previously. The dispersion functions are shown to be sensitive to the low frequency portion of the spectrum, indicating the need for careful measurement in those ranges.

The two forms for the crosswind and vertical dispersion functions may be used as input to Gaussian plume model calculations of pollutant spread. The values for σ_v and σ_w may be obtained from direct measurement or from accepted parameterization schemes (see Appendix H).

Care should be taken in the application of these dispersion formulae in the mixed layer itself ($z/z_i > 0.1$ say), where the low frequency end of the spectrum may be markedly different from the ones observed at much lower altitudes. An alternative approach for this regime is provided by Venkatram (1980) who expresses dispersion in terms of the mixed layer variables w_* and z_i.

Part Two:

THE DEPTH OF THE DAYTIME MIXED LAYER

5. Introduction

5.1 Specification of the Mixed Layer Depth

The atmospheric boundary layer is that portion of the Earth's gaseous mantle into which the frictional and thermal effects of the underlying surface extend. This layer is commonly in a state of highly turbulent motion which facilitates the uniform mixing of entropy and gaseous atmospheric constituents throughout its depth, hence the commonly used term "mixed layer" (Tennekes, 1974). The structure of the mixed layer is largely determined by the exchange of turbulent energy between the layer itself and the underlying surface, both of which can act as either source or sink, though the commonest configuration is for the surface to be a source of thermal and mechanical energy. In the case of a mechanically dominated layer, viscous drag at the surface provides a source of turbulent kinetic energy throughout the layer. This layer has no clear upper limit but can be defined as the height at which the turbulent fluxes (resulting from surface effects) have fallen to some (small) fraction of their surface values (Brost and Wyngaard, 1978), or some equivalent assumption (Niewstadt and Driedonks, 1979; Yamada, 1979). It is often observed that an inversion of synoptic origins provides an unambiguous upper limit to surface driven turbulent processes. It is the depth of this inversion-capped mixed layer in the presence of strong surface heating that is the concern of this part of the study.

The depth of a thermally-driven mixed layer generally exhibits strong diurnal variation and ranges from a few tens of metres to up to 2000 m in response to the diurnal variation of the surface sensible heat flux (Carson, 1973). This variation in depth, generally observed as a

monotonic increase, is principally achieved by entrainment in which the stable air above is eroded from below and mixed downward into the usually neutrally stable mixed layer. This entrainment is driven by the high levels of turbulence in the mixed layer which arise from upward heat transfer by thermal convection.

The depth of the mixed layer can be measured by a variety of means, each possessing its own definition of the exact height (Coulter, 1979). The principal methods of measurement being to sound directly some mixed layer parameter (usually temperature), and thereby detect the discontinuity at the inversion base, or to remotely detect some effect of the entrainment process. Rather than full-scale field measurement programmes, the atmospheric boundary layer can also be modelled on a laboratory scale so as to elucidate its properties, including the depth (Deardorff et al., 1969, and Heidt, 1977). A number of schemes for the estimation of (usually hourly) mixing depths from easily available meteorologic data have been developed (Holzworth, 1967; Miller, 1967; Deardorff, 1972; Benkley and Schulman, 1979) for use in air pollution modelling and as lower boundaries in general circulation models.

An alternative to direct measurement or rough estimation is the mathematical modelling of the mixed layer processes so as to elucidate the depth. This modelling has been extensively developed by a number of investigators whose work has been successful enough to prompt Tennekes (1976) to say "... the inversion rise problem may be regarded as solved". While this statement is in principle true, in detail there remain processes within the mixed layer and at the entrainment interface which are either poorly understood or need to be included in the models. Smith and Carson (1977) have considered the modelling of boundary layers in general and have detailed the requirements for this modelling on various scales, and in so doing have pointed out areas for further study.

In this study we address the short-range (see Smith and Carson, 1977) pseudo-two dimensional mathematical modelling of a dry, inversion-capped, convectively unstable boundary layer over a mid-latitude suburban surface near a large body of water.

5.2 Mathematical Modelling of the Mixed Layer Depth

The model which met with Tennekes' (1976) approval arose from a proposal of Ball (1960) later developed by Lilley (1968), Tennekes (1973), Betts (1973), Carson (1973), Mahrt and Lenschow (1976) and Stull (1976a,b), among others. Crucial to the success of these models was Ball's (1960) assumption that the downward sensible heat flux at the inversion base is proportional to the upward sensible heat flux at the surface (Ball actually assumed them equal). The complete model (as presented by Tennekes (1973)) is purely thermodynamic and parameterizes the entrainment processes by ascribing to the interface a finite temperature step or "jump". In the presence of free convection (a condition prevalent in this study), mechanically generated turbulence has a negligible effect on the entrainment process (Tennekes, 1973). In a regime of forced convection, the vertical heat convergence in the mixed layer would be represented by a purely mechanical term derived from the surface layer friction velocity (see Davidson et al., 1980).

The model equations are:

$$z_i \frac{d\overline{\theta}}{dt} = (\overline{w'\theta'})_s - (\overline{w'\theta'})_i \tag{5.1}$$

$$\Delta \frac{dz_i}{dt} = - (\overline{w'\theta'})_i \tag{5.2}$$

$$\frac{d\Delta}{dt} = - \frac{d\overline{\theta}}{dt} + \gamma \frac{dz_i}{dt} \tag{5.3}$$

$$(\overline{w'\theta'})_i = - c(\overline{w'\theta'})_s \tag{5.4}$$

where $\overline{\theta}$ is the mean potential temperature of the mixed layer, $\overline{w'\theta'}$ is a kinematic sensible heat flux where θ' and w' are the fluctuating components of potential temperature and vertical velocity respectively, γ is the potential temperature lapse rate above the inversion base, and Δ is the temperature "jump". The subscripts s and i refer to the surface and the inversion base respectively.

Equation (5.1) is the thermal energy budget equation for the mixed layer, the rate of change of temperature being related to the (vertical) convergence of turbulent sensible heat into that layer. Equation (5.2) relates the vertical movement of the entrainment interface to the eddy heat flux at that level and to the temperature step which serves to parameterize the entrainment process. The temporal behaviour of this step is given by equation (5.3) which is derived from the geometry of an idealized mixed layer potential temperature profile. Equation (5.4) is a parameterization of the heat flux at the inversion base from the surface layer heat flux, and serves to close the system of equations (5.1) to (5.3).

The parameter c is the basis of Ball's (1960) assumption, and has a range of reported values generally lying between 0.1 and 0.3 (Stull, 1976b). The exact value of c will vary throughout a given day in response to the complex interacting processes at the inversion base (Carson, 1973; Zilintinkevich, 1975; Tennekes, 1975; and Stull, 1976a). Carson (1973) shows how equations (5.1) to (5.3) can be solved analytically using a simple sinusoidal surface heat flux. He compares his model with the results of the 1953 O'Neill boundary layer observations (Lettau and Davidson, 1957) and shows that the data imply distinct phases in the evolution of the boundary layer. Each phase is characterised by a different set of values for the four governing parameters, including c. Stull

(1976a) uses a constant value of c to achieve agreement between his rather more complicated model and two different sets of daily data. His values for c are in the range (0.1 - 0.2). Most recently Caughey and Palmer (1979) present a direct measurement of the vertical profile of turbulent sensible heat flux that are in agreement with c = 0.2, albeit with large scatter. Mahrt and Lenschow (1976) conclude that the dynamics of the mixed layer are not very sensitive to the closure assumption.

Based on the above information, a constant value of 0.20 was used for c in all the simulations based on real data in this study. Yamada and Berman (1979) show that this assumption provides a more than adequate first-order model.

The basic ideas of the model have been applied to idealized metropolitan areas by including an advected heat flux term in equation (5.0)(Barnum and Rao, 1975) in order to simulate thermal internal boundary-layer development (Venkatram, 1977).

6. A Model of the Mixed Layer Depth

6.1 Characteristics of the Observed Mixed Layer

Observations of the daily course of the inversion height (see Appendices I and J) over the study area exhibit behaviour strongly at variance with the classic rise and decay modelled in previous studies over extensive homogeneous surfaces (e.g., Carson, 1973, and Stull, 1976b). The inversion shown by Carson (1973, his Figure 10) rises at an initial rate of 87 m h^{-1} six hours after sunrise, and ceases rising nine hours after sunrise, after which it stays at a constant height of 1800 m until twelve hours after sunrise. Figure 6.1 is an acoustic sounder record from August 1st, 1978, showing the typical inversion height behaviour observed in the present study. The broad features of the inversion height on this day are an approximately constant rise rate of 62 m h^{-1} lasting until approximately eight hours after sunrise, by which time the inversion has risen to its maximum height of 570 m. It then begins a rather ragged descent to nearly 50 m at sunset.

The presence of intense surface-based convection is indicated in Figure 6.1 by the intermittent "plumes" within the mixed layer. The apparent gap between the top of the plumes and the inversion base is due to the inability of the sensor to respond to signals scattered from upper parts of these "plumes" which are presumably decreasing in activity as they ascend through the mixed layer. The thickness of the entrainment interface cannot, for the same reason, be derived from the apparent thickness of the acoustic sounder representation. The sounder is, however, able to show quite clearly (even at this compressed time scale) the contorted nature of the base of the inversion (Carson and Smith, 1974;

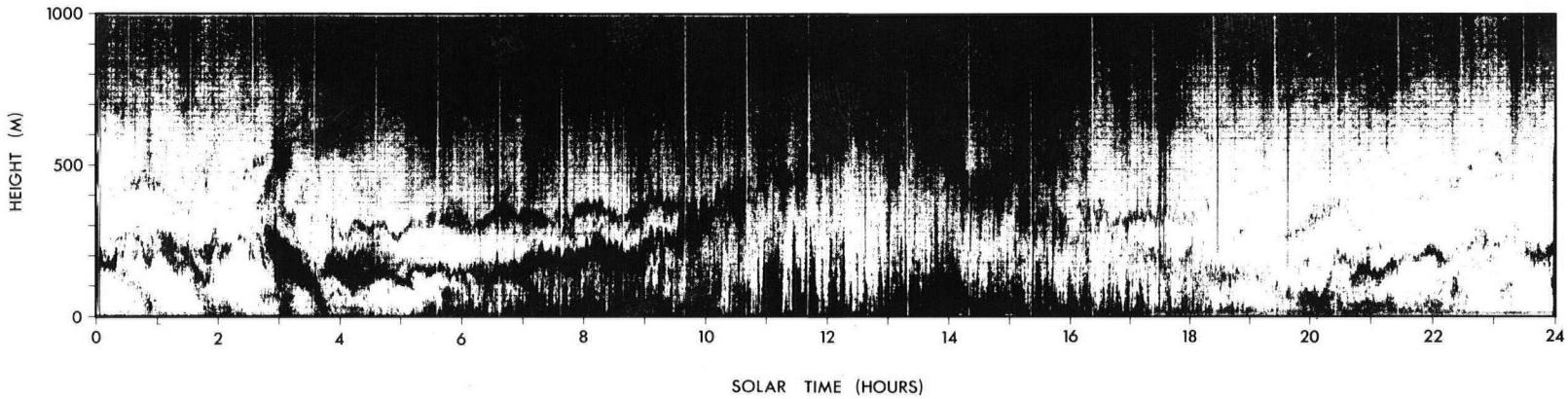

Figure 6.1: Acoustic sounder trace for August 1st.

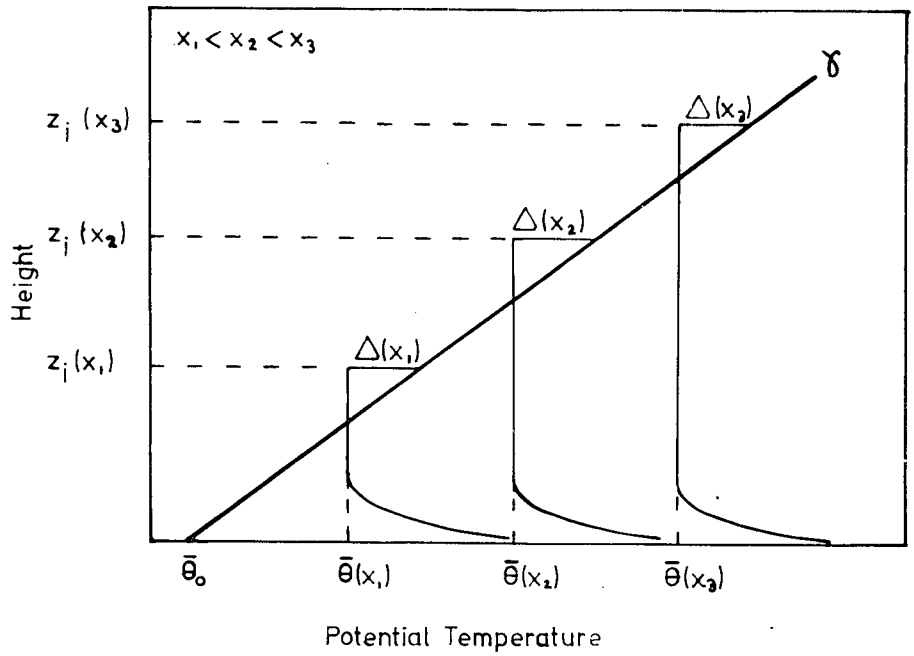

Figure 6.3: Potential Temperature Profiles at Various Distances Distances from the Upwind edge of a Thermal Internal Boundary-Layer.

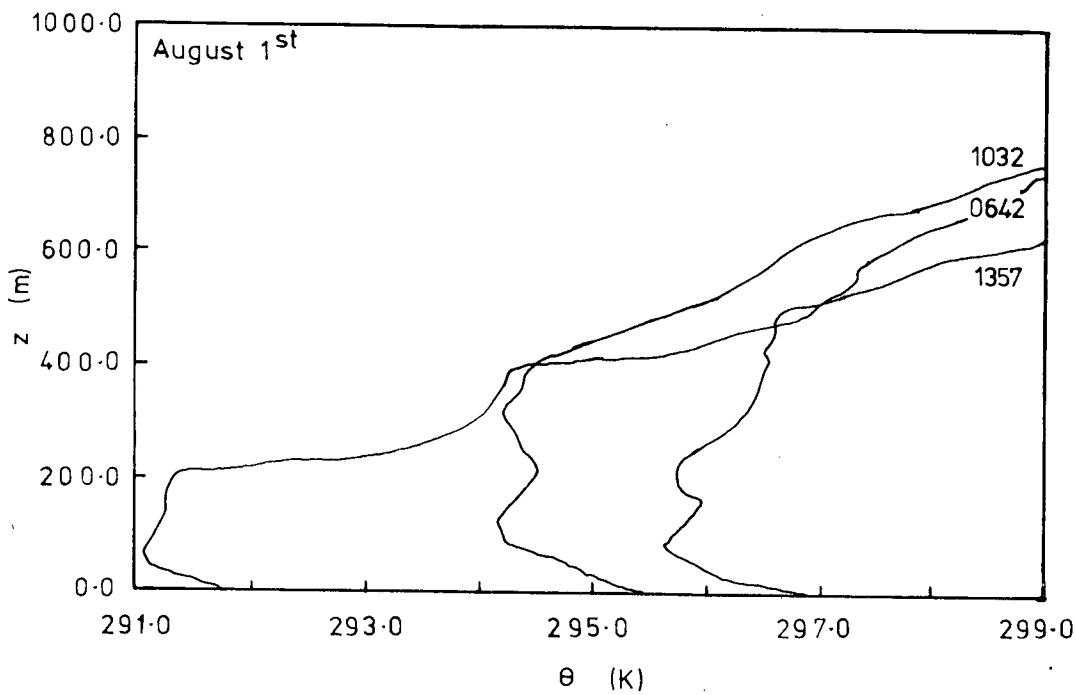

Figure 6.2: Potential Temperature Profiles for August 1st.

Stull, 1976a) as it is bombarded from below by the surface layer generated thermals. The model to be presented here is not intended to simulate this small-scale structure which is part of the entrainment process parameterized by equation (5.4). A fairly common feature of the acoustic sounder returns was the apparent disappearance of the inversion base especially beyond midday which, from the temperature soundings, continued undiminished in intensity. This phenomenon, which was often associated with descending inversions, remains unexplained in this study.

In interpreting these traces it must be remembered that the acoustic pulse has a length of 11 m, thus setting a lower limit to vertical resolution. The exact position of the inversion base on this often obscure trace was determined by comparing the trace with temperature soundings (see Appendix H), and the daily course was digitized at approximately ten minute intervals for comparison with the model results.

Potential temperature profiles, such as those shown in Figure 6.2, were used as verification of the inversion height from the acoustic sounder trace. They show the expected surface layer with strong lapse in the lower tens of metres and the near-adiabatic mixed layer capped by the strongly stable inversion layer, presumably associated with synoptic-scale subsidence (see Appendix C).

The mean characteristics of the elevated inversions are useful parameters. The mean inversion height from the acoustic sounder traces was 490 ± 122 m at noon, somewhat lower than the value of 590 m quoted by Morgan & Bornstein (1977) for San José, California at the same time of the year. This is as expected, as San José has considerably less maritime influence and is at a lower latitude. The mean inversion intensity (immediately above the mixed layer) from all balloon soundings was 0.019 ± 0.009 K m^{-1}, in good agreement with the San José figure of 0.012 K m^{-1}.

The following sections describe the development of a mixed layer model based on equations (5.1) to (5.2), modified so as to simulate in a general way the inversion height behaviour observed in this study.

6.2 Advection and Subsidence in the Mixed Layer Model

Growing boundary layers act as storage buffers for moisture, heat and momentum, thus implying non-zero and time-varying divergences of these quantities. Equation (5.1) expresses the thermal component of this characteristic; the two terms on the right hand side being the vertical divergence of heat (always positive in this case). In the case of finite fetch, there exists the possibility of non-zero horizontal divergence due to advected heat fluxes. Following Barnum and Rao (1975), we may rewrite equation (5.1) as:

$$z_i \frac{D\overline{\theta}}{Dt} = (1 + c)\, Q \qquad (6.1)$$

where $Q = (\overline{w'\theta'})_s$ and $\frac{D}{Dt} \equiv \frac{\partial}{\partial t} + \overline{u}\frac{\partial}{\partial x}$, x being the upwind distance to the surface discontinuity causing the bounday layer adjustment. This equation may be thought of as expressing the thermal energy balance of a column of air moving with the mean wind.

Similarly, equation (5.2) may be restated to include the effects of both advection and subsidence as follows:

$$\Delta \frac{Dz_i}{Dt} = cQ + \Delta w(z_i) \qquad (6.2)$$

where $w(z_i)$ is a vertical velocity of as yet unspecified origin.

Figure 6.3 shows schematically the spatial growth of an idealized thermal internal boundary layer. From it one may write:

$$\Delta(x,t) = \gamma z_i(x,t) - \overline{\theta}(x,t) + \overline{\theta}_0, \tag{6.3}$$

where $\overline{\theta}_0$ is the early morning value of the potential temperature at what will become the lower limit of the mixed layer. It ($\overline{\theta}_0$) is assumed independent of space and time, so that:

$$\frac{D\Delta}{Dt} = \gamma\frac{Dz_i}{Dt} - \frac{D\overline{\theta}}{Dt} + W(z_i,t), \tag{6.4}$$

where $W(z_i,t)$ is the heating effect of synoptic scale processes experienced at the top of the mixed layer.

In order to find the spatial behaviour of z_i and $\overline{\theta}$, an approximate first integral of equations (6.1), (6.2) and (6.4) must be found. This should produce more realistic results than those of Barnum and Rao (1975) who assumed a sinusoidal behaviour for both z_i and $\overline{\theta}$. It will be shown in Section 6.3 that the effects of subsidence are small and can, to first order, be ignored in equations (6.1), (6.2) and (6.4). Doing this and changing variables to a reduced time τ and dummy distance y, where:

$$\tau = t - x/\overline{u},$$

then $\quad \frac{\partial}{\partial t} = \frac{\partial}{\partial \tau}$ and $\frac{\partial}{\partial x} = -\frac{1}{\overline{u}}\frac{\partial}{\partial \tau} + \frac{\partial}{\partial y}$

results in

$$\frac{D}{Dt} \equiv \overline{u}\frac{\partial}{\partial y},$$

with $\overline{u}$ constant.

The model equations therefore become:

$$z_i\frac{\partial\overline{\theta}}{\partial y} = \frac{(1 + c)Q}{\overline{u}} \tag{6.5}$$

$$\Delta\frac{\partial z_i}{\partial y} = \frac{cQ}{\overline{u}} \tag{6.6}$$

$$\frac{\partial \Delta}{\partial y} = \gamma \frac{\partial z_i}{\partial y} - \frac{\partial \bar{\theta}}{\partial y} \tag{6.7}$$

(6.5) and (6.7) give: $z_i(\gamma \frac{\partial z_i}{\partial y} - \frac{\partial \bar{\theta}}{\partial y}) = \frac{(1 + c)Q}{\bar{u}}$

Subtracting (6.5) gives: $\gamma z_i \frac{\partial z_i}{\partial y} - \frac{\partial}{\partial y}(\Delta z_i) = \frac{Q}{\bar{u}}$

Which upon integration yields:

$$\tfrac{1}{2}\gamma z_i^2 - \Delta z_i = \frac{Qy}{\bar{u}} + f(\tau) \tag{6.8}$$

if Q is independent of y,

and $f(\tau)$ vanishes since $z_i = \Delta = 0$ when $Q = 0$.

If $2\Delta < \gamma z_i$, a zeroth approximation is:

$$z_i^o = \sqrt{\frac{2Qy}{\gamma \bar{u}}}$$

replacing this in (6.6) yields

$$\Delta^o = \sqrt{\frac{2\gamma c^2 Qy}{\bar{u}}}$$

The ratio $\frac{2\Delta^o}{\gamma z_i^o} \equiv 2c$ is less than unity, justifying our approximation.

Replacing Δz_i in (6.8) by $\Delta^o z_i^o$ yields:

$$z_i = \sqrt{\frac{2(1 + 2c)Qy}{\gamma \bar{u}}} \quad .$$

This form is in accord with Carson's (1973) integration of the non-advective equations. The quadratic spatial behaviour of z_i is supported by

the observations of Wiseman and Hirt (1975), Raynor et al. (1979) and Portelli (1979). Summer's (1965) thermodynamic model of an urban heat island (mixed layer) also has this quadratic behaviour, but is based on a stationary heat input to the mixed layer. The use of this form in the present context implies that the time scales at which the mixed layer adjusts to changes in heat input are smaller than the (diurnal) time scales at which the surface heat fluxes change. Replacing z_i (y) in equation (6.6) yields:

$$\Delta = \sqrt{\frac{2\gamma c^2 Qy}{(1 + 2c)\bar{u}}} .$$

Differentiating (6.4) by y (x) and replacing the above forms for z_i and Δ yields:

$$\frac{\partial\bar{\theta}}{\partial x} = \sqrt{\frac{\gamma Q}{2\bar{u}x}} \left[\sqrt{1 + 2c} - \frac{c}{\sqrt{1 + 2c}}\right]$$

while $$\frac{\partial z_i}{\partial x} = \sqrt{\frac{(1 + 2c)Q}{2\gamma\bar{u}x}} .$$

Using these forms for $\frac{\partial z_i}{\partial x}$ and $\frac{\partial\bar{\theta}}{\partial x}$, equations (6.5) and (6.6) can be used to yield Eulerian time derivative for z_i and $\bar{\theta}$. In addition, the Eulerian time derivative of Δ can be obtained from equation (6.3) to give a new set of equations which may be numerically solved to yield the temporal behaviour of z_i and $\bar{\theta}$ under the influence of both advection and subsidence.

6.3 Subsidence

6.3.1 Synoptic-Scale Subsidence

Commonly associated with the synoptic conditions encountered during this study (see Appendix C) is non-zero horizontal divergence in the momentum field. The equation of continuity has: $\nabla.(\rho\underset{\sim}{u}) = 0$

or, splitting the horizontal and vertical components

$$\rho \nabla_H \cdot \underset{\sim}{u} = - \frac{\partial}{\partial z} (\rho w)$$

where ∇_H is the horizontal divergence operator. Since the synoptic conditions were largely stationary we may, without much fear of oversimplification, assume the horizontal divergence to be constant over any given day, so

$$\frac{\partial}{\partial z} (\rho w) = - \rho \beta \tag{6.9}$$

where $\beta = \nabla_H(\underset{\sim}{u})$ is a constant (often erroneously called the subsidence parameter). A convenient formulation for the density of the atmosphere is (Schmidt, 1946):

$$\rho(z) = \theta(z) \frac{\rho_o}{\theta_o} e^{-bz} \tag{6.10}$$

where ρ_o and θ_o are the density and potential temperature at some reference level and $b = 10^{-4} m^{-1}$ is approximately constant. Using a two-layer thermal atmosphere, $\theta(z)$ becomes

$$\theta(z) = \theta_o \qquad 0 < z < z_i$$

$$\theta(z) = \theta_o + \gamma(z-z_i) \qquad z > z_i \tag{6.11}$$

Separating variables in equation (6.9), and substituting (6.10) and (6.11) leads to:

$$\beta\{\int_o^{z_i} \theta_o e^{-bz'} dz' + \int_{z_i}^{z} [\theta_o + \gamma(z' - z_i)] e^{-bz'} dz'\} =$$

$$\int_o^{w_i, z_i} d[w\theta_o e^{-bz'}] - \int_{w_i, z_i}^{w, z} d[w(\theta_o + \gamma(z' - z_i)) e^{-bz'}]$$

after integration, manipulation and substitution of αz for z_i the subsidence velocity is given by:

$$w = \frac{-\beta}{b(\theta_o + \gamma(1 - \alpha)z)} \left\{\theta_o(e^{bz} - 1) + \frac{\gamma}{b}\left[e^{bz(1 - \alpha)} - bz(1 - \alpha) - 1\right]\right\} \tag{6.12}$$

If we confine ourselves to lower layers of the atmosphere with moderately large z_i such that:

$$bz << 1$$

$$b(1 - \alpha)z << 1$$

equation (6.12) is well approximated by:

$$w = \frac{-\beta z\theta_o}{(\theta_o + \gamma(1 - \alpha)z)} \tag{6.13}$$

If, in addition,

$$\gamma(1 - \alpha)z << \theta_o$$

and

$$b\theta_o << \gamma(1 - \alpha)$$

the subsidence velocity is given by

$$w = -\beta z \tag{6.14}$$

This approximation will generally hold if α is not greater than 0.5. Equations (6.12) to (6.14) will be used to estimate the horizontal divergence from the subsidence of observed features on the upper portion of potential temperature profiles (Appendix K). The subsidence velocity at the inversion height is given from equation (6.13) as:

$$w_i = - \beta z_i$$

with the value for β calculated from (6.12) to (6.14) and can be substituted into equation (6.7) and used in the model.

In addition to imposing a vertical velocity at the entrainment interface, the subsidence produces a warming of the entire column of the atmosphere, and of direct importance in this context, results in a gradual increase of the temperature immediately above the entrainment zone (Davidson, 1980). This warming will affect changes in the magnitude of the temperature jump, and hence on the dynamics of the processes determining the depth and temperature of the mixed layer. Figure 6.4 shows (in idealized form) the manner in which this warming occurs. At a time, t, the "parcel" of air immediately above the inversion base (at a height of z_i') has a temperature $\theta(t)$. This "parcel" of air started its subsidence at a time t_o when it was at a height z_o. (Note that this initial height z_o, bears no relation to the surface roughness length usually given this symbol). The inversion must steepening since the subsidence velocity increases with height. In its simplest form,

$$w_s = \frac{dz}{dt} = - \beta z$$

integration leads to

$$z_o = z_i' \, e^{\beta(t - t_o)} \tag{6.15}$$

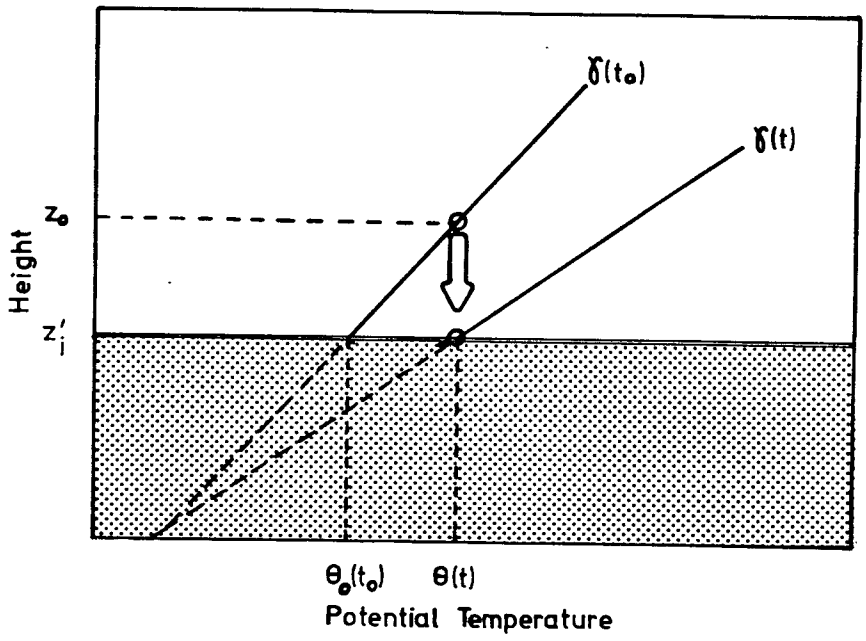

Figure 6.4: Subsidence Warming; for explanation see the text.

Now, $$\theta(t) = \gamma_o(z_o - z_i') + \theta_o$$

substituting (6.15) and differentiating leads to:

$$\frac{d\theta}{dt} = \beta\gamma_o z_i' e^{\beta(t - t_o)}$$

The value of γ_o will be chosen as the mean inversion intensity of the lowest 650 m of the atmosphere in the early morning temperature sounding. The figure of 650 m was chosen since this is the height z_o that would be a typical maximum for the conditions encountered in this study. ($z_i' = 500$ m, $t = 7h$, $\beta = 10^{-5}\ s^{-1}$). Adding this warming to the dynamics of the temperature "jump" changes equation (5.3) to

$$\frac{\partial\Delta}{\partial t} = \gamma\frac{\partial z_i}{\partial t} - \frac{\partial\bar{\theta}}{\partial t} + z_i\beta\gamma_o e^{\beta(t - t_o)} \qquad (6.16)$$

This is the complete equation for the dynamics of Δ and will be used in the model.

6.3.2 Meso-Scale Subsidence

The model as modified has no mechanism for producing the very rapid decrease in inversion height observed in the later part of most of the days studied. This rise and subsequent fall of the inversion has also been observed by Portelli (1979) at a lakeshore site. It is probably associated with the dynamics of a meso-scale sea-breeze circulation. While the detailed two-dimensional modelling of the sea-breeze circulation (e.g., Estoque, 1961 and 1962) would be the most proper way of approaching this problem, the intention in this study is to approximate the effects of such meso-scale circulations by providing order of magnitude estimates from the results of previous numerical and observational investigations.

Among the considerable literature on sea and land-breeze circulations Emslie (1968), Hoos and Packman (1974), Hay and Oke (1976) and Kalanda (1979) deal directly or indirectly with those phenomena in the Vancouver/Fraser Valley region. Guy (1979) uses wind-speed and direction profiles from 23 mini-sonde flights from this experiment (see Appendices B and I) to characterise the structure of the meso-scale circulations over the city. He finds very strong circulations on eleven of the fourteen days selected for investigation because of the absence of overriding synoptic flows. His calculations of the Biggs and Groves (1962) "Lake Breeze Index" show subcritical (i.e., conducive to thermally-induced meso-scale circulation) values on all days of the study, including the three days which showed an absence of sea-breeze circulation. The sea-breeze circulations occurring during this study had remarkably little effect on observations made within the surface layer, in particular the passage of the sea-breeze front was never evident in the wind-speed and direction, temperature and humidity measurements made on the tower (Guy, 1979). There are, however, slow trends in both wind-speed and -direction that indicate quite clearly the existence of these circulations. The typical sequence being light easterly to south easterly winds in the morning freshening by about 1.0 m s^{-1} by noon and gradually swinging through south to south south west by late afternoon.

As dramatically illustrated by the tetroon flight patterns of Lyons and Olsson (1973), sea breeze circulations have regions of uplift and subsidence at their landward and seaward extremities respectively of between 1 and 2 m s^{-1}. An examination of the two-dimensional flow fields presented by Estoque (1961 and 1962) reveals a slow landward migration of the subsidence zone as the sea-breeze front advances. The Estoque

(1961) flow field for 1700 h shows that the region of maximum horizontal vorticity has migrated inland to 16 km from the coastline. An analysis of the vertical velocities at 8 km inland (the approximate distance of the present study site from the coastline) shows a horizontal divergence of $5 \times 10^{-4} s^{-1}$, approximately an order of magnitude larger than that due to synoptic-scale processes (see Appendix J). This increase in subsidence at a given inland position will be gradual as the circulation matures and migrates inland. To accommodate this feature, in the model, the horizontal divergence was kept at its measured synoptic value until 1130 LST, when it was forced to increase exponentially in time so that it reached ten times its original value by 1900 h, viz

$$\beta(t) = \beta_s \qquad t < 1130$$

$$\beta(t) = \beta_s e^{0.35(t - 11.50)} \qquad t > 1130 \qquad (6.17)$$

This form was used wherever β appeared in the model.

Because of the approximate nature of the foregoing analysis, the modelling is expected to provide only order of magnitude estimates of the afternoon subsidence of the inversion. A major weakness of this approximation being that the time of onset of this effect will in general be dependent on the upwind fetch. Whereas the form used in the model has a time of onset appropriate to a fetch of 8 km, the actual fetch does vary from 6 to 12 km depending on wind direction.

7. Implementation of the Mixed Layer Model

7.1 Computational Scheme

Collecting the mixed layer model equations ((6.1), (6.2) and from (6.3)) and substituting the derived forms for $\frac{\partial z_i}{\partial x}$, $\frac{\partial \bar{\theta}}{\partial x}$, $w(z_i)$ and $W(z_i,t)$ produces the following system of first order non-linear differential equations:

$$\frac{\partial \bar{\theta}}{\partial t} = \frac{a_1}{z_i} - a_2 \tag{7.1}$$

$$\frac{\partial z_i}{\partial t} = \frac{a_3}{\Delta} - a_4 z_i - a_5 \tag{7.2}$$

$$\frac{\partial \Delta}{\partial t} = a_6 \frac{\partial z_i}{\partial t} - \frac{\partial \bar{\theta}}{\partial t} - a_7 z_i \tag{7.3}$$

where $a_1 = (1 + c)Q$

$$a_2 = \sqrt{\frac{Q\gamma\bar{u}}{2x}} \left[\sqrt{1 + 2c} - \frac{c}{\sqrt{1 + 2c}} \right]$$

$$a_3 = cQ$$

$$a_4 = \beta$$

$$a_5 = \sqrt{\frac{(1 + 2c)\overline{u}Q}{2\gamma x}}$$

$$a_6 = \gamma$$

$$a_7 = \beta\gamma_o e^{\beta(t - t_o)}$$

The coefficients a_1 to a_7 are all in general time-dependent and their values will be calculated from the measured meteorologic variables. All initial values were input as hourly averages, and the system of equations advanced in six minute steps through each hour. The surface sensible heat flux values being linearly interpolated for each six minute interval, and the horizontal divergence being set according to equation (6.17). The solution to the system of differential equations was provided by a library program in The University of British Columbia Computing Centre. This program (called DE) is based on a modified divided difference representation of the Adams predictor-corrector formulas and provides variable internal step length to control local error with special devices to control propagated round-off error (Shampine and Gordon, 1974). A listing of the FORTRAN IV code to perform the simulation for one day and plots of the variables is given in Appendix L. The running time for a 14 h simulation on an Amdahl 470 v/6 model II varied from 1.1 to 2.8s, depending on the "stiffness" of the equations.

An example of the input data needed to run the simulation for 14 h is provided in Appendix L. The first two lines contain sixteen hourly averaged surface sensible heat flux values (Wm^{-2})(see Appendix E). The first and last of these are the pre- and post-sunrise values which are

used in the interpolation. The next two lines contain fourteen values for the inversion strength (K m^{-1}) interpolated linearly from the temperature soundings (Appendix I). The next two lines contain fourteen hourly averaged mean wind speeds (m s^{-1}). The values used here were measured at level 4 of the tower (see Appendix B) and are taken to represent the mean wind in the mixed layer. Figure I.1 is a plot of the mean wind at level 4 and the mean wind in the mixed layer estimated from the wind speed profiles provided by the theodolite-tracked balloons. It shows that the tower measured wind is a good approximation for the mixed layer wind. The next two lines contain fourteen hourly averaged wind directions (in degrees from true north) also measured at level 4 of the tower. These directions are used to calculate the distance x in coefficients a_2 and a_5, equation (7.1) and (7.3). The calculation was made on the basis of an assumed elliptical plan of the urbanized part of Vancouver (see Figure A.1). The next line contains the initial inversion height, mixed layer temperature (K), synoptic horizontal divergence (s^{-1}), a data level, an optional model adjustment parameter which will be referred to in the next section, the time of onset of meso-scale subsidence as simulation step number, the exponential parameter for this subsidence (equation (6.17)), and the early morning inversion intensity (K m^{-1}) for calculating subsidence warming. The last line shown contains up to six pairs of time (decimal hours) and mean mixed layer temperature (K) for validation of the model. Not shown in these data is a sequence of digitized mixed layer depth and times for model validation. At initiation the temperature step was set to 0.1 K on all days.

7.2 Results of Mixed Layer Modelling

Complete data sets for mixed layer modelling were available on thirteen days during the study period. Figures 7.1 to 7.13 show the results in graphic form. The overall performance of the model varies from poor (July 23rd) to excellent (July 31st and August 8th). The height of the observed inversion base was digitized so as to include fluctuations with characteristic times slower than roughly 10 min, which is much faster than the characteristic times of the modelled inversion height. These high frequency fluctuations are presumably caused by a combination of thermal bombardment of the inversion base and breaking gravity waves at this interface, neither of which are explicitly modelled here. There are, however, cases in which the observed inversion height deviates markedly from the modelled one at time scales larger than the aforementioned ones but shorter than the apparent response time of the model (three to four hours). These intermediate frequency fluctuations are presumably of synoptic origin, and are not evident in the surface layer (where the input data are measured) because of the previously mentioned buffering nature of the mixed layer.

The magnitude of the potential temperature "jump" generated in the model is difficult to validate as it is a mean property of the profile and would require much more frequent soundings than available in this study. Its general behaviour is, however, quite conservative and displays a gentle rise from its initial value (0.1K) to a maximum of between 1.5 and 2.5 K some three to four hours after sunrise. It remains steady at this value usually for about four hours and then begins a slow decline.

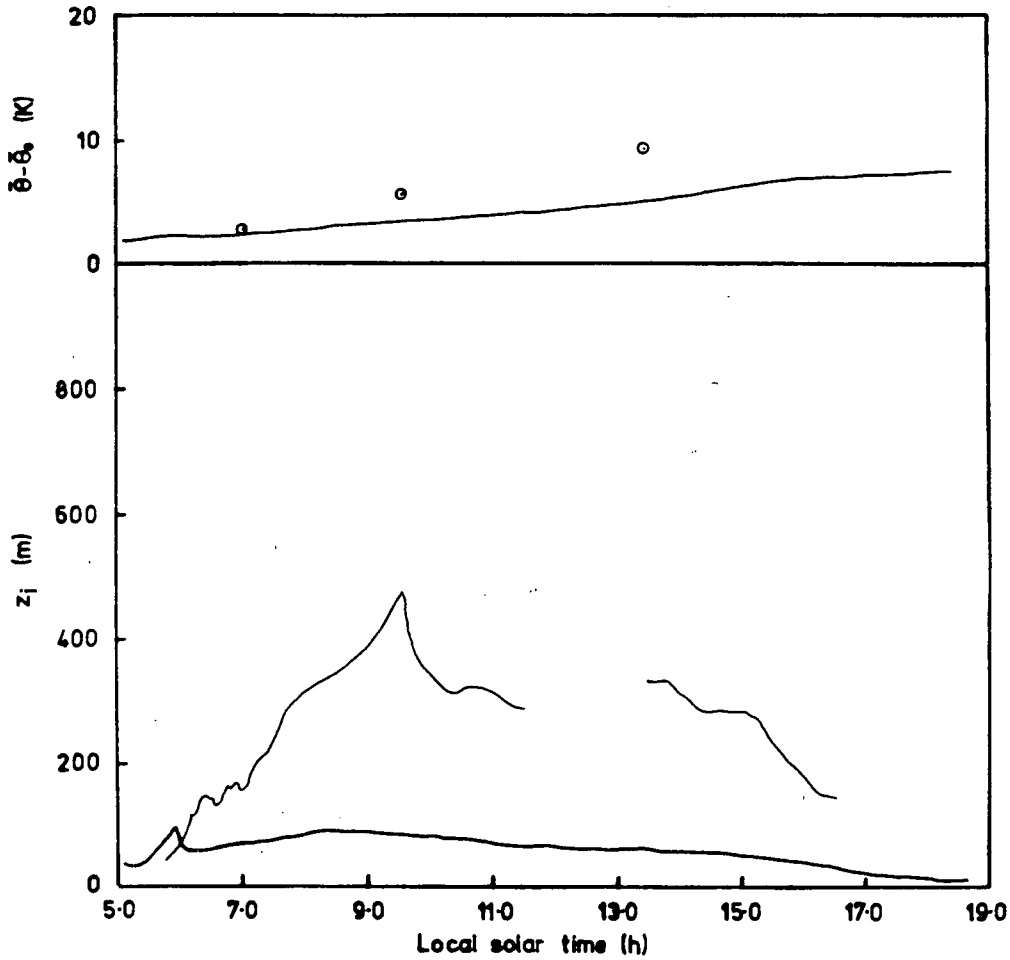

Figure 7.1: Inversion Rise Modelling for July 20th.

⊙ Observed mixed layer potential temperature.

△ Observed (Balloon Sonde) inversion height

($\bar{\theta}_o$ = 290.5K)

The heavy line is the modelled inversion height.

The light line is the inversion height from the acoustic sounder.

The overall behaviour of the model is very poor on this day which was characterized by only moderate surface heating (due to a thin cover of continuous cloud).

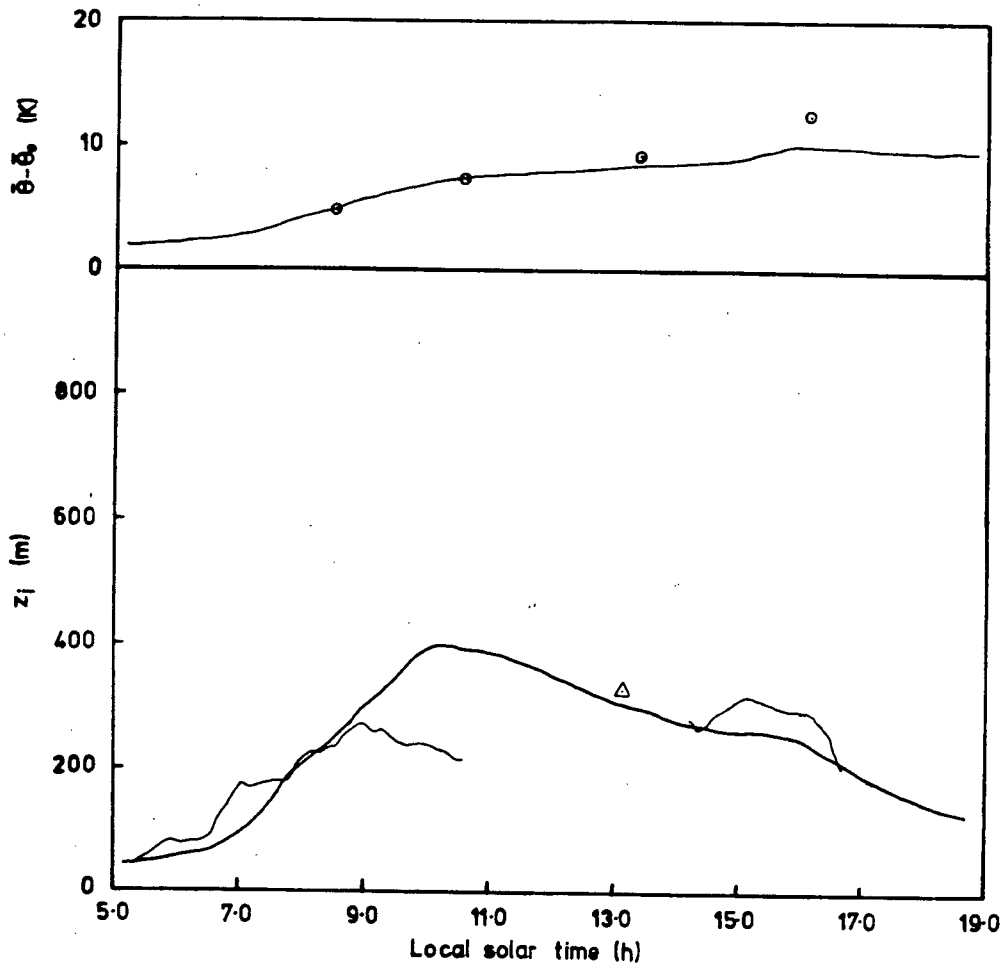

Figure 7.2: Inversion Rise Modelling for July 22nd.

Symbols as for Figure 7.1 ($\overline{\theta}_o$ = 292.5K)

The overall behaviour of the model is good with an underestimation of inversion height and temperature in the latter part of the day.

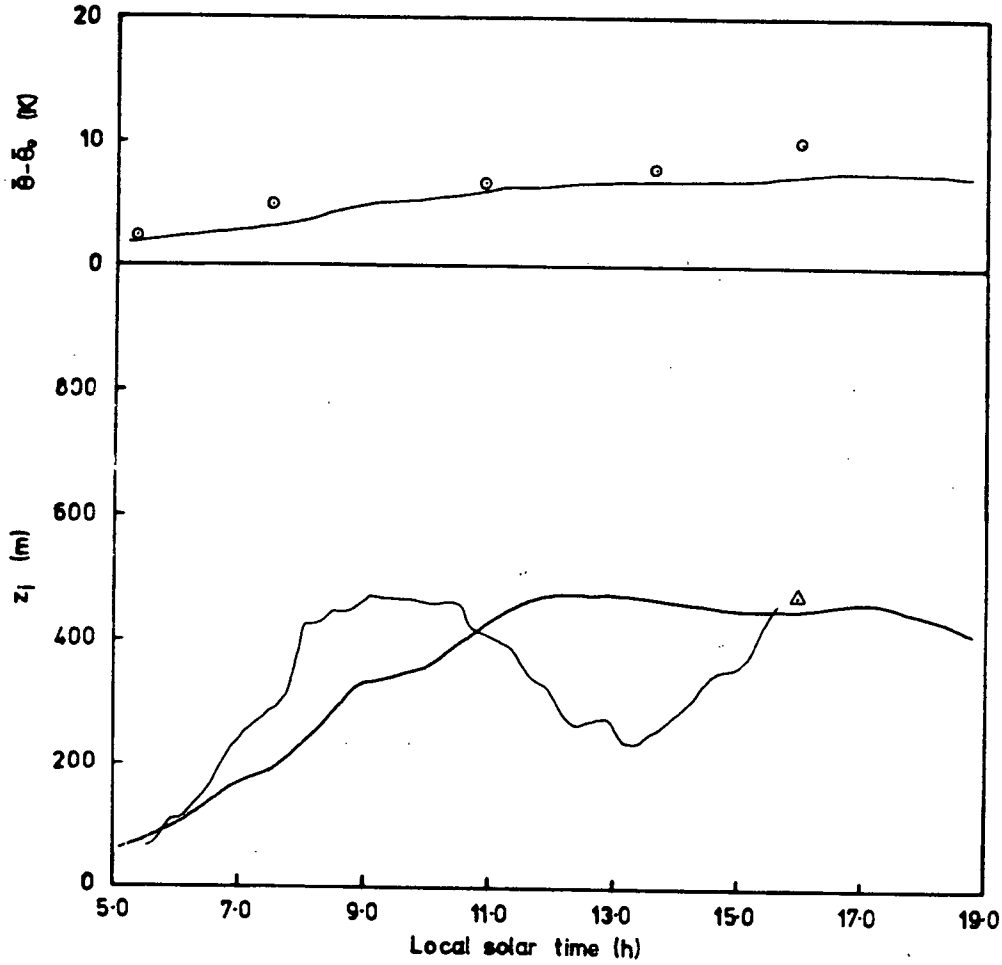

Figure 7.3: Inversion Rise Modelling for July 23rd.

Symbols as for Figure 7.1 ($\overline{\theta}_o$ = 289.7K)

The model appears unable to simulate much of the inversion height variation on this day, almost certainly due to the passage of an elevated frontal system (see Appendix C).

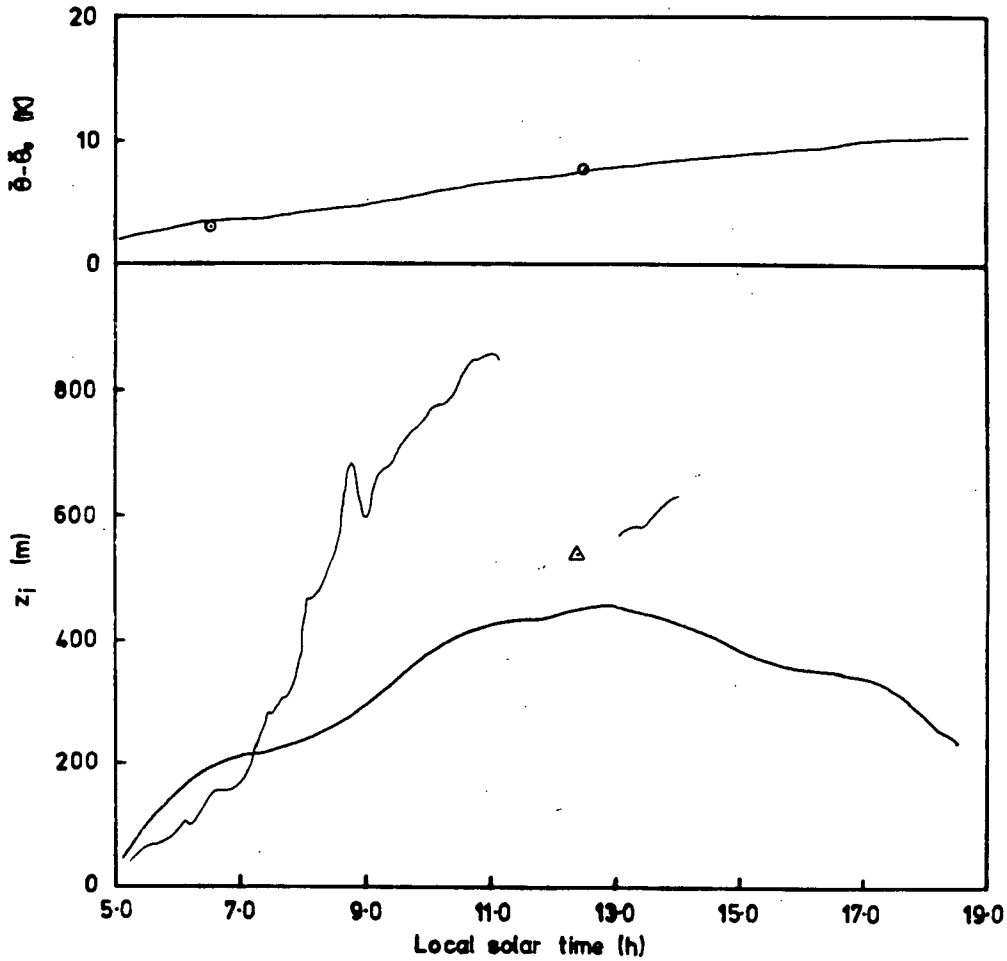

Figure 7.4: Inversion Rise Modelling for July 28th.

Symbols as for Figure 7.1 ($\overline{\theta}_o$ = 286.7K)

This day was marked by unsettled synoptic conditions, as a surface ridge developed. This non-stationarity is reflected in the relatively poor behaviour of the model. The development of this ridge led to a sequence of days with remarkably stationary weather, reflected in the next nine simulations.

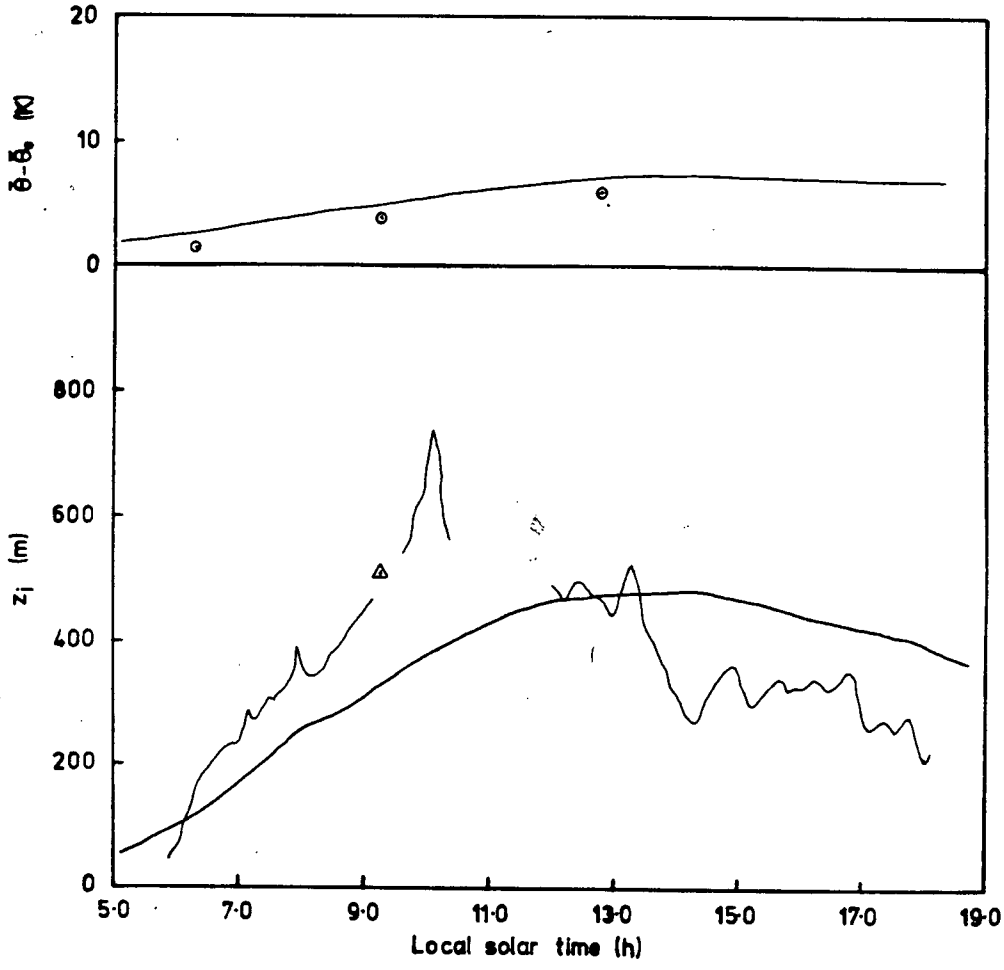

Figure 7.5: Inversion Rise Modelling for July 29th.

Symbols as for Figure 7.1 ($\overline{\theta}_o$ = 288.6K)

The model behaves fairly well in the first half of the day, following the mixed layer temperature well but consistently underestimating the inversion height. The model is unable to follow the sharp decrease in height observed in the latter half of this day.

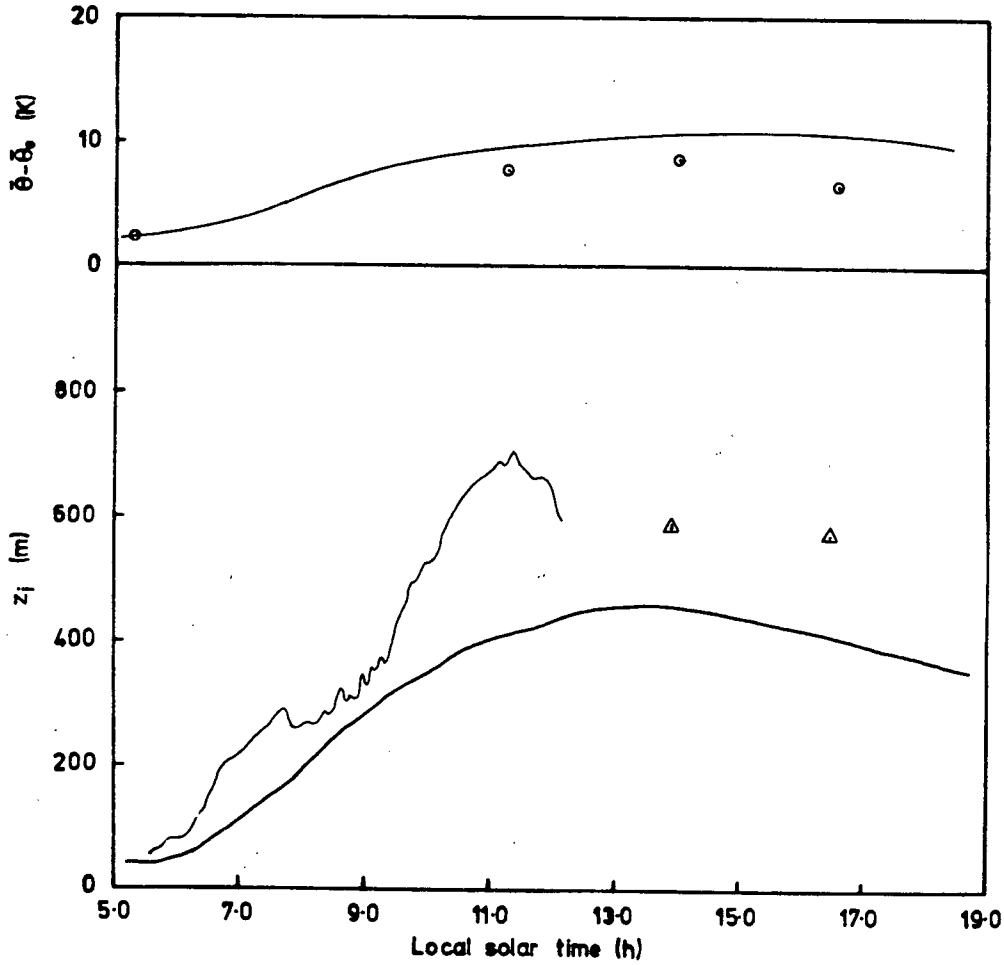

Figure 7.6: Inversion Rise Modelling for July 30th.

Symbols as for Figure 7.1 ($\overline{\theta}_o$ = 290.3K)

The simulation of both inversion height and temperature on this day is remarkably good, the sharp peak in mid-morning inversion height being an anomaly with no apparent synoptic origin.

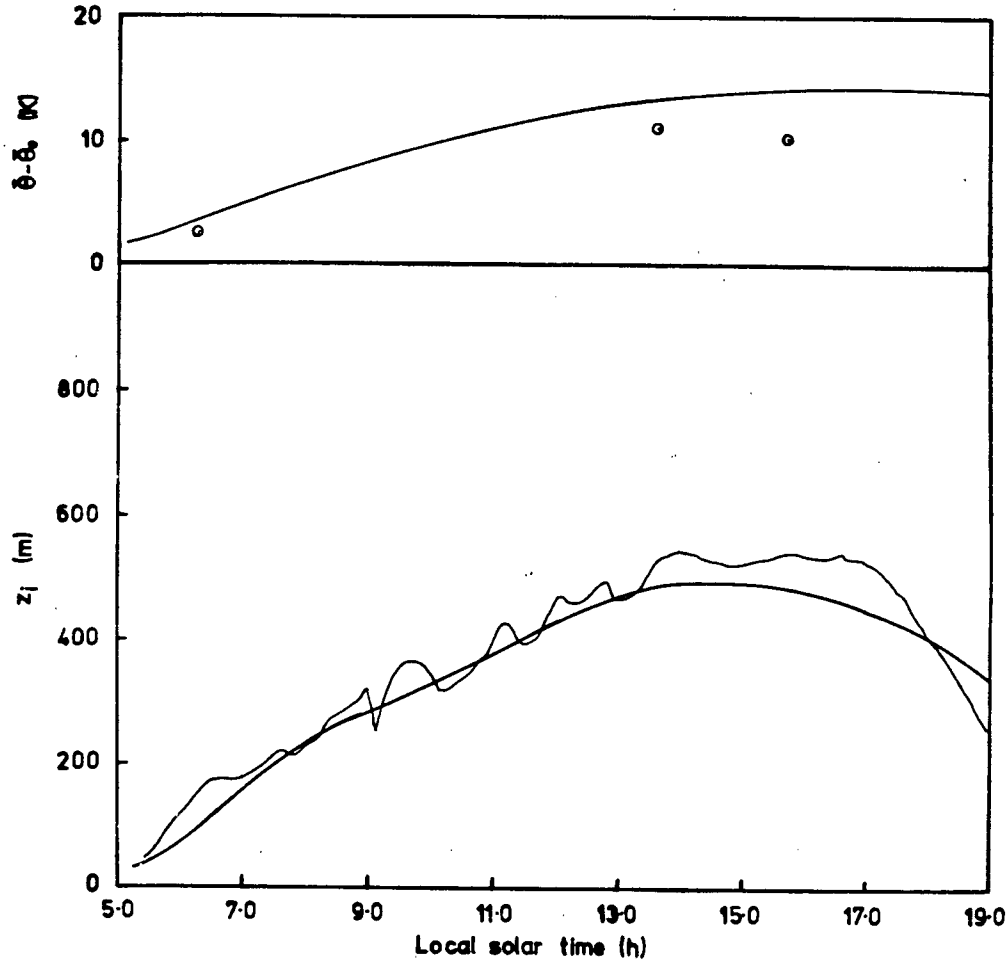

Figure 7.7: Inversion Rise Modelling for July 31st.

Symbols as for Figure 7.1 ($\overline{\theta}_o$ = 284.0K)

The model has near-perfect behaviour, the only disagreement being in the exact form of the inversion's descent in the late afternoon. As this phenomenon is treated by a rough approximation the disagreement is not fundamental.

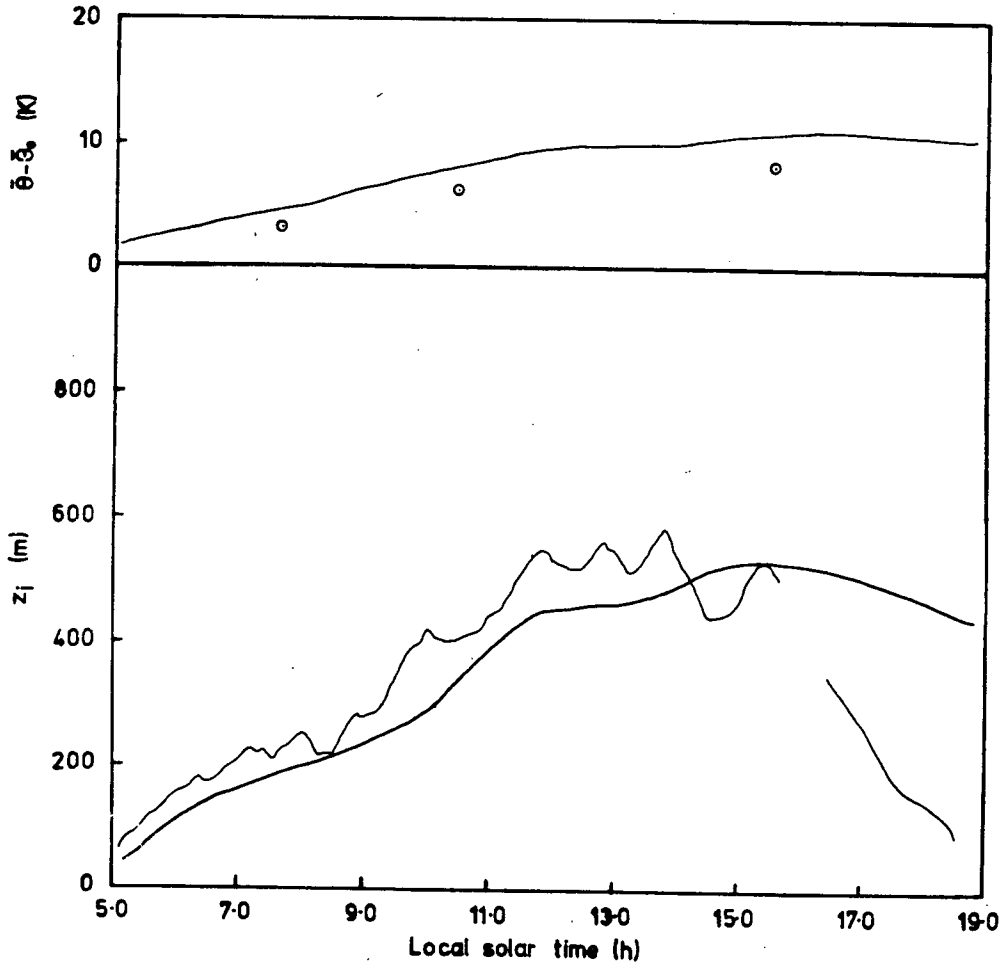

Figure 7.8: Inversion Rise Modelling for August 1st.

Symbols as for Figure 7.1 ($\overline{\theta}_o$ = 288.0K)

The remarks for July 31st apply to this simulation as well.

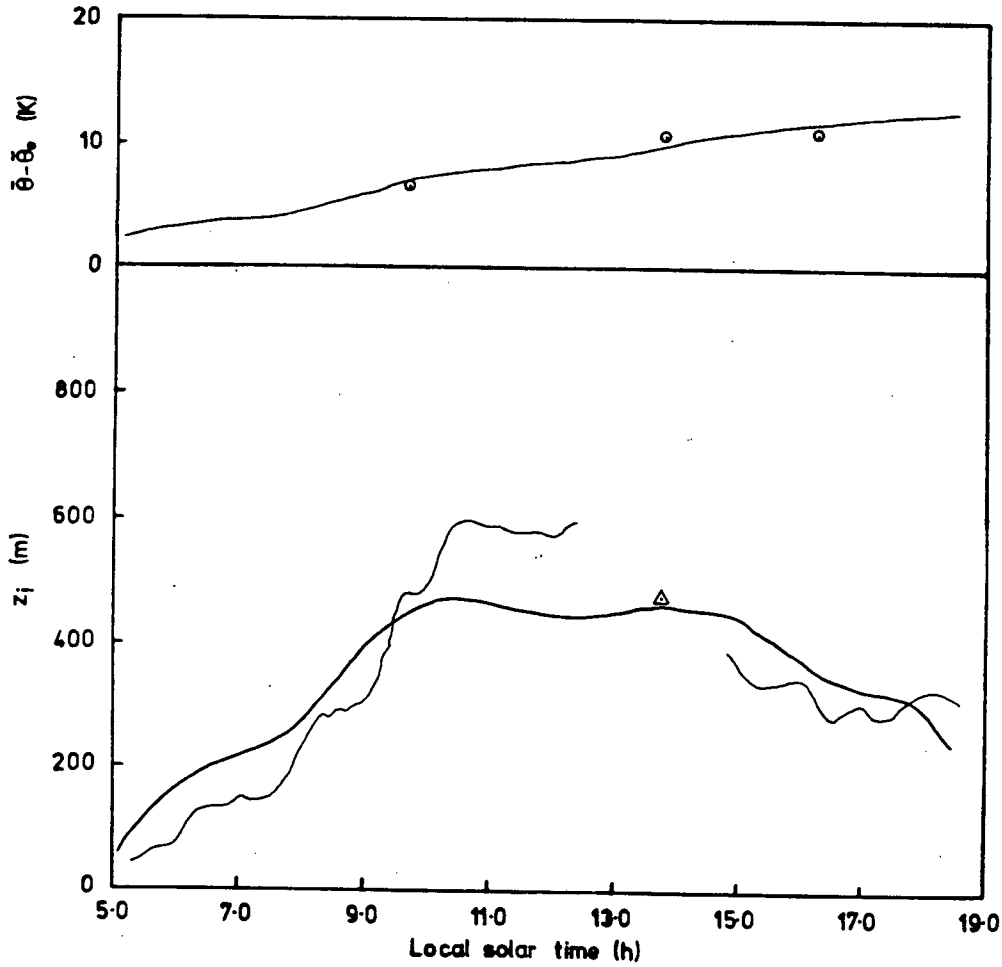

Figure 7.9: Inversion Rise Modelling for August 2nd.

Symbols as for Figure 7.1 ($\overline{\theta}_o$ = 286.7K)

In spite of the rather complex behaviour of the inversion height, the model tracks very well.

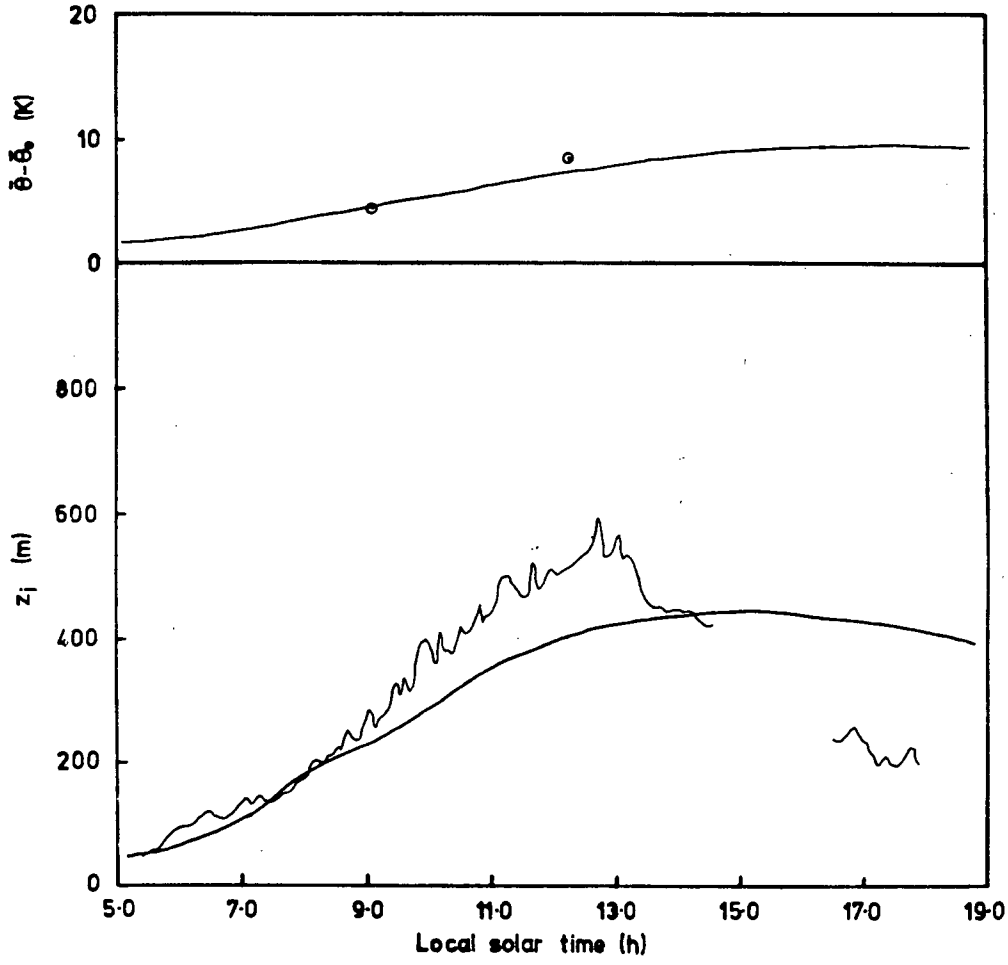

Figure 7.10: Inversion Rise Modelling for August 3rd.

Symbols as for Figure 7.1 ($\overline{\theta}_o$ = 290.0K)

As on the previous day, the inversion height is well modelled, but the calculated temperature drops off in the afternoon.

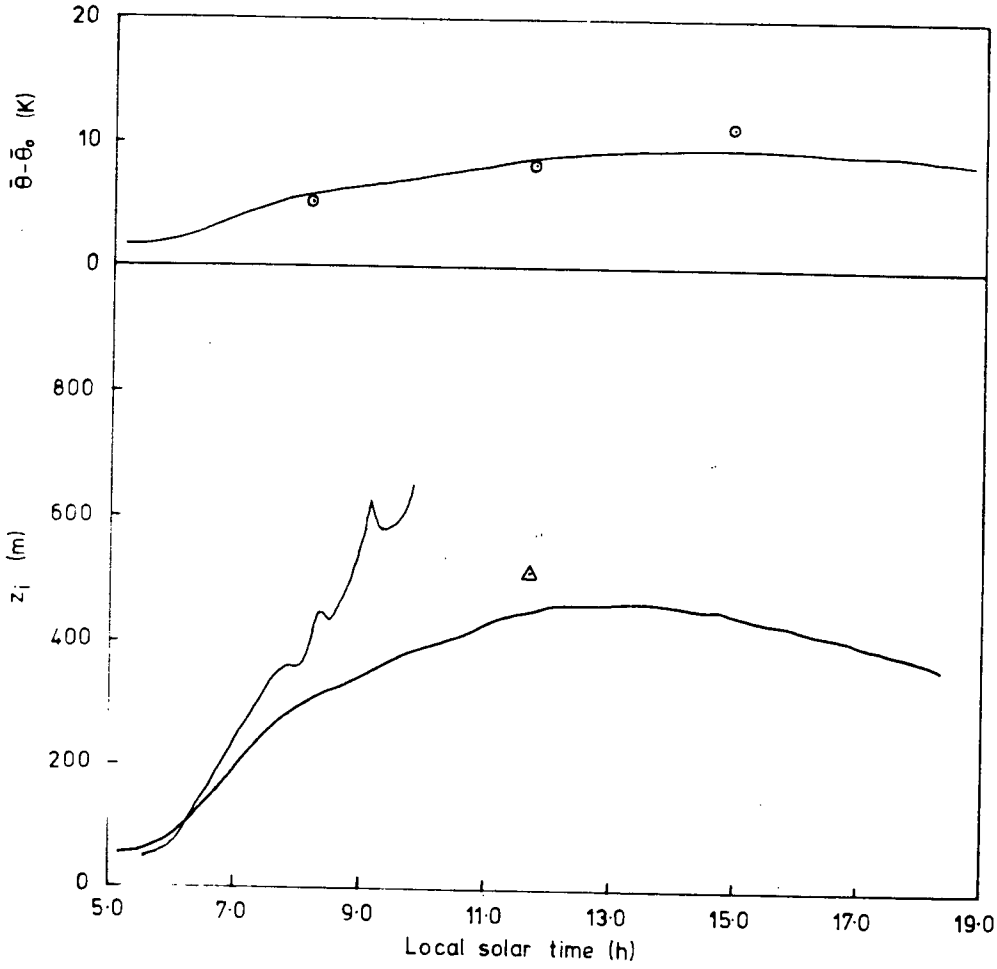

Figure 7.11: Inversion Rise Modelling for August 4th.

Symbols as for Figure 7.1 ($\overline{\theta}_o$ = 284.3K)

The acoustic sounder record for this day was difficult to interpret, but the rapid early morning rise that was evident is well followed by the model.

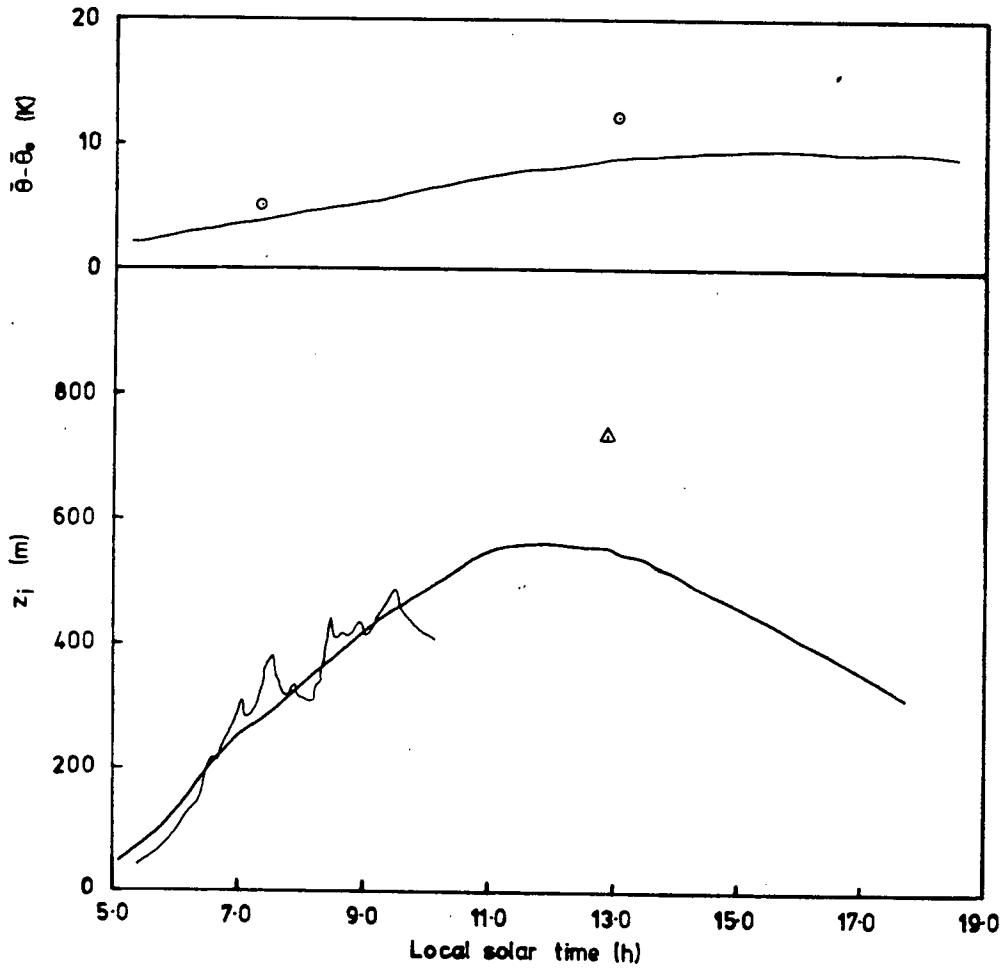

Figure 7.12: Inversion Rise Modelling for August 5th.

Symbols as for Figure 7.1 ($\overline{\theta}_o$ = 283.2K)

The model performs very well in the early morning when the height of the inversion is evident from the acoustic sounder trace.

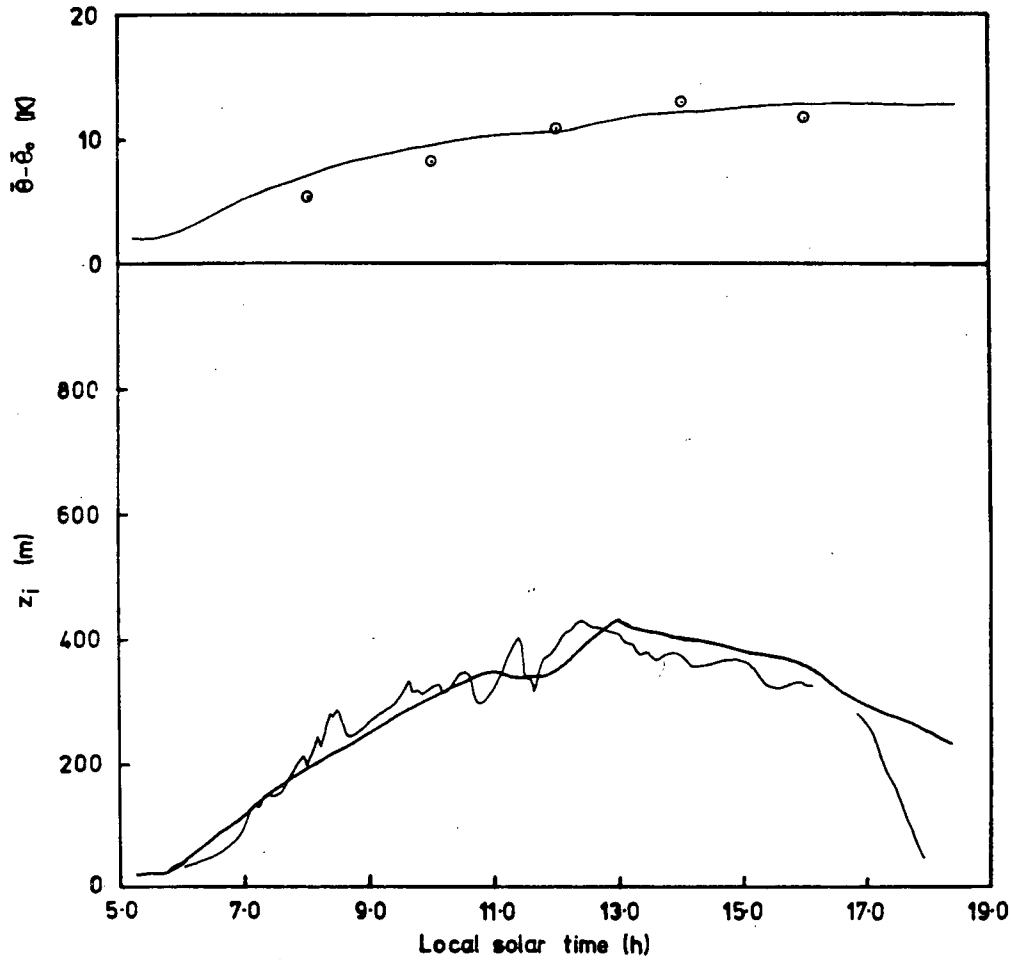

Figure 7.13: Inversion Rise Modelling for August 8th.

Symbols as for Figure 7.1 ($\overline{\theta}_o$ = 292.0K)

The model performs particularly well on this day, simulating both inversion height and mixed layer temperature accurately.

Since the input values of the inversion intensity are derived from the linearized segment of the potential temperature profile immediately above the mixed layer, they will be too large due to "contamination" by the thermal "jump". This problem is not easily resolved as the extent of the "jump" is never clear. The best solution seemed to be the use of the measured values of γ reduced by a variable multiplicative factor (the adjustment parameter mentioned previously). By trial and error it was found that a value of 0.70 for this parameter reduced the inversion intensity to a value which gave good agreement between observed and modelled inversion heights and mixed layer temperatures. This adjustment is used for all days modelled. The overall sensitivity of the model to a change of this magnitude can be extracted from Figure 7.17 which indicates an increase in maximum inversion height of some 120 m for a 30% reduction in γ from its mean value in this study (0.019 K m^{-1}).

A day-by-day discussion of the performance of the model follows. In most of the graphs the effect of the singularity in equations (7.1) and (7.3) is evidenced by sharply decreasing modelled temperatures in mid- to late afternoon.

7.3 Sensitivity Analysis

In order to examine the sensitivity of the model to the magnitude of the input variables, a synthetic data set was created based on mean values of the observed variables. The basic data set consisted of a sinusoidal surface sensible heat flux given by:

$$Q_H = Q_{H_{max}} \sin\left(\frac{\pi(t - 5)}{14}\right)$$

with $Q_{H_{max}} = 340$ W m^{-2}.

The inversion intensity (γ) was set constant at 0.015 K m^{-1}, the mean wind speed ($\overline{u}$) constant at 2.5 m s^{-1}, the wind direction constant at 180°, an initial inversion height (z_{i_0}) of 10 m and mixed layer temperature (θ_0) of 290 K with horizontal divergence (β) of 1.0 x 10^{-5} s^{-1} were used. This mean wind direction implies an upwind urban fetch of 8 km. The meso-scale subsidence was set to start at 1130 h and to provide a ten-fold increase in the horizontal divergence by 1900 h. With this data set, the model produces a smoothly increasing mixed layer depth rising to a maximum of 690 m by 1406 h (9.1 h after sunrise). The basic variables were then adjusted one at a time to investigate the behaviour of this maximum inversion height which invariably occurred at the same time. Figures 7.14 to 7.18 show the dependence of $z_{i_{max}}$ on $Q_{H_{max}}$, mean wind, inversion intensity, horizontal divergence and the entrainment parameter (c).

In all of these analyses, the initial rise rate of the inversion is between 113 and 190 m h^{-1} and decreases monotonically from sunrise to 1400 h when it reaches zero (the results shown on Figure 7.18 are an exception to this). The model can be seen to be sensitive to all the tested variables (which are in reality boundary conditions). The most sensitive being the inversion intensity which also exhibits the greatest non-linearity, the least sensitive variable being mean wind speed, the maximum inversion height being all but independent of winds greater than 4.0 m s^{-1}: the dependence of maximum inversion height on upwind fetch cannot be completely rationally investigated in this model as the present formulation is appropriate to a constant fetch of 8 km as described in Section 6.3.2. A rough indication of the model sensitivity to fetch is possible in the region of 8 km. This is indicated in Table 7.1 as a mean gradient of maximum inversion height with fetch, together with

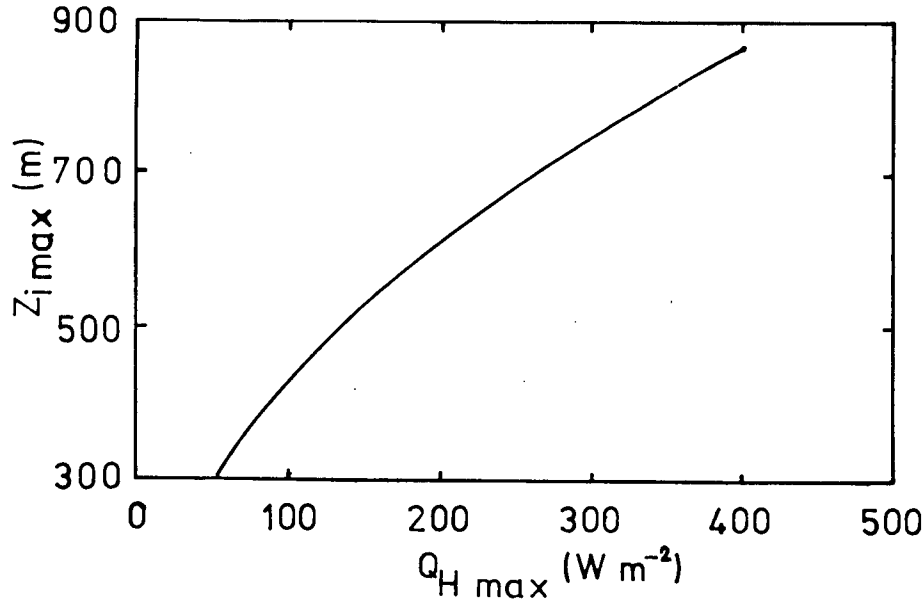

Figure 7.14: Maximum Inversion Height vs Maximum Surface Sensible Heat Flux.

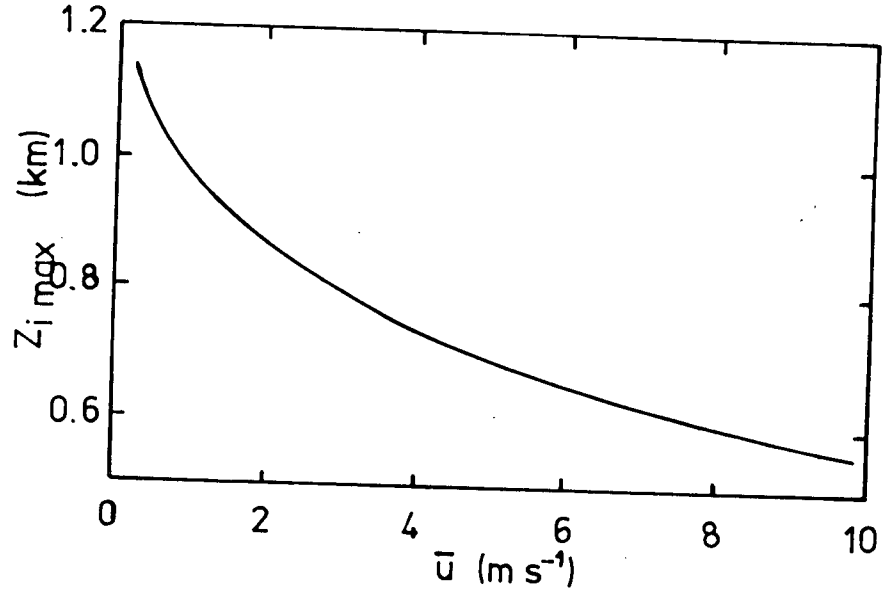

Figure 7.15: Maximum Inversion Height vs Mean Wind Speed in Mixed Layer.

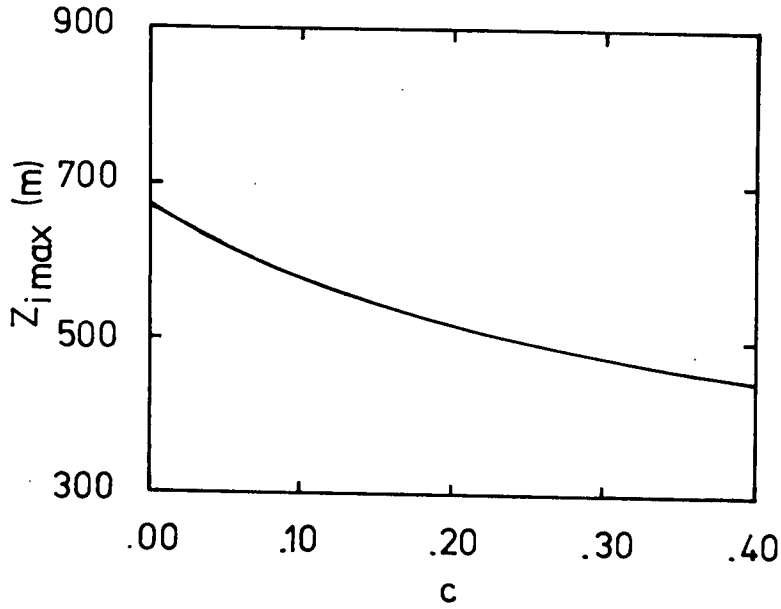

Figure 7.16: Maximum Inversion Height vs Entrainment Parameter.

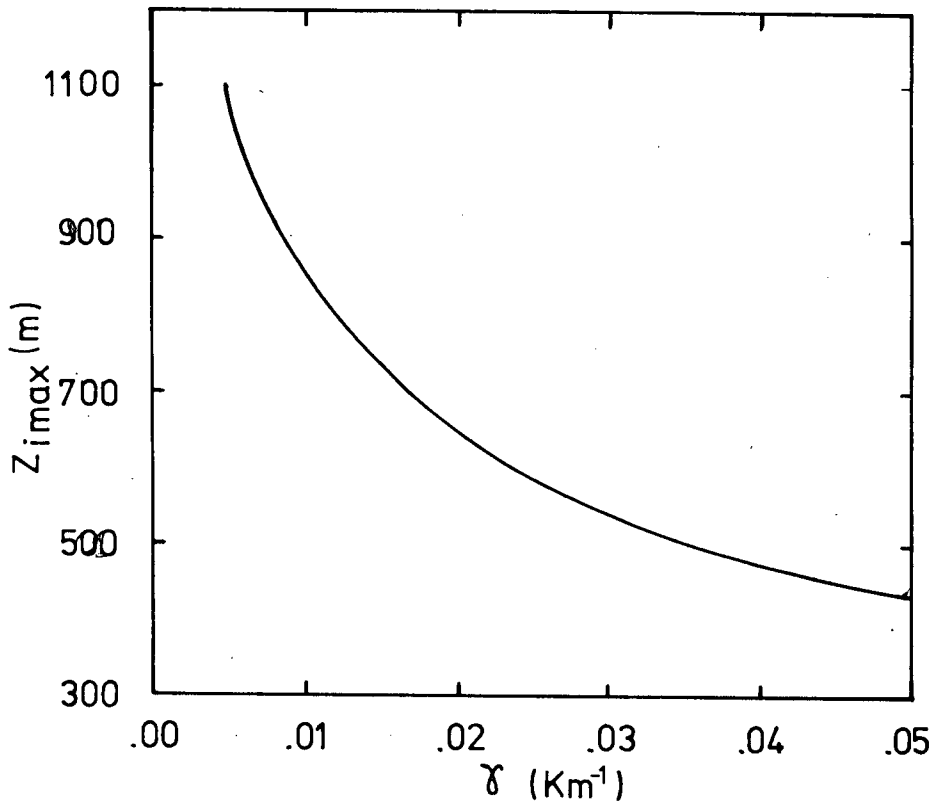

Figure 7.17: Maximum Inversion Height vs Inversion Intensity.

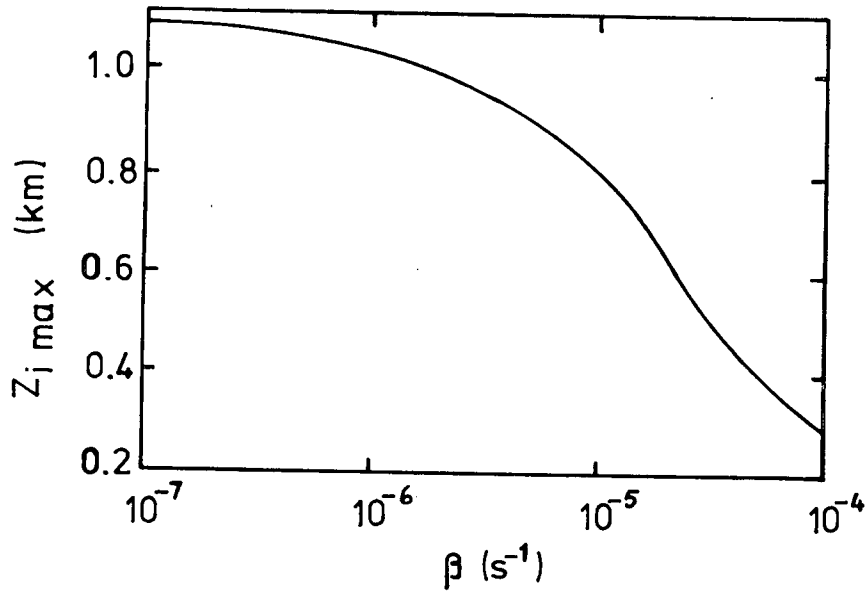

Figure 7.18: Maximum Inversion Height vs Horizontal Divergence.

the mean gradients for the other parameters investigated. The gradients are all determined at the basic values of the parameters.

Table 7.1: Mixed Layer Model Sensitivity

Parameter	Basic Value	Gradient
Q_H	340 W m^{-2}	1.13 m^3W^{-1}
$\overline{u}$	2.0 m s^{-1}	158 s
γ	0.010 K m^{-1}	2.82×10^4 m^2 K^{-1}
c	0.020	250 m
β	1.0×10^{-5} s^{-1}	9.3×10^3 m s
x	8.00 km	1.26×10^{-2}

8. Conclusion

This part of the study has shown that the accepted forms of inversion rise models (typified by that of Tennekes (1973)) can be successfully generalized to include the effects of advection and subsidence. The effects of advection have been modelled by including an advected heat flux term into the thermal budget equation for the mixed layer. The magnitude of this flux is determined from observed forms of the spatial structure of growing thermal internal boundary layers. The effects of subsidence have been taken into account in the model by allowing subsidence-induced warming of the atmosphere above the growing layer as well as imposing a subsidence velocity on the entrainment interface. This subsidence is driven by atmospheric divergence on both synoptic- and meso-scales. The magnitude of the synoptic-scale divergence has been estimated from observations of subsidence in potential temperature profiles, while the meso-scale effect has been approximated from modelled results of thermally induced meso-scale circulations. The inclusion of these processes in the model allow its application to areas in which meso-scale phenomena may have a considerable effect on the diurnal behaviour of the mixed layer depth (e.g., coastal regions).

The model has been applied to observations of mixed-layer depth and surface-layer variables made over a mid-latitude coastal city. These observations show the diurnal behaviour of the daytime mixed layer depth to be quite different from the behaviour expected over wide stretches of homogeneously featureless terrain. In general the maximum mixed layer observed in the present study was approximately half that observed over flat terrain, and showed a decline in mid- to late afternoon that is absent in the contrasted environment.

The results of the modelling are generally in reasonable agreement with the observed mixed layer depth and mean temperature. This success is an indication that the generalizations are necessary and at least partially sufficient to account for the mixed layer properties in this type of environment. It is probable that the model will be able to estimate quite reasonably the daytime inversion height from parameterized or climatologic input variables. As none of the model properties are explicitly urban or in any way related to the character of the underlying surface or surface-layer it should have general applicability in all aspects excepting the details of meso-scale subsidence which have been approximately treated.

The most obvious extensions of the model would be in the detailed modelling of meso-scale, thermally driven circulations so as to explicitly compute the imposed subsidence field. This sort of extension would need spatially-resolved mixing heights for proper validation. The entrainment processes at the inversion base are stochastic in nature and it is unlikely that the high frequency fluctuations of the inversion height will yield to simple modelling of this kind. A surprising feature of this part of the study was the apparent absence of any effect related to the passage of the sea-breeze front. This may be a regional characteristic due to the complexity of the coastline, and not generally true.

It must be emphasized that the model performs well in the restricted and very "simple" synoptic conditions encountered during this study but produces very poor results in the presence of synoptic scale non-stationarities, as shown by Figure 7.3 which depicts a day during which a very weak front passed over the study area.

9. Summary of Conclusions

The two major themes of this study (turbulent diffusion and mixed layer depth) have been developed using a body of data gathered over a coastally situated suburban surface under conditions approaching free convection.

In developing the first theme, the following conclusions have been drawn:

- The non-dimensional integral turbulence statistics σ_i/u_* over very rough surfaces (z_0 = 0.5 m) have adiabatic limits that agree with those measured over much smoother surfaces.
- The behaviour of these statistics with increasing instability is consistent with previous results but somewhat obscured by large scatter.
- The integral statistics are all related to the mixed layer variable $-z_i/L$ and show strong increasing trends with this variable.
- Turbulent velocity spectra can be successfully measured in these highly turbulent flows with an orthogonal array of helicoid propeller anemometers.
- The velocity spectra thus produced are remarkably consistent with unstable spectra measured over much smoother surfaces. In particular the horizontal components show the three spectral regions defined by Kaimal (1978).
- The statistical theory of diffusion may be used as a basis for a convenient form of dispersion function whose determination reduces to the integration of the appropriate energy spectrum, multiplied by an averaging function. The form presented here has an internal scaling time that is relatively easily available and can be related to the more proper Lagrangian integral time scale.

- The dispersion function thus derived is in good agreement with previous estimates made from measurements of tracer spread and from turbulence measurements. The crosswind and vertical dispersion functions are presented as empirical forms which may be used to perform diffusion calculations if the conditions of diffusion are consistent with the assumptions underlying the statistical theory of diffusion.

In developing the second theme, the following conclusions have been drawn:

- In situations such as the one presently being studied, the behaviour of the daytime mixed layer depth may be quite different from that observed over homogeneous terrain. In particular, the mixed layer depths are notably lower than expected and show downward trends in mid- to late-afternoon.
- The behaviour of the mixed layer depth may be successfully modelled by including the effects of advection and subsidence (at both synoptic- and meso-scales) in currently available mathematical models.
- Under non-stationary synoptic conditions the model results can be only poor reflections of the actual mixed layer depth.
- The generalized model is sensitive to all input variables, the sensitivity being roughly 100 m for the expected range of values of surface sensible heat flux, mean wind, inversion strength and subsidence parameter.

In addition to these conclusions, during the course of the data analysis the following techniques have been utilized.

- The closure of an open energy budget was achieved by distributing the budget residual among the turbulent flux terms, thus providing a more certain estimate of the fluxes.
- The horizontal divergence parameter was determined by applying a simple model of a compressible atmosphere to observed rates of subsidence of thermal features from temperature soundings. The form of the subsidence velocity is a simple function of height which, under successive approximations, can be shown to reduce to the incompressible form.

LIST OF SYMBOLS

Symbols are defined on first introduction in the text, and for ease of reference are summarized here. In a few cases the symbolism is not unique; this is indicated by a multiple definition in the list below, and will be obvious from the context within the text. Subscripting is used for axis (x,y,z), velocity component (u,v,w), level (s,i for surface and inversion base respectively) and frame of reference (L,E for Lagrangian and Eulerian respectively). An overbar represents a mean value and primes represent departures from a mean.

Symbol	Meaning	S.I. Unit
a	Constant in mixed layer scaling	(-)
a_1	Coefficient in mixed layer model	$(K\ m\ s^{-1})$
a_2	Coefficient in mixed layer model	$(K\ s)$
a_3	Coefficient in mixed layer model	$(K\ m\ s^{-1})$
a_4	Coefficient in mixed layer model	(s^{-1})
a_5	Coefficient in mixed layer model	$(m\ s^{-1})$
a_6	Coefficient in mixed layer model	$(K\ m^{-1})$
a_7	Coefficient in mixed layer model	$(K\ m^{-1}\ s^{-1})$
b	i) Constant in mixed layer scaling	(-)
	ii) Constant in approximate formulation for height dependence of atmospheric density and temperature	(m^{-1})
c	Entrainment closure parameter	(-)

d	Displacement height	(m)
f	Non-dimensional frequency	(-)
h^*	Height of roughness elements	(m)
i	Longitudinal turbulent intensity	(-)
k	von Karman's constant	(- _
L	Monin-Obukhov stability length	(m)
n	Frequency	(s^{-1})
Q	Kinematic eddy heat flux	(K m s^{-1})
Q_E	Turbulent latent heat flux	(W m^{-2})
Q_H	Turbulent sensible heat flux	(W m^{-2})
Q^*	Net all-wave radiation	(W m^{-2})
r	i) Error ratio	(-)
	ii) Ratio of Lagrangian to Eulerian time scales	(-)
R	Velocity autocorrelation function	(-)
S	Non-dimensional dispersion function	(-)
s	Silhouette area of roughness elements	(m^2)
t	Time	(s)
t_E	Eulerian integral time scale	(s)
t_i	Empirical scaling time for dispersion function	(s)
t_L	Lagrangian integral time scale	(s)
t_s	Surface layer scaling time for dispersion function	(s)
t_u	Scaling time for vertical diffusion in unstable conditions	(s)
t^*	Non-dimensional diffusion time	(-)

u	Longitudinal component of wind velocity	$(m\ s^{-1})$
$\overline{u}$	Mean wind speed	$(m\ s^{-1})$
u_*	Surface layer friction velocity	$(m\ s^{-1})$
v	Cross-stream component of wind velocity	$(m\ s^{-1})$
W	Warming due to subsidence	$(K\ s^{-1})$
w	Vertical component of wind velocity	$(m\ s^{-1})$
w_s	Subsidence velocity	$(m\ s^{-1})$
w_*	Convective velocity scale	$(m\ s^{-1})$
$\overline{w'\theta'}$	Kinematic heat flux (subscripted s for surface layer, i for inversion base)	$(K\ m\ s^{-1})$
x	Upwind distance or fetch	(m)
y	Dummy distance variable	(m)
z	Height	(m)
z_i	Inversion height	(m)
z_o	Surface roughness length	(m)
α	Scale height	(-)
β	i) Constant in Hay-Pasquill form of Lagrangian-Eulerian transform	(-)
	ii) Bowen's ratio	(-)
γ	Inversion intensity (lapse rate), subscripted o for some initial state	$(K\ m^{-1})$
δ	Depth of adjusted layer	(m)
Δ	Potential temperature "step" at inversion base	(K)
ΔQ_s	Heat storage in urban canopy layer	$(W\ m^{-2})$
ε	Residual in energy budget closure	$(W\ m^{-2})$

ϕ	Non-dimensional wind velocity variance	(-)
$\Phi_{u,L}$	Non-dimensional turbulent energy density spectrum (subscripted for component (u, v or w) and frame of reference (Lagrangian or Eulerian))	(-)
λ	Wavelength	(m)
ρ	Density (of air) subscripted 0 for a reference state	(k g m^{-3})
σ_y, σ_z	Crosswind and vertical RMS plume dimensions respectively	(m)
σ_u, σ_v, σ_w	Alongwind crosswind and vertical standard deviations of wind velocity respectively	(m s^{-1})
θ	Potential temperature	(K)
$\overline{\theta}$	Mean potential temperature of mixed layer	(K)
θ_o	Potential temperature of some reference state	(K)
τ	Reduced time	(s)
τ	Lag in auto correlation function	(s)
ζ	Monin-Obukhov stability parameter (z/L)	(-)
ζ_i	Mixed layer stability parameter (z_i/L)	(-)

REFERENCES

Angell, J.K., 1964: Measurement of Lagrangian and Eulerian Properties of Turbulence at a Height of 2300 ft. Quart. J. Roy. Meteorol. Soc. 90, 57-71.

Ariel, N.Z. and E.K. Buttener, 1966: Relation Between the Lagrange Correlation and the Maxima of the Euler Space-Time Correlation Function for the Atmospheric Layer near the Earth Surface. Izv. Atmos. Ocean. Phys., 2, 993-996.

Bailey, W.G., 1977: Atmospheric and Surface Control on Evapotranspiration During Soybean Maturation. Ph.D. Thesis, McMaster University, Hamilton, Ontario, 162 pp.

Ball, F.K., 1960: Control of Inversion Height by Surface Heating. Quart. J. Roy. Meteorol. Soc., 86, 482-494.

Barnum, D.C. and B.V. Rao, 1975: Role of Advection and Penetrative Convection in Affecting the Mixing-Height variations over an Idealized Metropolitan area. Boundary-Layer Meteorol., 8, 497-514.

Benkley, C.W. and L.L. Schulman, 1979: Estimating Hourly Mixing Depths from Historical Meteorological Data. J. Appl. Meteorol., 18, 772-780.

Bennett, R., 1975: Acoustic Radar Studies of Planetary Boundary Layer Structures Associated with Gravity Waves, Fronts and Lake Breezes. Ph.D. thesis, University of Toronto, Toronto, Ontario.

Beran, D.W. and F.F. Hall Jr., 1974: Remote Sensing for Air Pollution Meteorology. Bull. Am. Meteorol. Soc., 55, 1097-1105.

Betts, A.K., 1973: Non-Precipitating Convection and its Parameterization. Quart. J. Roy. Meteorol. Soc., 99, 178-196.

Biggs, W.G. and M.E. Groves, 1962: A Lake Breeze Index. J. Appl. Meteorol., 1, 474-480.

Binkowski, F.S., 1979: A Simple Semi-Empirical Theory for Turbulence in the Atmospheric Surface Layer. Atm. Env., 13, 247-253.

Black, T.A. and K.G. McNaughton, 1971: Psychrometric Apparatus for Bowen Ratio Determination over Forests. Boundary-Layer Meteorol., 2. 246-254.

Bowne, N.E. and J.T. Ball, 1970: Observational Comparison of Rural and Urban Boundary Layer Turbulence. J. Appl. Meteorol., 9, 862-873.

Briggs, G.A., 1973: Diffusion Estimation for Small Emissions. In Environmental Res. Lab., Air Resources Atmos. Turb. and Diffusion Lab., 1973 Annual Rep., ATDL - 106, USDOC - NOAA.

Brook, R.R., 1974: A Study of Wind Structure in an Urban Environment. Ph.D. Thesis, University of Melbourne, Melbourne, 232 pp.

Brost, R.A. and J.C. Wyngaard, 1978: A Model Study of the Stably Stratified Planetary Boundary Layer. J. Atm. Sci., 35, 1427-1440.

Busch, N.E., 1973: The Surface Boundary Layer. Boundary-Layer Meteorol., 4, 213-240.

Carson, D.J., 1973: The Development of a Dry Inversion-Capped Convectively Unstable Boundary Layer. Quart. J. Roy. Meteorol. Soc., 99, 450-467.

Carson, D.J. and F.B. Smith, 1973: The Leipzig Wind Profile and the Boundary Layer Wind-Stress Relationship. Quart. J. Roy. Meteorol. Soc., 99, 171-177.

Carson, D.J. and F.B. Smith, 1974: A Thermodynamic Model for the Development of a Convectively Unstable Boundary-Layer. Adv. in Geophys., 18A, 111-124.

Caughey, S.J. and S.G. Palmer, 1979: Some Aspects of Turbulence Structure Through the Depth of the Convective Boundary-Layer. Quart. J. Roy. Meteorol. Soc., 105, 811-827.

Christiansen, O., 1971: Wind Velocity Sensing by means of Four-bladed Helicoid Propellers. Univ. of Mich., Dept. of Meteorology and Oceanography report, 100 pp.

Clarke, J.F., J.K.S. Ching, F.S. Binkowski and J.M. Godowitch, 1978: Turbulent Structure of the Urban Surface Boundary Layer. Presented at the NATO/CCMS Ninth International Technical Meeting on Air Pollution Modelling and its Application, Aug. 28-31, 1978, Toronto, Ontario, Canada.

Coppin, P.A. 1979: Turbulent Fluxes Over a Uniform Urban Surface. Ph.D. Thesis, The Flinders University of South Australia, Flinders, 196 pp.

Corrsin, S., 1959: Progress Report on some Turbulent Diffusion Research, Atmospheric Diffusion and Air Pollution. Adv. Geophys., 6, 161.

Corrsin, S., 1963: Estimation of the Relation between Eulerian and Lagrangian Scales in Large Reynolds Number Turbulence. J. Atmos. Sci., 20, 115-119.

Coulter, R.L., 1979: A Comparison of Three methods for Measuring Mixing-Layer Height. J. Appl. Meteorol., 18, 1495-1499.

Counihan, J., 1971: Wind Tunnel Determination of the Roughness Length as a Function of the Fetch and Density of Three-Dimensional Roughness Elements. Atmos. Environ., 5, 637-642.

Counihan, J., 1975: Adiabatic Atmospheric Boundary Layers. A Review and Analysis of Data from the Period 1880-1972. Atm. Env., 9, 871-905.

Davenport, A.G., 1967. Instrumentation and Measurement of Wind Speed Spectra in a City. Proceedings of the First Canadian Conference on Micrometeorology. Toronto, Canada, Dept. of Transport, Meteorological Branch, part II, 361-368.

Davidson, K.L., G.E. Schacher, C.W. Fairall and T.M. Houlihan, 1980: Observations of Atmospheric Mixed-Layer Changes off the California Coast. Second Conference on Coastal Meteorology (Preprints), January 1980, 63-70, Los Angeles, California.

Deardorff, J.W., 1972: Parameterization of the Planetary Boundary Layer for use in General Circulation Models. Mon. Wea. Rev., 100, 93-106.

Deardorff, J.W., G.E. Willis and D.K. Lilley, 1969: Laboratory Investigation of Non-steady Penetrative Convection. J. Fluid. Mech., 35, 7-31.

Deardorff, J.W. and G.E. Willis, 1975: A Parameterization of Diffusion into the Mixed Layer. J. Appl. Meteorol., 14, 1451-1458.

Deland, R.J., 1978: A Study of Atmospheric Turbulence over a City. New York University, Geophysical Sciences Laboratory Report TR-68-14.

Draxler, R.R., 1976: Determination of Atmospheric Diffusion Parameters. Atmos. Env., 10, 99-105.

Drinkrow, R., 1972: A Solution to the Paired Gill-Anemometer Response Function. J. Appl. Meteorol., 11, 76-80.

Duchêne-Marullaz, P., 1975: Turbulence atmosphérique au voisonage d'une ville. Report EN. CLI 75-2, Centre Scientif. Tech. Batiment, Nantes.

Dyer, A.J. and B.C. Hicks. 1972: The Spatial Variability of Eddy Fluxes in the Constant Flux Layer. Q.J. Roy. Meteorol. Soc., 98, 206-212.

Emslie, J.H., 1968: Wind Flow in Burrard Inlet, Vancouver, B.C. A Summary of Six Years of Data. TEC 686, 14 pp.

Estoque, M.A., 1961: A Theoretical Investigation of the Sea Breeze. Quart. J. Roy. Meteorol. Soc., 87, 136-146.

Estoque, M.A., 1962: The Sea Breeze as a Function of the Prevailing Synoptic Situation. J. Atm. Sci., 19, 244-250.

Fichtl, G.H. and G.E. McVehil, 1969: Longitudinal and Lateral Spectra of Turbulence in the Atmospheric Boundary-Layer. A.G.A.R.D., cp. 48.

Fichtl, G.H. and P. Kumar, 1974: The Response of a Propeller Anemometer to Turbulent Flow with the Mean Wind Vector Perpendicular to the Axis of Rotation. Boundary-Layer Meteorol., 6, 363-379.

Fuchs, M. and C.B. Tanner, 1970: Error Analysis of Bowen Ratio Measured by Differential Psychrometry. Agr. Meteorol., 7, 329-334.

Gifford, F.A., 1975: Atmospheric Dispersion Models for Environmental Applications. In Lectures on Air Pollution and Environmental Impact Analyses, ed. D.A. Haugen, Amer. Meteorol. Soc., Boston, Mass.

Gill, G.C., 1975: Development and Use of the Gill UVW Anemometer. Third Symposium on Meteorological Instruments and Observations (Preprints) February 1975, 65-72, Boston, Mass.

Golder, D., 1972: Relations among Stability Parameters in the Surface Layer. Boundary-Layer Meteorol., 3, 47-58.

Guy, B., 1979: Land and Sea Breeze Circulations in the Vancouver/Fraser Valley Area. Unpublished Graduating Thesis, Dept. of Geography, U.B.C., Vancouver, B.C., 80 pp.

Haering, P., 1978: Failure of Computer Products to Handle Convective Precipitation. Pacific Region Technical Notes, No. 78-028, Environment Canada.

Hanna, S.R., G.A. Briggs, J. Deardorff, B.A. Eagen, F.A. Gifford and F. Pasquill, 1977: A.M.S. Workshop on Stability Classification Schemes and Sigma-curves Summary of Recommendations, Bull. Amer.

Meteorol. Soc., 58, 1305-1309.

Haugen, D.A., 1966: Some Lagrangian Properties of Turbulence Deduced from Atmospheric Diffusion Experiments. J. Appl. Meteorol., 5, 646-652.

Hay, J.E. and T.R. Oke, 1976: The Climate of Vancouver, Tantalus Research Ltd., Vancouver, B.C., 48 pp.

Hay, J.S. and F. Pasquill, 1959: Diffusion from a Continuous Source in Relation to the Spectrum and Scale of Turbulence. Atmospheric Diffusion and Air Pollution, ed. F.N. Frenkiel and P.A. Sheppard, Advances in Geophysics, Acad. Press., 6, 345.

Heidt, F.D., 1977: The Growth of the Mixed Layer in a Stratified Fluid Due to Penetrative Convection. Boundary-Layer Meteorol., 12, 439-461.

Hicks, B.B., 1972: Propeller Anemometers as Sensors of Atmospheric Turbulence. Boundary-Layer Meteorol., 3, 214-228.

Holzworth, G.C., 1967: Mixing Depths, Wind Speeds and Air Pollution Potential from Selected Locations in the United States. J. Appl. Meteorol., 6, 1039-1044.

Hoos, L.M. and G.A. Packman, 1974: The Fraser River Estuary, Status of Environmental Knowledge to 1974. Environment Canada, Special Estuary Series, no. 1, 518 pp.

Horst, T.W., 1972: A Computer Algorithm for Correcting Non-cosine Response in the Gill Anemometer. Pacific Northwest Laboratory Annual Report for 1977 to the US AEC Division of Biology and Medicine, Vol. II: Physical Sciences Part 1: Atmospheric Sciences, BNWL-1651-1. Batelle, Richland, Washington.

Horst, T.W., 1973: Corrections for Response errors in a Three-Component Propeller Anemometer. J. Appl. Meteorol., 12, 716-725.

Hunt, J.C.R. and A.H. Weber, 1979: A Lagrangian Statistical Analysis of Diffusion from a Ground-Level Source in a Turbulent Boundary Layer. Quart. J. Roy. Meteorol. Soc., 105, 423-443.

Irwin, J.S., 1979: Estimating Plume Dispersion - A Recommended Generalized Scheme. Fourth Symposium on Turbulence, Diffusion and Air Pollution (Preprints), Jan. 15-18, 1979. Reno, Nev.

Jensen, N.O. and E.L. Petersen, 1979: The Box Model and the Acoustic Sounder, A Case Study. Atmos. Env., 13, 717-720.

Kaimal, J.C., 1978: Horizontal Velocity Spectra in an Unstable Surface Layer. J. Atm. Sci., 35, 18-24.

Kalanda, B.D., 1979: Suburban Evaporation Estimates in Vancouver. M.Sc. Thesis, The University of British Columbia, Vancouver.

Kalanda, B.D., T.R. Oke and D. Spittlehouse, 1980: Suburban Energy Balance Estimates for Vancouver, B.C. using the Bowen Ratio-Energy Balance Approach. J. Appl. Meteorol., (in press).

Koper, C.A., W.Z. Sadeh and R.E. Turner, 1978: A Relation Between the Lagrangian and Eulerian Turbulent Velocity Autocorrelations. AIAA Journal, 16, 969-975.

Kutzbach, J.E., 1961: Investigations of the Modification of Wind Profiles from Artificially controlled Surface Roughness. Annual Report. Dept. of Meteorology, University of Wisconsin

Lettau, H.H. and B. Davidson, 1957: Exploring the Atmosphere's First Mile. Pergamon Press, London. 2 volumes.

Lettau, H.H., 1969. Note on Aerodynamic Roughness-Parameter Estimation on the Basis of Roughness-Element Description. J. Appl. Meteorol., 8, 828-832.

Lilley, D.K., 1968: Models of Cloud Topped Mixed Layers Under a Strong Inversion. Quart. J. Roy. Meteorol. Soc., 94, 292-309.

Lumley, J.L. and H.A. Panofsky, 1964: Structure of Atmospheric Turbulence. Wiley-Interscience, New York.

Lyons, W.A. and L.E. Olsson, 1973: Detailed Mesometeorological Studies of Air Pollution Dispersion in the Chicago Lake Breeze. Mon. Wea. Rev., 101, 387-403.

MacReady, P.B. Jr. and H.R. Jex, 1964: Response Characteristics and Meteorologic Utilization of Propellers and Vane Wind Sensors. J. Appl. Meteorol., 3, 182-193.

Madderom, P., 1978: Integration (Quadrature) Routines. U.B.C. Computing Centre Manual, Sept. 1978, 44 pp.

Mahrt, L. and D.H. Lenschow, 1976: Growth Dynamics of the Convectively mixed Layer. J. Atmos. Sci., 33, 41-51.

McAllister, L.G., 1968: Acoustic Sounding of the Lower Troposphere. J. Atmos. Terr. Phys., 30, 1439-1440.

McBean, G.A., 1972: Instrument Requirements for Eddy Correlation Measurements. J. Appl. Meteorol., 11, 1078-1084.

McElroy, J.L. and F. Pooler, 1968: St. Louis Dispersion Study, U.S. Public Health Service, National Air Pollution Control Administration, Report AP-53.

Melling, H., 1979: The Urban Convective Boundary Layer as Studied by Acoustic Echo Sounder. Ph.D. Thesis, University of Toronto, Toronto, Ont.

Miller, M.C., 1967: Forecasting Afternoon Mixing Depths and Transport Wind Speeds, Mon. Wea. Rev., 95, 35-44.

Monin, A.S. and A.M. Yaglom, 1975: Statistical Fluid Mechanics: Mechanics of Turbulence. Vol. II, The M.I.T. Press, Cambridge.

Morgan, T. and R.D. Bornstein, 1977: Inversion Climatology at San José California. Mon. Wea. Rev., 105, 653-656.

Moses, H. and H.G. Daubeck, 1961: Errors in Wind Measurements Associated with Tower-mounted Anemometers. Bull. Amer. Meteorol. Soc., 42, 190-194.

Munro, D.S. and T.R. Oke, 1975: Aerodynamic Boundary-Layer Adjustment Over a Crop in Neutral Stability. Boundary-Layer Meteorol., 9, 53-61.

Netterville, D.D.J. and S.G. Djurfors, 1979: Controlling Inherent Uncertainties in Double Theodolite Measurements. J. Appl. Meteorol., 18, 1371-1375.

Nicholas, F., 1974: Parameterization of the Urban Fabric: A Study of Surface Roughness. Ph.D. Dissertation, University of Maryland, 161 pp.

Nicholson, S.E., 1975: A Pollution Model for Street-Level Air. Atmos. Env., 9, 19-31.

Niewstadt, F.T.N. and A.G.M. Driedonks, 1979: The Nocturnal Boundary Layer: A Case Study Compared with Model Calculations: J. Appl. Meteorol., 18, 1397-1405.

Nunge, R.J., 1974: Application of an Analytical Solution for Unsteady, Advective Diffusion to Dispersion in the Atmosphere -I-II. Atm. Env., 8, 969-1001.

Oke, T.R., 1976: The Distinction Between Canopy and Boundary-Layer Urban Heat Islands. Atmosphere, 14, 268-277.

Oke, T.R., 1978: Surface Heat Fluxes and the Urban Boundary Layer. Proc. WMO Symp. Boundary Layer Physics Appl. Specific Problems Air Poll., WMO No. 510, WMO, Geneva, 63-69.

Oke, T.R., B.D. Kalanda and D.G. Steyn, 1979: Parameterization of Heat Storage in Urban Areas. Submitted to Urban Ecology. (Sept., 1979).

Panofsky, H.A., H. Tennekes, D.H. Lenschow and J.C. Wyngaard, 1977: The Characteristics of Turbulent Velocity Components in the Surface Layer under Convective Conditions. Boundary-Layer Meteorol., 11, 355-361.

Pasquill, F., 1961: The Estimation of Windborne Material. Meteorol. Mag., 2, 225-250.

Pasquill, F., 1968: Some Outstanding Issues in the Theory and Practice of Estimating Diffusion from Sources, Sandia Laboratories, Symposium on the Theory and Measurement of Atmospheric Turbulence and Diffusion in the Planetary Boundary Layer, 17-30.

Pasquill, F., 1971: Atmospheric Dispersion of Pollution. Quart. J. Roy. Meteorol. Soc., 97, 369-395.

Pasquill, F., 1974: Atmospheric Diffusion (2nd Ed.), Ellis Horwood, 429 pp.

Pasquill, F., 1975a: Some Topics Relating to Modelling of Dispersion in the Boundary Layer, EPA-650.4-75-015, U.S. Environmental Protection Agency, Research Triangle Park, N.C., 1975.

Pasquill, F., 1975b: The Dispersion of Materials in the Atmospheric Boundary-Layer, The Basis for Generalization. In Lectures on Air Pollution and Environmental Impact Analysis, ed. D.A. Haugen, A.M.S., Boston, Mass.

Peterson, E.W., 1969: Modification of Mean Flow and Turbulent Energy by a Change in Surface Roughness Under Conditions of Neutral Stability. Quart. J. Roy. Meteorol. Soc., 95, 561-575.

Philip, J.R., 1967: Relation Between Eulerian and Lagrangian Statistics, Boundary Layers and Turbulence. Phys. Fluid Suppl., 69-71.

Pond, S., W.G. Large, M. Miyake and R.W. Burling, 1979: A Gill Twin Propeller-Vane Anemometer for Flux Measurements During Moderate and Strong Winds. Boundary-Layer Meteorol., 16, 351-364.

Portelli, R.V., 1980: The Nanticoke Study: Experimental Investigation of Diffusion from Tall Stacks in a Shoreline Environment. Submitted for Presentation to 10th NATO/CCMS Meeting, Rome, Nov., 1979.

Randerson, D., 1979: Review Panel on Sigma Computations. Bull. Amer. Meteorol. Soc., 60, 682-683.

Raupach, M.R., 1977: Atmospheric Flux Measurement by Eddy Correlation, Ph.D. Thesis, The Flinders University of South Australia, 207 pp.

Raynor, G.S., S. Sethuraman and R.M. Brown, 1979: Formation and Characteristics of Coastal Internal Boundary Layers During Onshore Flows, Boundary-Layer Meteorol., 16, 487-514.

Saffman, P.G., 1963: An Approximate Calculation of the Lagrangian Autocorrelation Coefficient for Stationary Homogeneous Turbulence. Appl. Sci. Res. A, 11, 245-255.

Sawford, B.L., 1979: Wind Direction Statistics and Lateral Dispersion. Quart. J. Roy. Meteorol. Soc., 105, 841-848.

Schaefer, J.T. and C.A. Doswell, 1978: The Inherent Position errors in Double-Theodolite Pibal Measurements. J. Appl. Meteorol., 17, 911-915.

Schmidt, F.H., 1946: On the Causes of Pressure Variations at the Ground K. Ned. Meteor. Inst. Meded. Verh., B, 2.

Scorer, R.S., 1976: The Meaningfulness of Mathematical Theories of Atmospheric Dispersion. Symposium on External Flows, Bristol University.

Shampine, L.F. and M.K. Gordon, 1974: Computer Solution of Ordinary Differential Equations: The Initial Value Problem. Freeman.

Slade, D.H. (ed.), 1968: Meteorology and Atomic Energy, USHEC TID-24190. 445 pp.

Smedman-Högstrom, A.S. and U. Högstrom, 1975: Spectral Gap in Surface-Layer Measurements. J. Atm. Sci., 32, 340-350.

Smith, F.B., 1972: A Scheme for Estimating the Vertical Dispersion of a Plume from a Source near Ground Level. In Proceedings of the Third Meeting of the Expert Panel on Air Pollution Modelling, NATO-CCMS Report 14, North Atlantic Treaty Organization, Brussels, 1972.

Smith, F.B. and D.J. Carson, 1977: Some Thoughts on the Specification of the Boundary Layer Relevant to Numerical Modelling. Boundary-Layer Meteorol., 12, 307-330.

Spagnol, J., 1978: Stratus Advection into the Southern Georgia Strait. Pacific Region Technical Notes, No. 78-035.

Steenbergen, J.D., 1971: Comparison of Urban and Rural Turbulence Statistics at Edmonton, Alta. M.Sc. Thesis, University of Edmonton.

Steyn, D.G. and T.R. Oke, 1980: Effects of a Small Scrub Fire on the Surface Radiation Budget. Weather, (in press).

Stull, R.B., 1976a: Mixed-Layer Depth Model based on Turbulence Energetics, J. Atmos. Sci., 33, 1268-1278.

Stull, R.B., 1976b: The Energetics of Entrainment Across a Density Interface. J. Atmos. Sci., 33, 1260-1267.

Summers, P.W., 1965: An Urban Heat Island Model: Its rôle in Air Pollution, with application to Montréal. First Canadian conference on Micrometeorology, April 1965, Toronto, Ont.

Sutton, O.G., 1953: Micrometeorology. New York, McGraw-Hill.

Tanner, C.B. and G.W. Thurtell, 1970: Sensible Heat Flux Measurements with a Yaw Sphere and Thermometer. Boundary-Layer Meteorol., 1, 195-200.

Taylor, G.I., 1921: Diffusion by Continuous Movements. Proc. London Math. Soc., Ser. 2, 20, 196.

Tennekes, H., 1973: A Model for the Dynamics of the Inversion above a Convective Boundary Layer. J. Atmos. Sci., 30, 558-567.

Tennekes, H., 1974: The Atmospheric Boundary Layer, Physics Today, 27, 52-63.

Tennekes, H., 1975: Reply. J. Atmos. Sci., 32, 992-995.

Tennekes, H., 1976: Observations on the Dynamics and Statistics of Simple Box Models with a Variable Inversion Lid. Third Symposium on Atmospheric Turbulence, Diffusion and Air Quality (Preprints). Rayleigh N. C., Amer. Meteorol. Soc., 397-402.

Thyer, N., 1962: Double Theodolite Pibal Evaluation by Computer. J. Appl. Meteorol., 1, 66-68.

Turner, D.B., 1967: Workbook of Atmospheric Dispersion Estimates, USDHEW, PHS No. 995-AP-26, 84 pp.

Venkatram, A., 1977: A Model of Internal Boundary-Layer Development. Boundary-Layer Meteorol., 11, 419-437.

Venkatram, A., 1980: Dispersion from an Elevated Source in a Convective Boundary Layer. Atm. Env., 14, 1-10.

Wandel, C.F. and O. Kofoed-Hansen, 1962: On the Eulerian-Lagrangian Transform in the Statistical Theory of Turbulence. J. Geophys. Res., 67, 3089-3093.

Weisman, B. and M.S. Hirt, 1975: Dispersion Governed by the Thermal Internal Boundary Layer. 68th Meeting of the Air Pollution Control Association, June 1975, Boston, Mass.

Wyngaard, J.C., 1973: On Surface Layer Turbulence. In Workshop on Micrometeorology. Ed. D.A. Haugen. Amer. Meteorol. Soc., Boston, Mass., 392 pp.

Wyngaard, J.C. and O.R. Coté, 1974: The Evolution of a Convective Planetary Boundary Layer - A Higher-Order Closure Model Study. Boundary-Layer Meteorol., 7, 289-308.

Yamada, T., 1979: Prediction of the Nocturnal Surface Inversion Height. J. Appl. Meteorol., 18, 526-531.

Yamada, T. and S. Berman, 1979: A Critical Evaluation of a Simple Mixed-Layer Model with Penetrative Convection. J. Appl. Meteorol., 18, 781-786.

Yap, D., T.A. Black and T.R. Oke, 1974: Calibration and Tests of a Yaw Sphere-Thermometer System for Sensible Heat Flux Measurements. J. Appl. Meteorol., 13, 40-45.

Yap, D. and T.R. Oke, 1974: Sensible Heat Fluxes over an Urban Area - Vancouver, B.C., J. Appl. Meteorol., 13, 880-890.

Zilintinkevich, S.S., 1975: Comments on a Model for the Dynamics of the Inversion above a Convective Boundary-Layer. J. Atmos. Sci., 32, 991-992.

APPENDICES

A. The Observational Site

A.1 General Requirements

Observational studies in micrometeorology are plagued by the need to assume that surfaces surrounding the site of observation are homogeneous in all properties which may affect the atmospheric surface layer. While this may not present any problems in studies of the marine surface layer, it has led to the selection of environmentally extreme sites for terrestrial studies. This is particularly true for sites at which pioneering studies have been carried out.

A prime criterion on which site selection must be based is the fetch required for the surface layer to adjust to a change in surface characteristics. This adjustment must be completely propagated through the layer of atmosphere being studied, so that no flux divergences exist due to upwind changes in surface properties. The process of adjustment has been investigated both theoretically and experimentally, and reviewed by Munro and Oke (1975) who present the relation

$$\delta'(x) = 0.1x^{4/5}\, z_0^{\,1/5} \qquad (A.1)$$

for the depth of complete adjustment $\delta'(x)$ as a function of fetch (x) and surface aerodynamic roughness length (z_0). This relation describes the adjustment of an adiabatic turbulent surface layer in transition from a smooth-to-rough surface. The depth of adjustment will be greater for increasing instability, and smaller for a transition from rough-to-smooth (Peterson, 1969) or increasing stability.

The relation (A.1) gives the required fetch which must be homogeneous for a given roughness length and tower height (assumed equal to $\delta'(x)$). The present study was directed at surfaces with a roughness length of $\sim$ 0.5 m, and utilized a tower 30 m in height, thus requiring a fetch of 1485 m for smooth to rough transitions in an adiabatic atmosphere.

In addition to this theoretical requirement, for logistical reasons it was necessary to find a site with easily accessible electric power, reasonable security, and one at which the erection of a 30 m steel tower would not be in violation of city zoning laws.

A.2 The Selected Site

The requirement of 1.5 km of homogeneous fetch makes it all but impossible to find a site truly representative of urban meteorology, but it is relatively easy to find a site surrounded by homogeneous suburban surfaces, particularly in North American cities. Nevertheless because of the restrictive nature of the ideal requirements, it was inevitable that some compromise would have to be made in selecting the site. The site finally chosen is a transformer station (operated by the British Columbia Hydro and Power Authority) known as the Mainwaring Substation. The substation is situated in suburban South Vancouver, in the 6400 block of Inverness Street (Kalanda, 1979). The setting of the city of Vancouver has been described by Hay and Oke (1975) from a meteorologic point of view, while the general environs of the study area, the near site topographic details and land use are shown in Figure A.1. As can be seen from these figures, the site is surrounded by suburbia in all directions for well over the requisite 1.5 km, and these surrounds are essentially flat except for a gradient of 1:16 to the southwest, starting 1.0 km away. The visual impression of the surrounding topography

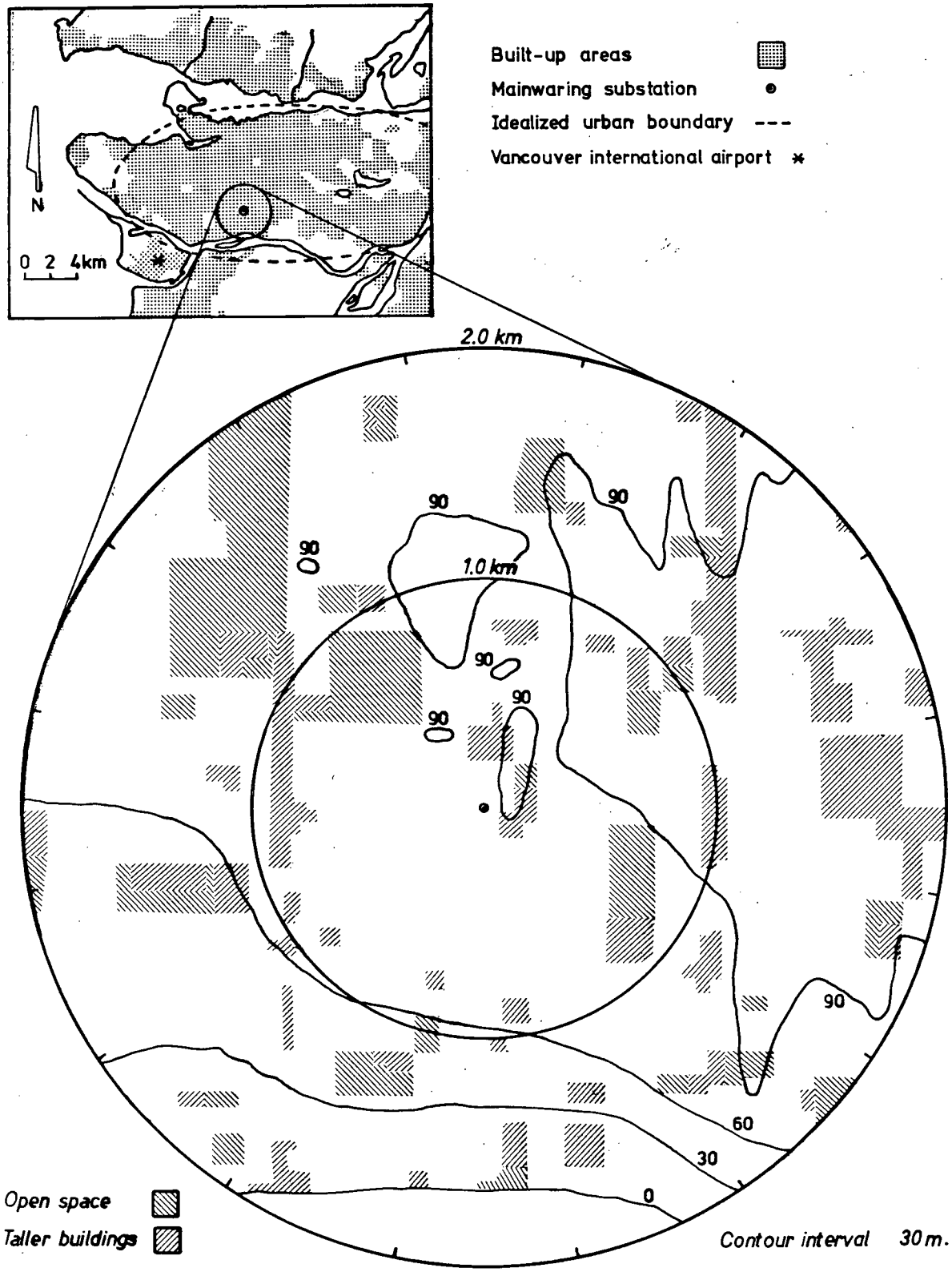

Figure A.1: General Environs of the Study Area, near-site Topography and Land-use.

Figure A.2a: Photographic view from the top of the tower to the west.

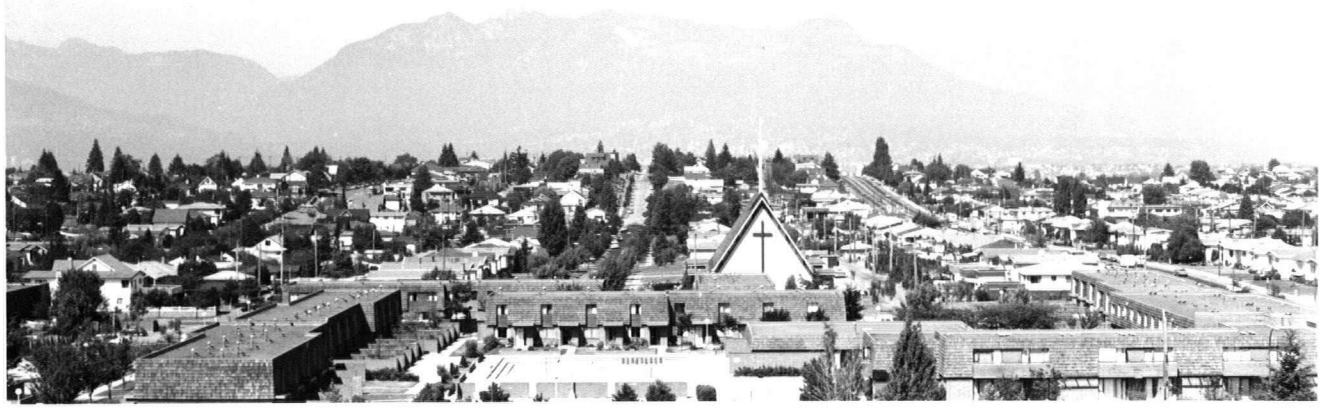

Figure A.2b: Photographic view from the top of the tower to the north.

Figure A.2c: Photographic view from the top of the tower to the east.

Figure A.2d: Photographic view from the top of the tower to the south.

is "gently rolling" with a vertical length scale of about ten metres. This is borne out by Figure A.2 (a,b,c, and d), four photographic views from the top of the tower. The large building in Figure A.2c is a three storey school which is situated 200 m to the east of the tower. As the mean wind was seldom from this direction, it was easy to ensure that wake effects from this building did not contaminate the results of the turbulence measurements.

In order to quantify the degree of horizontal homogeneity of the roughness length a land-use analysis was performed using a 1:10,000 photomosaic of the city. (Figure A.1 is based on this analysis). The surface roughness length is most properly determined from wind profile measurements, a task of considerable complexity in this environment, so a surrogate approach was taken.

A.3 Sectorial Roughness Length Analysis

For irregular arrays of reasonably homogeneous roughness elements, the surface roughness length can be estimated (Lettau, 1969) by

$$z_0 = 0.5h^* \frac{s}{S} \qquad (A.2)$$

where h^* is the height, s is the silhouette area, and S the total area of the roughness elements. Similar estimators using different formulae have been presented by Kutzbach (1961) and Counihan (1971) and the technique has been applied to urban surfaces by Nicholas (1974) and Clarke et al. (1978).

In order to apply this method of analysis to Vancouver, a land-use classification scheme was designed which served to differentiate between the different types of roughness elements in the area. Figure

A.1 shows the results of this classification which differentiates between purely residential use (mostly single family dwellings and garages, the mean frontal dimensions being 10.5 m and 6.0 m respectively and the mean heights being 8.5 m and 3.5 m respectively), commercial and multi-family dwelling use (having a mean frontal dimension of 41.5 m and a mean height of 15.0 m), and open areas (mainly parkland, parking lots and playing fields). The mean number density of roughness elements in the first two land-use types was found by counting those elements on representative sample areas on the map, and was used to determine the total number of roughness elements in each of sixteen 22.5° sectors centred on the tower. Because of the diversity of roughness elements, the terms in equation (A.2) were replaced by composite values as follows:

$$h^* = \sum_{i=1}^{m} \frac{n_i}{N} h_i^*$$

$$s = \sum_{i=1}^{m} \frac{n_i}{N} S_i$$

$$S = \sum_{i=1}^{m} \frac{A}{n_i}$$

where m is the number of roughness element types, n_i is the number of elements of the ith type in the sector being considered, N is the total number of elements in that sector, h_i^* is the height of the ith element type, s_i is the silhouette area of that element type, and A is the area of the sector.

The results of this analysis are shown in Table A.1. While the absolute value of z_0 thus produced is not expected to be much more

than an order of magnitude estimate, the homogeneity of the parameter among the 16 sectors is a powerful indication that the assumption of surface homogeneity is at least a fair one. The mean roughness length of 0.52 m is somewhat lower than the values reported by Counihan (1975) and Clarke et al. (1978) for this kind of surface (0.7 to 1.7 m). The standard deviation of 0.09 m indicates the degree of homogeneity.

Table A.1: Sectorial Analysis of Roughness Length

Sector	No. of houses	No. of garages	No. of larger buildings	Percentage open space	z_o (m)
S	760	388	42	64	0.49
SSW	941	500	16	64	0.50
SW	1148	543	10	42	0.57
WSW	1149	790	23	54	0.61
W	1219	745	75	0	0.70
WNW	867	350	45	46	0.48
NNW	1073	553	7	27	0.53
N	1045	459	15	0	0.53
NNE	1117	406	19	0	0.56
NE	880	445	60	48	0.52
ENE	796	449	31	0	0.43
E	1100	677	32	55	0.59
ESE	972	572	9	60	0.49
SE	811	530	14	57	0.43
SSE	1005	680	13	64	0.54

Overall roughness length 0.52 m ± 0.09 m (mean and standard deviation)

A.4 Displacement Length

Outside the laminar sublayer which surrounds all surfaces exposed to the atmosphere, there exists a highly turbulent wake layer which contains constantly fluctuating horizontal inhomogeneities. This layer, called the urban canopy layer by Oke (1976), provides a lower boundary for the surface layer in which our measurements are made, and must be accounted for in any calculations involving height. In effect, the top of this layer must serve as a zero for all height measurements when using surface layer theory.

The momentum surface layer is taken to be based a distance d (the aerodynamic displacement height) from the ground's surface. This height is usually determined from measurements of mean wind profiles, but can be estimated from land-use analyses. Estimation formulae have been presented by Kutzbach (1961), Counihan (1971) and Nicholson (1975). This sort of analysis has been applied by Clarke et al. (1978) to suburban surfaces, and will be used here. The Kutzbach (1961) form gives d/h as a function of the fraction area covered by roughness elements of height h. Using a weighted mean for the different types of roughness elements yields a displacement height of 3.7 m. The Nicholson (1975) form is derived from Lettau's results and is a somewhat more complicated function of roughness length and building height. This yields a value of 3.2 m for d, in close agreement with the first estimation. A displacement height of 3.5 m was used in all analyses to adjust all height measurements on the tower to a more realistic datum for the surface layer.

B. The Tower, Instrumentation and Data Logging Systems

B.1 The Tower

The instruments probing the surface layer in this study were mounted on a triangular section, steel lattice free-standing tower constructed by the LeBlanc and Royle company to their LR324 series S/S specifications. The tower consisted of six lattice sections (A,A,B,C,D and E of their specifications), having a base of 2.03 m, tapering to 0.5 m at an elevation of 18.40 m, and thence being parallel-sided to 27.45 m. A tubular extension of 1.60 m was added to give a total elevation of 29.05 m. The tower was fitted with an external climbing ladder on the tapered section, while horizontal rungs were incorporated into the upper sections. The instruments were mounted on booms fixed to these upper sections (Figure B.1 and B.2). The upper sections have a shadow fraction of 0.14, and the booms are all at least two tower diameters in length, thus ensuring that tower influences on the measurements will be at an acceptable minimum (Moses and Daubeck, 1961).

The tower was erected in the south-east corner of the Mainwaring substation, some three metres from the embankments and hedges of the south and east boundaries, the base being 6.0 m below the base of the hedges. A trailer at the base of the tower housed the recording and logging equipment (Figure B.1).

The surrounding houses are built at the same level as the base of the hedges, and allowing 3.5 m for the displacement length (see Appendix A), 9.0 m must be subtracted from all tower station elevations to obtain heights in the surface layer (Figure B.1).

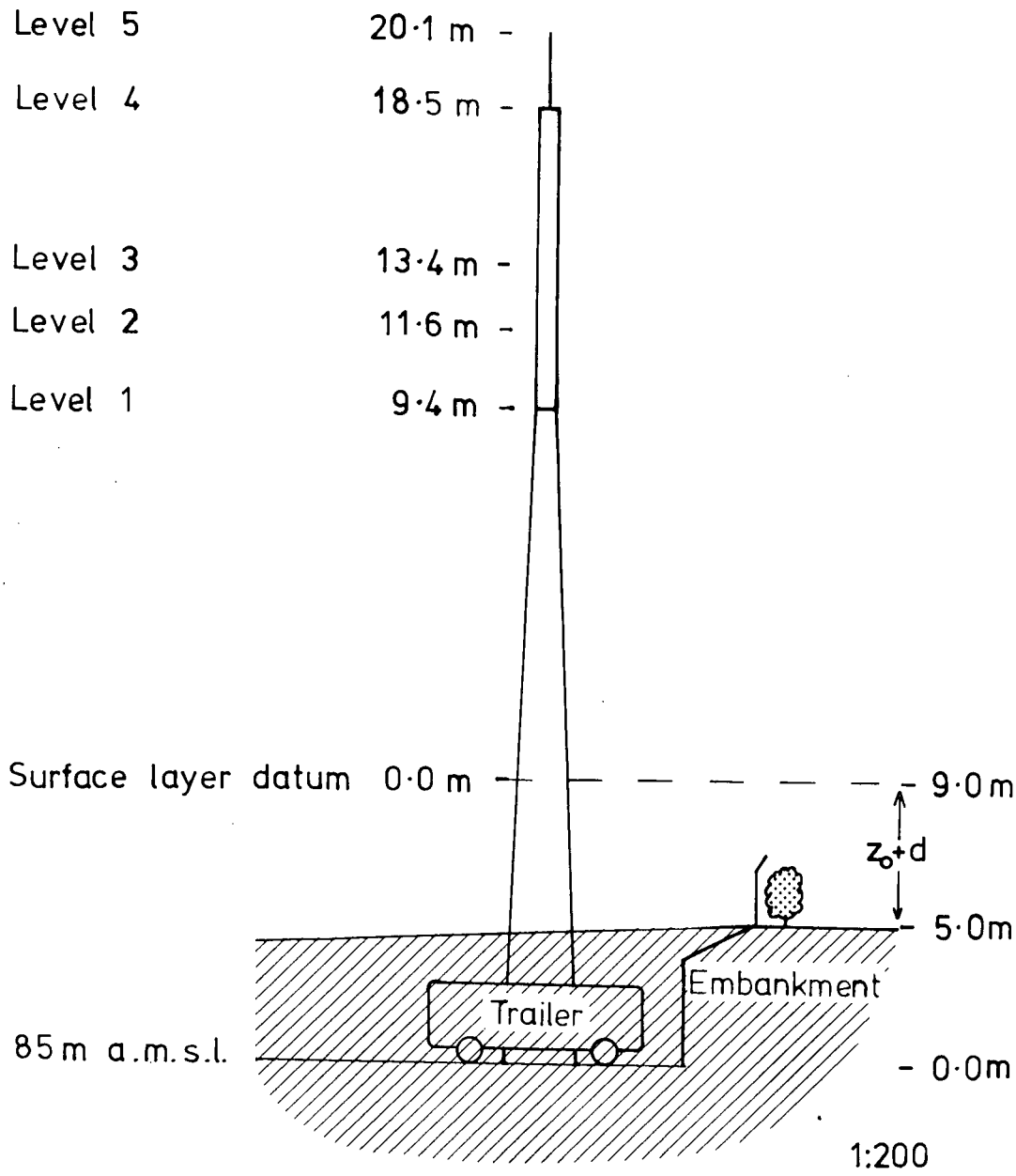

Figure B.1: The Tower and Embankments

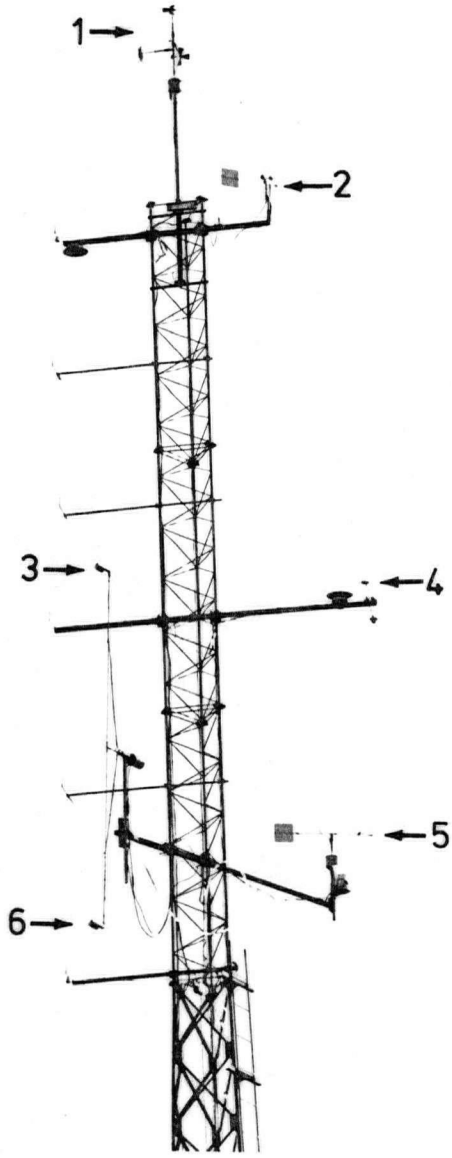

Figure B.2: Upper sections of the tower showing surface layer instrumentation.

1. U.V.W. Anemometer.
2. Microvane and cup anemometer.
3. Differential psychrometer, upper sensor.
4. Net pyrradiometer.
5. Yaw sphere-thermometer.
6. Differential psychrometer, lower sensor.

B.2 Instrumentation

B.2.1 U.V.W. Anemometer

This instrument consists of an orthogonal triplet of helicoid propellor anemometers, each driving a miniature DC tachometer (Gill, 1974b). The instrument has been intensively studied (Drinkrow, 1972; Fichtl and Kumar, 1974; Hicks, 1973; Horst, 1973; McBean, 1972) and used in studies of the urban atmosphere (Brook, 1974; Coppin, 1979; Clarke et al., 1978). The instrument used in this study was the stock model manufactured by R.M. Young Co. with 0.3 m pitch, four-blade polystyrene propellors. The response length (MacReady and Jex, 1964) has been found to be a function of the angle of attack (Raupach, 1977), and for the RMS angles of attack (approximated by $\tan^{-1}(\sigma_w/\overline{u})$) encountered in the study should be 1.3 m for the horizontal sensors and 1.5 m for the vertical. The starting speed of the sensors is in the region of 0.15 m s^{-1} (McBean, 1972). Different configurations of these three sensors have been considered (Gill, 1975; Christiansen, 1971; Pond et al., 1979) in order to minimise the effective response length, which can be unacceptably long in conditions of high horizontal wind velocities and small vertical velocity variances. This problem was not encountered in this study so the more standard and simpler orthogonal triplet was utilized.

This instrument was used as a sensor of turbulent wind velocity fluctuations and was mounted at level 5 (Figures B.1 and B.2) of the tower. The instrument was mounted on top of the tubular extension to the tower and was levelled as accurately as possible with a spirit level. The levelling required an operator at the top of the tower, and the flexing of the tower would certainly alter the levelling; it is, however, expected that the plane of the horizontal sensors is within at most 1° of true

horizontal, thus ensuring a tilt error of less than 14% in the measured velocity covariance (Dyer and Hicks, 1972). The three signals were led down the tower to the trailer where, after passing through an active low-pass filter with a signal reduction of 3.2 dB at 25 Hz, with ten-fold amplification, they were recorded on an FM analogue instrumentation tape recorder (Hewlett-Packard model 3960A). The data tapes were subsequently played back into an analogue to digital converter (having 12 bit resolution) linked to a minicomputer (PDP Model 10) which wrote the sampled data onto a computer-compatible 9-track magnetic tape. The analysis of the data is described in Appendix F.

B.2.2 Yaw Sphere-Thermometer Eddy Correlation System

Turbulent fluxes of sensible heat can be directly measured by determining the correlation of temperature and vertical velocity fluctuations. Any of a wide range of velocity and temperature sensors can be used to achieve this end. A particularly convenient combination is a vane mounted pressure-sphere anemometer and platinum resistance thermometer (called a Yaw Sphere-Thermometer or YST) as described by Tanner and Thurtell (1970) and Yap et al. (1974). A YST system has been used to estimate turbulent sensible heat fluxes over an urban (really suburban) surface (Yap and Oke, 1974; Oke, 1978), and was utilised for that purpose in this study. The sensor assembly was mounted at level 2 on the tower and the signals were led down the tower where they were transformed and conditioned to produce an hourly averaged value of the turbulent sensible heat flux.

In atmospheric environments such as the one presently under study, a compromise must be reached between the need for long averaging

times (to achieve statistical stationarity in signals with large variances), and the need for short averaging times (to satisfy the assumption of temporal stationarity in the signals). The problem of statistical stationarity has been approached by Wyngaard (1973) whose results, when applied to the conditions of this study indicate a desired averaging time of one hour for a 10% accuracy in flux estimates at a mean wind speed of between 2.0 and 3.0 m s^{-1}. As this is one order of magnitude less than the diurnal cycle, it should be within the dominant temporal variations, and so will be used as the basic averaging time. This choice is consistent with a number of previous urban meteorology studies (Brook, 1974; Clarke et al., 1978; Coppin, 1979; and Yap and Oke, 1974). The estimation of a detailed energy budget is described in Appendix E. The errors in fluxes determined with this instrument amount to 5% to 15%, dependent on mean wind and the range settings used.

B.2.3 Differential Psychrometer System

The ratio of turbulent sensible- to turbulent latent-heat flux in the surface layer may be estimated by measuring simultaneously the vertical gradients of atmospheric temperature and humidity. The method, as implemented in this study utilises a pair of vertically separated wet-bulb/dry-bulb temperature sensors, as described by Black and McNaughton (1971). The system used in this study is described by Kalanda (1979), and Kalanda et al. (1980), and was used to give hourly averaged estimates of the Bowen ratio. The system was fixed to the tower so that the sensor positions were at levels 1 and 3 (Figures B.1 and B.2). These data were used in conjunction with other measurements to provide estimates of the surface energy budget as described in Appendix E.

A detailed error analysis of fluxes determined by this system has been presented by Kalanda (1979), who finds errors in the range 10% to 20%.

B.2.4 Microvane and Cup Anemometer

Wind speed and direction at level 4 (Figure B.1 and B.2) were sensed by a three-cup anemometer and microvane manufactured by the R.M. Young Co. (Model 12101 cup and 12301 vane). The cup has a distance constant of 3.0 m, and the vane a delay distance of 1.0 m and a damping ratio of 0.44. The analogue signals from these sensors were conditioned and integrated by a Campbell Scientific data logging system (Model CR5) to produce hourly averaged values of mean wind speed and direction.

B.2.5 Pyrradiometer

The net all-wave radiant flux density of the surface was measured with a net pyrradiometer (manufactured by Swissteco Pty. Ltd., Model S1) mounted at level 3 (Figures B.1 and B.2) and 1.8 m from the tower. The polyethylene domes were kept inflated and free of internal condensation by a stream of dry commercial-grade nitrogen piped up the tower. The signal from the sensor was led down the tower where it was integrated and logged on the CR5 data logger to produce hourly average values of the net radiant flux density. Appendix E details how these data were used (in conjunction with others) to estimate surface energy budgets.

At this height (29.05 m) the gravel-coated transformer site has a view factor of approximately 0.24 (the site is rectangular with dimensions 140 m x 110 m). This represents a considerable fraction, and though there are no installations in the site with temperatures significantly different from those of the surrounding suburbia, the net radiation

may not be entirely representative of a suburban surface. A radiation budget study based on the data gathered during this study (Steyn and Oke, 1980) shows this site and the surrounding suburbia to be represented by an albedo of between 0.12 and 0.14, in good agreement with albedos typical of urbanized surfaces (Oke, 1974).

B.2.6 Theodolite tracked Mini-Sonde System

The thermal structure of the planetary boundary layer was probed intermittently with miniature radio transmitting temperature sensors. The sensors were of the "mini-T-sonde" variety (manufactured by Sangamo Co.), and provided an accuracy of $\pm$ 0.1°C and a time constant of 2.5 to 3.5 s using a miniature thermistor as a temperature transducer. The sondes were carried aloft on Helium-filled pilot balloons inflated to provide an ascent rate of $\sim$ 3m s^{-1}. The temperature was transmitted as an FM analogue radio signal centred on 403 MHz. The receiver demodulator (Beukers Model 4700B) was fitted with an output lineariser and chart recorder which provided a temperature-time plot. In order to transform to a temperature-height plot, the position of the balloon was tracked with two tracking-theodolites (Askania Model 5700), having a vernier least count of 0.1 and a high power telescope with graticule circles at 0.5° and 0.1°). They were set up on a 301.4 m baseline just to the west of the substation. The baseline was aligned in a N-S orientation to accommodate the expected preponderance of E-W flows.

Each flight was tracked for 15 min, with azimuth and zenith sightings being taken every 30 s. The cueing for these readings was provided by a controlling operator with a portable radio transmitter, each of the trackers having a receiver. The angles were read into portable tape recorders for subsequent transfer to data sheets for computer coding. The temperature traces were digitized at each of the sighting times and

coded with that data. The analysis of this data is detailed in Appendices I and J.

B.2.7 Acoustic Sounder

The atmosphere can be probed remotely and continuously in a semi-quantitative manner by a monostatic acoustic sounder (McAllister, 1968; Beran and Hall, 1974). The instrument in its most basic form transmits a pulse of sound vertically into the atmosphere and then detects any echoes scattered by thermal structures. A commercially available model (Aerovironment, Model 300) was used in this study to produce a continuous record of the height of thermal turbulence structure above the site. The transmit/receive unit was located inside the transformer station approximately 10 m from the tower. The transceiver and display unit were set up inside the instrument trailer. The instrument used in this study produced a 25 W pulse of sound at 16 Hz every 18 s. The recording system was adjusted to display the lowest 1000 m of the atmosphere on a time base of 30.5 mm per hour.

This form of sounding has been used in an urban environment (Bennett, 1975; Melling, 1979; Jensen and Petersen, 1979) where the major problem is interference by ambient (particularly traffic) noise. With the above settings this interference was at an acceptable minimum, producing a light but continuous darkening at upper levels. Apart from chart paper changes every 28 days, the instrument operated without attention. The traces from the sounder were digitized and analysed as detailed in Appendices I and J.

C. Synoptic Background to the Observational Period

The climate of Vancouver (49° 13' 37" N, 123° 4' 37" W) is characterised by its mid-latitude location on the west coast of a large continent with a very mountainous hinterland (Hay and Oke, 1976). This study was undertaken from mid-July to mid-August of 1978 in what was an extreme example of the typical anti-cyclonic régime which dominates the summer weather in this region. The following is a synoptic sketch of the weather during the observation period extracted from surface, and 500 mb charts, hourly observation sheets from Vancouver International Airport observing station (for location see Figure A.1) and visible band satellite imagery (data provided by the Atmospheric Environment Service, Dept. of the Environment, Canada).

The weather over the first half of the study period was dominated by a broad anticyclone centred at approximately 150°W, 50°N and covering all of the Eastern Pacific Ocean, with a dry thermal trough over the western United States of America. Associated with these surface features was an upper level ridge parallel to the west coast. This régime brought clear skies to the region with only occasional bursts of marine stratus advected up the coastal inlets (Spagnol, 1978). During this period a weak short wave moved through the long wave ridge on the 23rd of July bringing some scattered cloud but no precipitation. This régime persisted until the 26th/27th when a deepening closed vortex over the Pacific Ocean began to dominate the flow at all levels. In the transition between these two régimes, large-scale motions without frontal origin realised potential instability, producing wide-spread convective activity over the entire region. Recording stations in Vancouver reported 4 to 6 mm of rain the 26th (Haering, 1978). After the 27th, the cold Low persisted and remained stationary, with an associated front taking on a

N-S orientation some distance to the west of the coastline. In response to this cold Low, a surface ridge of moderate amplitude developed bringing further clear skies and continued subsidence of warm air to the Southwestern British Columbia region. This régime was remarkably persistent, and lasted from the 28th July to the 9th of August when a strengthening westerly upper flow over the Pacific finally drove the Low over the coast bringing cloud and precipitation to the region and heralding the end of both the summer and of the observational phase of this study.

D. The Data-Set

The data gathered in this study (by the instrumentation detailed in Appendix B) will be compiled and prepared for general teaching and research use by interested parties after the completion of the thesis. This appendix serves as an outline of the scope and extent of the data which consists of:

- Digitized (at varying sampling rates) measurements of daytime (0500-1900 Solar Time) mixed layer depths for July 20th, 22nd, 23rd, 28th, 29th to August 8th.
- Complete hourly averaged surface radiation and energy budgets from July 16th to August 8th with occasional missing data points in some of the earlier days.
- Mean hourly averaged wind speed and direction at level 4 (Figure B.1) from July 16th to August 8th.
- Potential temperature profiles of the planetary boundary layer taken intermittently throughout each of the days with at least three flights on each day.
- Hourly blocks of three-dimensional turbulence statistics taken intermittently throughout each of the days (a total of 62 blocks of useable data were taken).

These data are all stored in data files in The University of British Columbia Computing Centre where they were subjected to the analyses described in this thesis.

E. Estimation of the Surface Energy Budget

E.1 Budget Closure by Distribution of Residuals

As described in Sections B.2.2, 3 and 5, turbulent sensible heat flux, Bowen ratio and net all-wave radiant heat flux were independently measured within the surface layer. From these three quantities an estimate of the four terms in the following idealized energy budget had to be made:

$$Q^* = Q_H + Q_E + \Delta Q_S \qquad (E.1)$$

Q^* is the net all-wave radiant flux density, Q_H the turbulent sensible heat flux density, Q_E the turbulent latent heat flux density and ΔQ_S the canopy layer heat storage.

At first sight the above would appear to be no more than a trivial algebraic problem, but it must be remembered that the measurements of the turbulent fluxes are subject to relatively large errors which would appear in the residual (canopy layer storage term) and mask most of its real variations. A more detailed look must be taken at the various possible ways of estimating the energy budget terms.

Because of the extreme inhomogeneity (in both material and conformational senses) of the suburban surface, the direct measurement of canopy layer storage is an all but impossible task, and was not attempted in this study. Fortunately the canopy layer storage is expected to be a very conservative variable, and can be parameterized from the net all-wave radiation (Kalanda, 1979; and Oke, et al., 1979). This parameterization has the form:

$$\Delta Q_S = 0.24(Q^* - 17.0) \qquad (E.2)$$

when $Q^* \geq 5.5\ W m^{-2}$

and $$\Delta Q_s = 0.70\ Q^* \tag{E.3}$$

otherwise.

Given the three measured quantities and this parameterization, there are five different energy budgets that can be constructed (three closed and two open). The following (unfortunately somewhat complicated) notation is introduced in order to illustrate the five budgets.

Q^* - net radiation as measured.

ΔQ_s - canopy layer heat storage, parameterised as eqns (E.2) and (E.3).

Q_H - turbulent sensible heat flux as measured by the YST system.

β - Bowen ratio as measured by the differential psychrometer system.

Q_H' - turbulent sensible heat flux, calculated as $\frac{\beta}{(1+\beta)}(Q^* - \Delta Q_s)$

Q_E' - turbulent latent heat flux, calculated as $\frac{1}{(1+\beta)}(Q^* - \Delta Q_s)$

Q_E'' - turbulent latent heat flux, calculated as Q_H/β.

Q_E''' - turbulent latent heat flux, calculated as $Q^* - Q_H - \Delta Q_s$.

$\Delta Q_s'$ - canopy layer heat storage calculated as $Q^* - Q_H - Q_E''$.

The three closed budgets are:

$$Q^* = Q_H' + Q_E' + \Delta Q_s \tag{E.4}$$

This budget is independent of the YST system.

$$Q^* = Q_H + Q_E'' + \Delta Q_s' \tag{E.5}$$

This budget uses data from both the differential psychrometer and YST systems and does not use the parameterizations for canopy layer heat storage.

$$Q^* = Q_H + Q_E''' + \Delta Q_s \qquad (E.6)$$

This budget is independent of the differential psychrometer system. The two open budgets are:

$$Q^* = Q_H + Q_E' + Q_s + \varepsilon_1 \qquad (E.7)$$

and

$$Q^* = Q_H + Q_E'' + Q_s + \varepsilon_2 \qquad (E.8)$$

Both open budgets utilize data from both the differential psychrometer and yaw sphere-thermometer systems and are closed by the residuals ε_1 and ε_2.

The core observational period consisted of some 480 hourly intervals. If, during a given interval, the yaw sphere-thermometer system was not operative, the budget shown in (E.4) had to be used. Similarly (E.6) was used when the differential psychrometer system was not operative. These cases covered 220 hourly intervals. Some decision network had to be set up in order to decide on the best estimates of the various fluxes during the remaining intervals. One rational approach to this problem was to divide these 260 intervals into four classes as follows (based on the open budgets).

i) Complete agreement.

The two budgets given by (E.5) and (E.6) were judged to be in complete agreement when there was termwise agreement of the three right hand terms to within a (small) error, here taken to be $0.125Q^* + 10.0$ W m^{-2}.

ii) Obvious error in one term.

A budget was judged to be obviously in error if it met any of the following conditions

a) positive canopy layer heat storage with negative net radiation (or the converse).

b) turbulent sensible heat flux greater than net radiation.

c) turbulent latent heat flux greater than 1.25 times net radiation.

iii) Incomplete Agreement.

The two budgets were judged to be in incomplete agreement if they passed the "obvious error" filter, had both turbulent terms less than $0.70Q^*$, and did not fit into class i).

iv) All cases not fitting into the above classes.

In the class i) budgets, the best estimates of the fluxes were taken to be the means of the fluxes in the budgets (E.5) and (E.6). In the class ii) budgets, the budget obviously in error was rejected and the alternative one used as the best estimate. The class iv) budgets were generally for intervals when Q^* was very small, the ambiguities being the result of measurement errors masking the actual fluxes. An examination of the terms usually showed one or the other budget to be in error. The class iii) budgets were subjected to scheme whereby the residuals ε_1 and ε_2 were distributed into the turbulent terms in the ratio of the absolute magnitude of estimated errors in those terms. The decision tree whereby the budgets were determined is schematically shown in Figure E.1, the bracketed numbers being the number of cases (hourly averages) that fell into each category.

The open budgets were considered to be open because of measurement errors rather than advective effects. This is consistent with our assumption of effective surface homogeneity (see Appendix A) and is supported by Figure E.2 which shows the residual ε_1 to be independent of wind direction (ε_2 has a similarly random distribution). For these reasons the residuals are considered to be energy which must be distributed amongst the two turbulent terms, these being subject to the most uncertainty in measurement.

Figure E.3 shows the frequency distribution of the residuals ε_1 and ε_2. They both have near-zero means and are strongly leptokurtic, ε_1 being the more extreme. For this reason (E.7) was chosen as the open budget, and ε_1 was distributed between Q_H and Q_E' according to the following scheme.

Consider the following open energy budget:

$$Q^* = Q_H + Q_E + \Delta Q_s + \varepsilon$$

(the complex notation has been dropped for clarity). The residual ε is assumed to be composed of two portions arising from measurement errors in the two turbulent terms only viz:

$$Q^* = (Q_H + \varepsilon_H) + (Q_E + \varepsilon_E) + \Delta Q_s$$

where $\varepsilon_H + \varepsilon_E = \varepsilon$, and our estimated turbulent fluxes are:

$$\hat{Q}_H = Q_H + \varepsilon_H$$

$$\hat{Q}_E = Q_E + \varepsilon_E.$$

No Q_H	Use $Q^* = Q_H' + Q_E' + \Delta Q_S$	(68)
Budgets 1, 2 and 3 agree to within δQ[1]	Use $Q^* = \frac{Q_H + Q_H'}{2} + \frac{Q_E' + Q_E'}{2} + \frac{\Delta Q_S + \Delta Q_S'}{2}$	(8)
If $Q^* > 0$ and $Q_H > Q_*$	Use $Q^* = Q_H' + Q_E' + \Delta Q_S$	(41)
If $Q^* > 0$ and $Q_E' > 1.25\ Q^*$	Use $Q^* = Q_H + Q_E''' + \Delta Q_S$	(19)
If $Q^* < 0$ and $\Delta Q_S' > 0$	Use $Q^* = Q_H' + Q_E' + \Delta Q_S$	(1)
If $Q^* \geq 0$ and $\Delta Q_S' < 0$	Use $Q^* = Q_H' + Q_E' + \Delta Q_S$	(14)
Q_H, Q_H', Q_E, Q_E', all less than $\delta Q'$[2]	Use distributed residual budget.	(62)
Class IV budget (subjective decision necessary).		(35)

Figure E.1: Decision tree for closure of energy budget.

The number of cases in each category is given on the right.

Notes: 1. $\delta Q = 0.125\ Q^* + 10.0\ W\ m^{-2}$

2. $\delta Q' = 0.7\ Q^*$

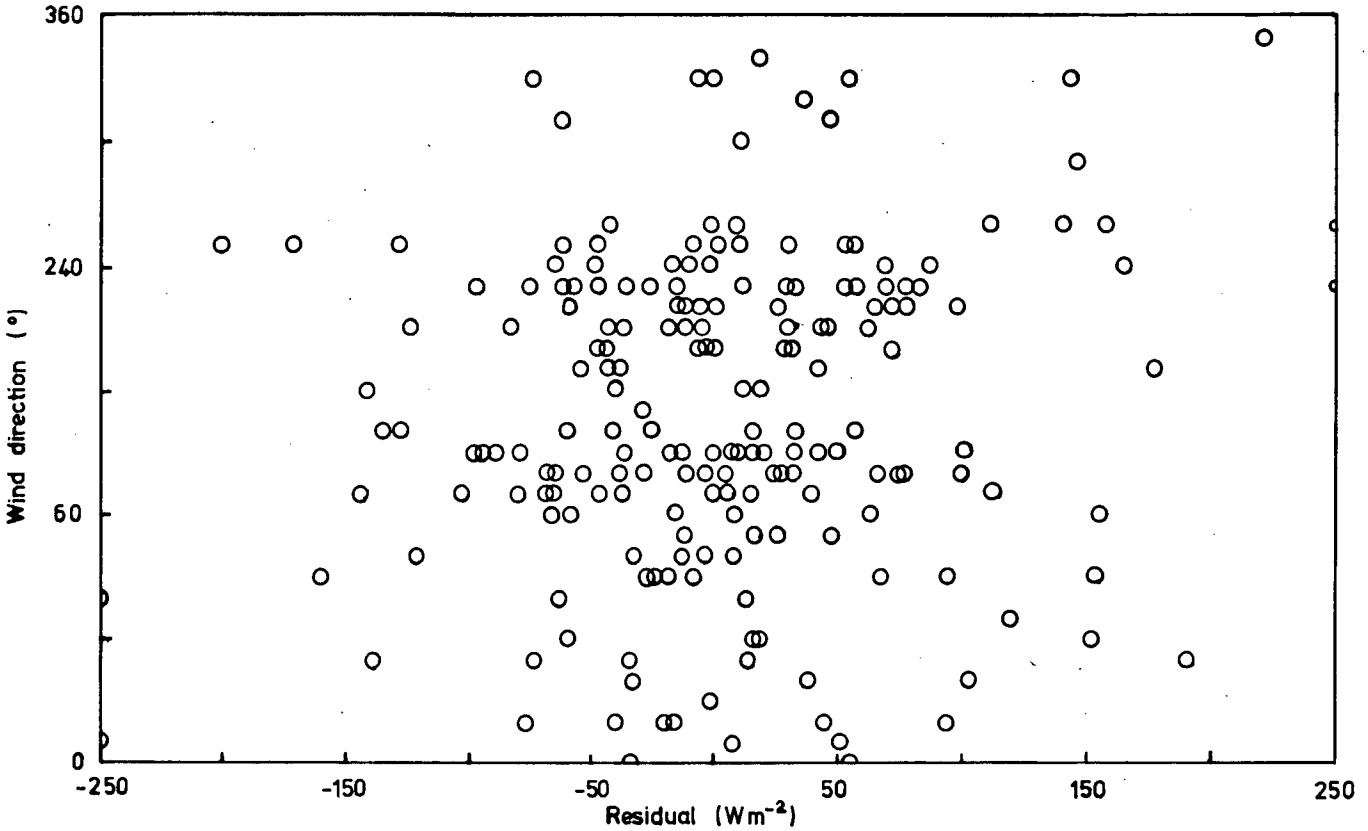

Figure E.2: Residual ε_1 vs Wind Direction

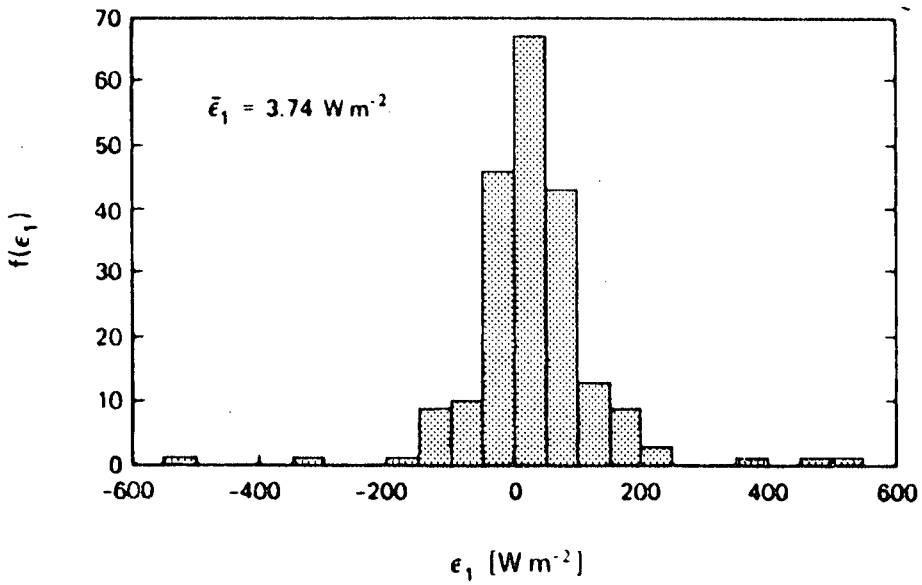

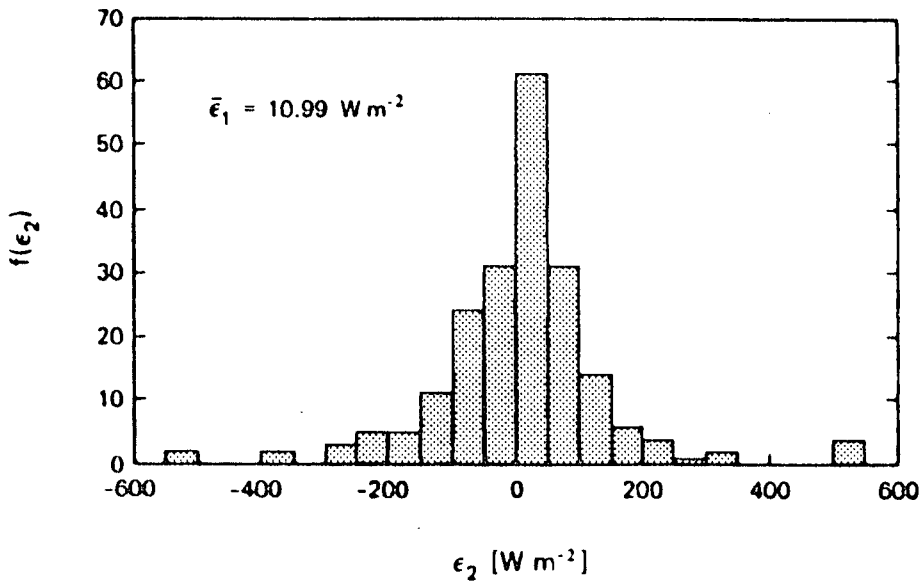

Figure E.3: Frequency Distribution of ε_1 and ε_2.

A statistical treatment of experimental data yields probable errors δQ_H and δQ_E in the two fluxes (Fuchs and Tanner, 1970; Bailey, 1977; Kalanda, 1979). We require that:

$$\varepsilon_H/\varepsilon_E = \pm\ \delta Q_H/\delta Q_E = \pm\ r$$

Solving for ε_H and ε_E leads to

$$\varepsilon_H = \varepsilon/(1 \pm r)$$

$$\varepsilon_E = \varepsilon/(1 \pm 1/r)$$

where the positive sign is for δQ_H and δQ_E having the same sign and the negative for their having opposite signs. Since the sign of the error cannot be determined from the error analysis, the residuals must be calculated for both cases and the resulting energy budgets examined. The most reasonable estimate of fluxes will always be obvious. An example is drawn from the data on the 27th of July for the hour ending 1700 LST (Local Solar Time).

$$\begin{array}{ccccccccc} Q^* & & Q_H & & Q_E' & & Q_S & \varepsilon & \delta Q_H \quad \delta Q_E \\ 149.1 & = & 95.0 & + & 67.8 & + & 34.3 & - 48.0; & 17.3,\ 19.2 \end{array}$$

(all fluxes in W m^{-2}).

For the positive sign,

$$149.1 = 69.7 + 45.8 + 34.3$$

For the negative sign,

$$149.1 = 389.8 - 504.5 + 34.3.$$

Quite obviously the first form is the more realistic one, and both fluxes had been overestimated by the instrumentation. A second example is from the hour ending 0900 LST on the 5th of August.

$$Q^* \quad Q_H \quad Q_E' \quad Q_s \quad \varepsilon \quad \delta Q_H \quad \delta Q_E$$

$$382.5 = 313.0 + 46.1 + 87.7 - 64.3; \quad 17.1; \quad 36.3$$

Positive r: $382.5 = 269.3 + 25.5 + 87.7$

Negative r: $382.5 = 191.7 + 103.1 + 87.7$.

The second case is taken to be the best estimate as the Bowen's ratio in the first case is unrealistically high. The instrumentation overestimated Q_H and underestimated Q_E in this case.

E.2 Examples of an Urban Surface Energy Budget

A previous energy budget study at this site (Kalanda, 1979; Kalanda et al., 1980) utilized only the differential psychrometer system for estimating the turbulent fluxes (the budget is as eqn. (E.4)). Energy budgets measured in that study are not significantly different from those of the present study and exhibit the usual temporal variation of fluxes and the relative magnitudes of Q_H, Q_E and ΔQ_s now known to typify urban surfaces (Oke, 1978). Figure E.4 is an example of a 24 h surface energy budget for the urban surfaces surrounding the Mainwaring Substation. The entire energy budget is not explicitly utilized in this study, but the surface turbulent sensible heat flux is a crucial parameter in both Parts One and Two. The extra effort involved in determining the entire budget was deemed justified by the increased confidence in Q_H when the other three terms were determined and shown to be reasonable.

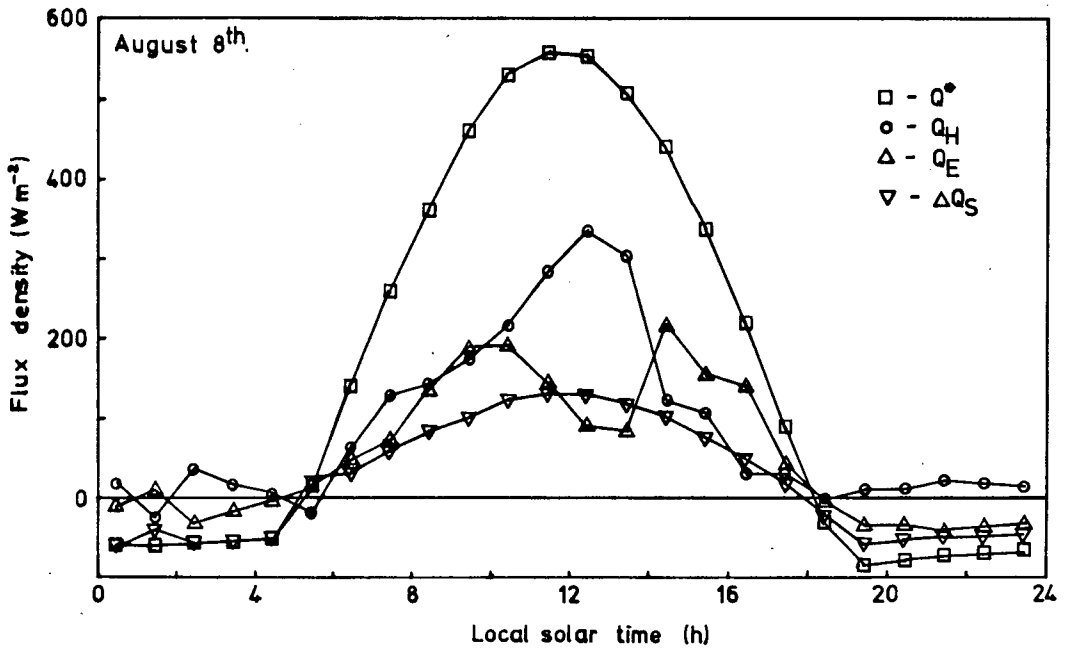

Figure E.4: Suburban Surface Energy Budget.

F. Spectral Analysis

The magnetic tapes containing the Gill UVW signals, collected, filtered and recorded as in Section B.2.1 were transferred to The University of British Columbia Computing Centre for analysis. The first step in this analysis was to sweep the data off the PDP tapes and demultiplex the three velocity signals. At this step, single- and double-point data spikes were removed by replacing them with adjacent values. Each triplet (u, v and w) was then transformed according to Horst (1973) to remove the by now well-known response errors inherent in this instrument (Drinkrow, 1972; Hicks, 1972; Gill, 1973; and Fichtl and Kumar, 1974). The data thus transformed was calibrated using coefficients determined before and checked after the study period, and written to magnetic tape in blocks of 2048 triplets. Each raw data block was slightly over an hour in extent. At a sampling rate of 2.5 Hz, four of these smaller blocks gave some 54 min of data, allowing leading and trailing discards of approximately 5 min each. This selected subset of data was then examined for trends and discontinuities and those hours with strong trends or marked discontinuities discarded, leaving 62 "hours" of usable data for further analysis. This selected data was then transformed into flow co-ordinates using the means produced by the previous program and standard co-ordinate rotation forms. After transformation, the time series was split into mean and fluctuating parts by subtraction of a linear trend, the fluctuating part being saved for further analysis. The signals produced by this process were used to generate the integral statistics presented in Section 3.2.1. The next stage of analysis involved the use of a standard Fast Fourier Transform (FFT) routine to produce energy density spectra of the three velocity components. The data blocks were grouped into

stability (z/L) classes as described in Section 3.2.1, and the spectra combined to produce ones representative of each stability class. This was achieved by averaging the spectral amplitudes from all eight data blocks in each z/L class into bands, each of width 0.1 units of non-dimensional frequency ($f = nz/\overline{u}$) in log space. Because of this form of band-averaging, the high frequency points are averages of large numbers of determinations ($\sim$ 4000), the low frequency points being derived from a much smaller number ($\sim$ 8), thus resulting in some scatter at the low frequency end. The spectra were then plotted in a variance-preserving form and a smooth curve drawn by eye. Figure F.1 shows a typical spectrum, illustrating the low frequency scatter. The slight scatter in the high frequency points is due to a small amount of aliasing in the spectral analysis of some of the runs. These smoothed spectra were then replotted (on one set of axes for each component). Figure F.2 (a, b, and c) shows the results of this replotting, and indicates that spectral forms are largely independent of stability. No systematic ordering of curves with stability could be discerned, presumably due to purely statistical fluctuation masking the weak trends with stability mentioned in Section 3.2.2.

A single smoothed spectrum was drawn by eye from the mean position of the cluster of lines in Figure F.2, and digitized for use in determining the dispersion functions. These are the spectra shown in Figure 3.4. For the reasons given in Section 3.3.2, no attempt was made to correct the spectra for the less than perfect high-frequency response of the sensors.

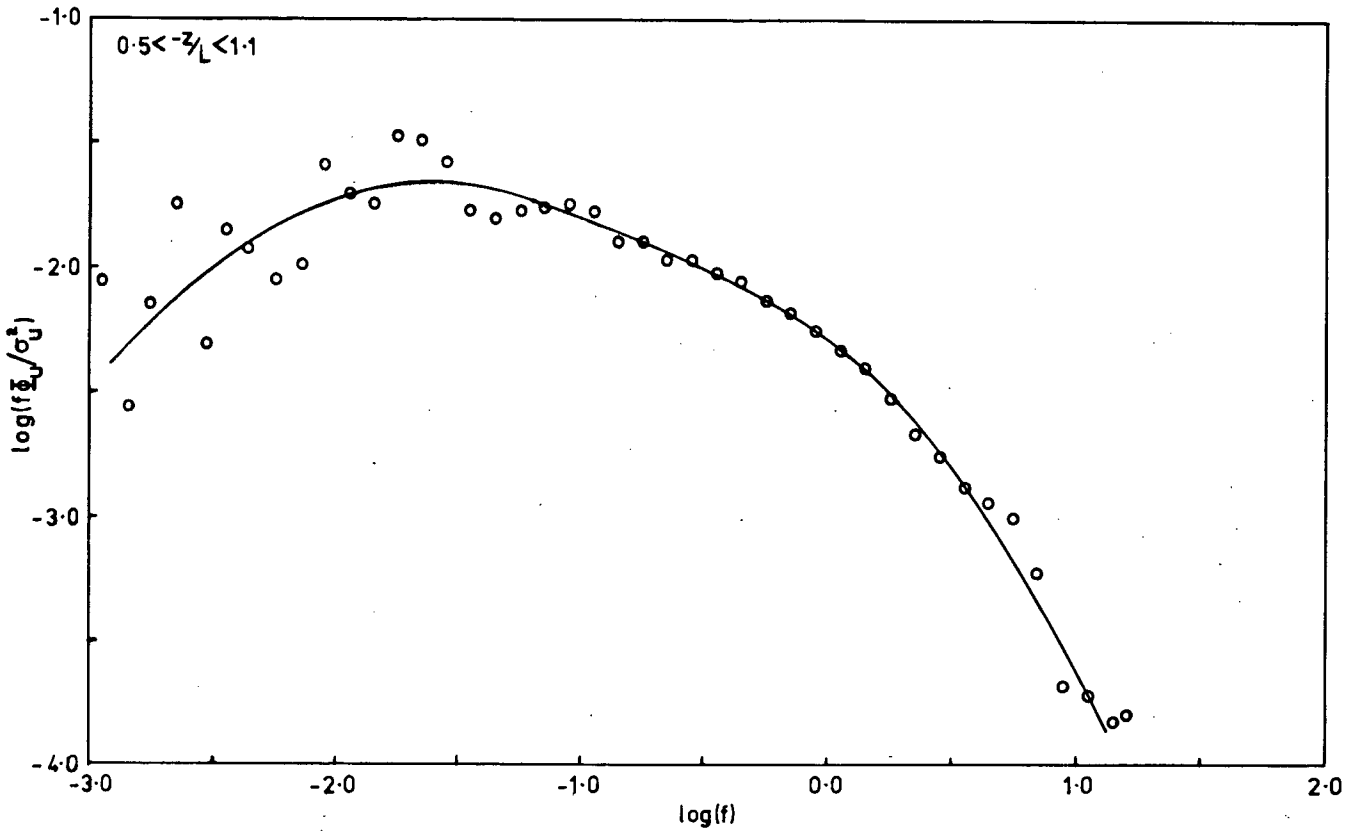

Figure F.1: Spectrum for a Single Stability Class.

Symbols indicate individual amplitudes.

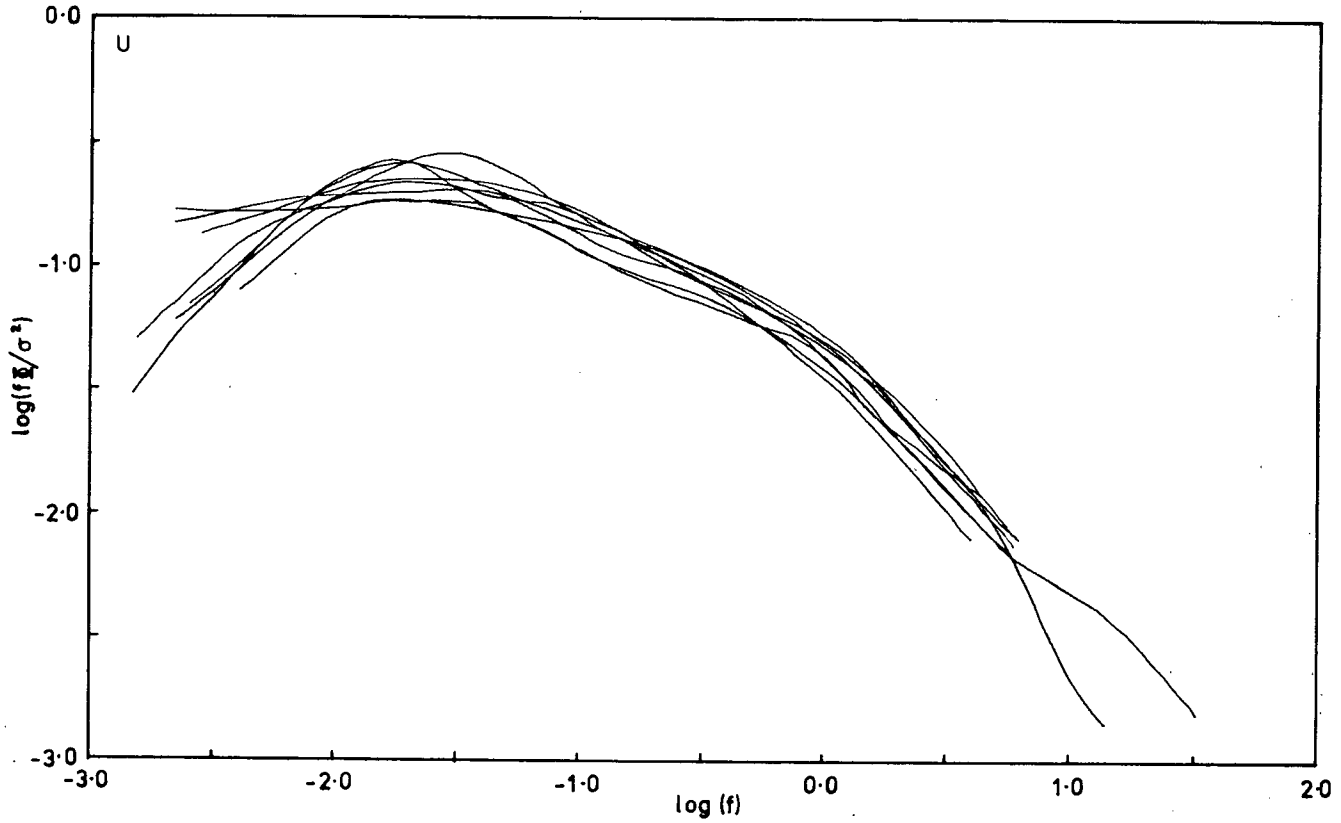

Figure F.2a: Construction of Composite Spectrum.

Alongwind component.

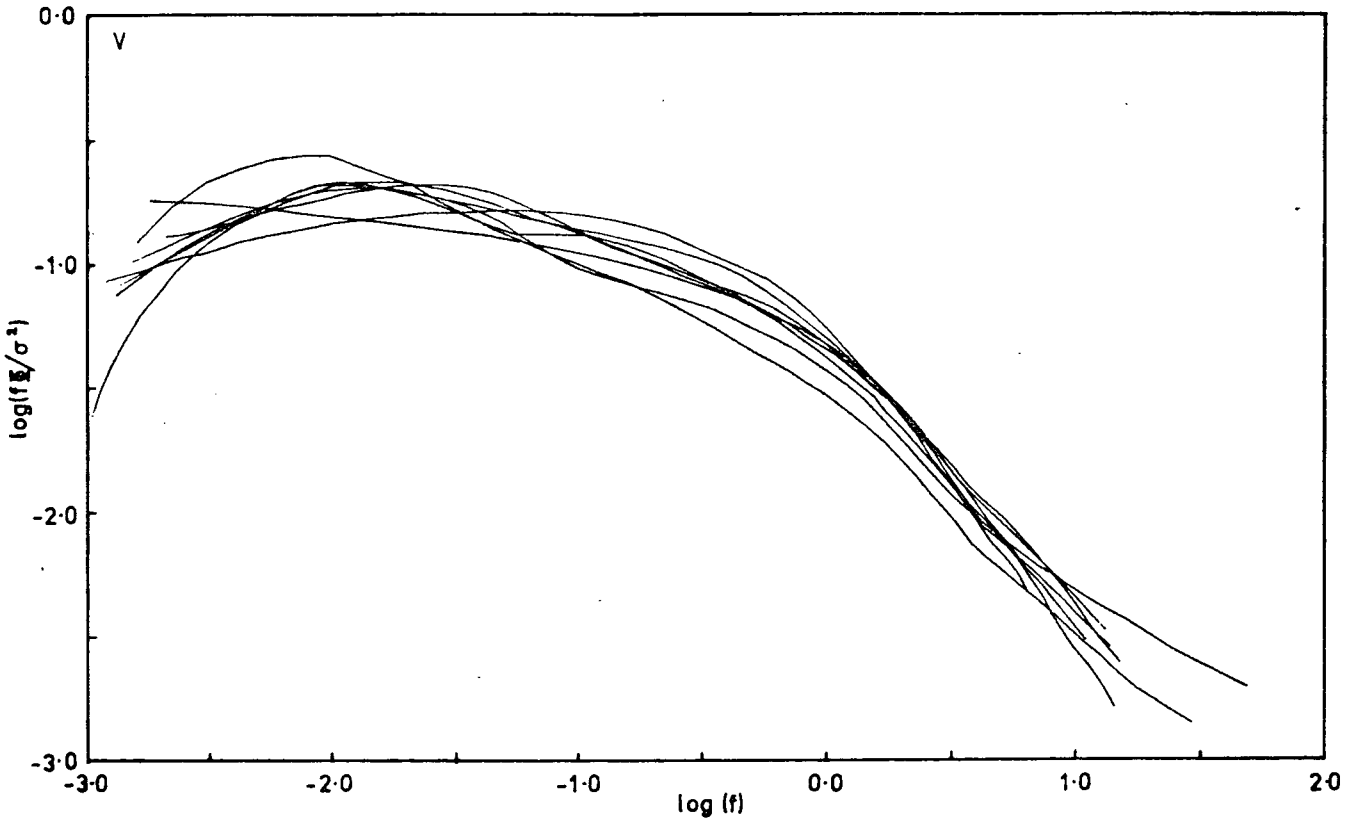

Figure F.2b: Construction of Composite Spectrum.

Crosswind Component.

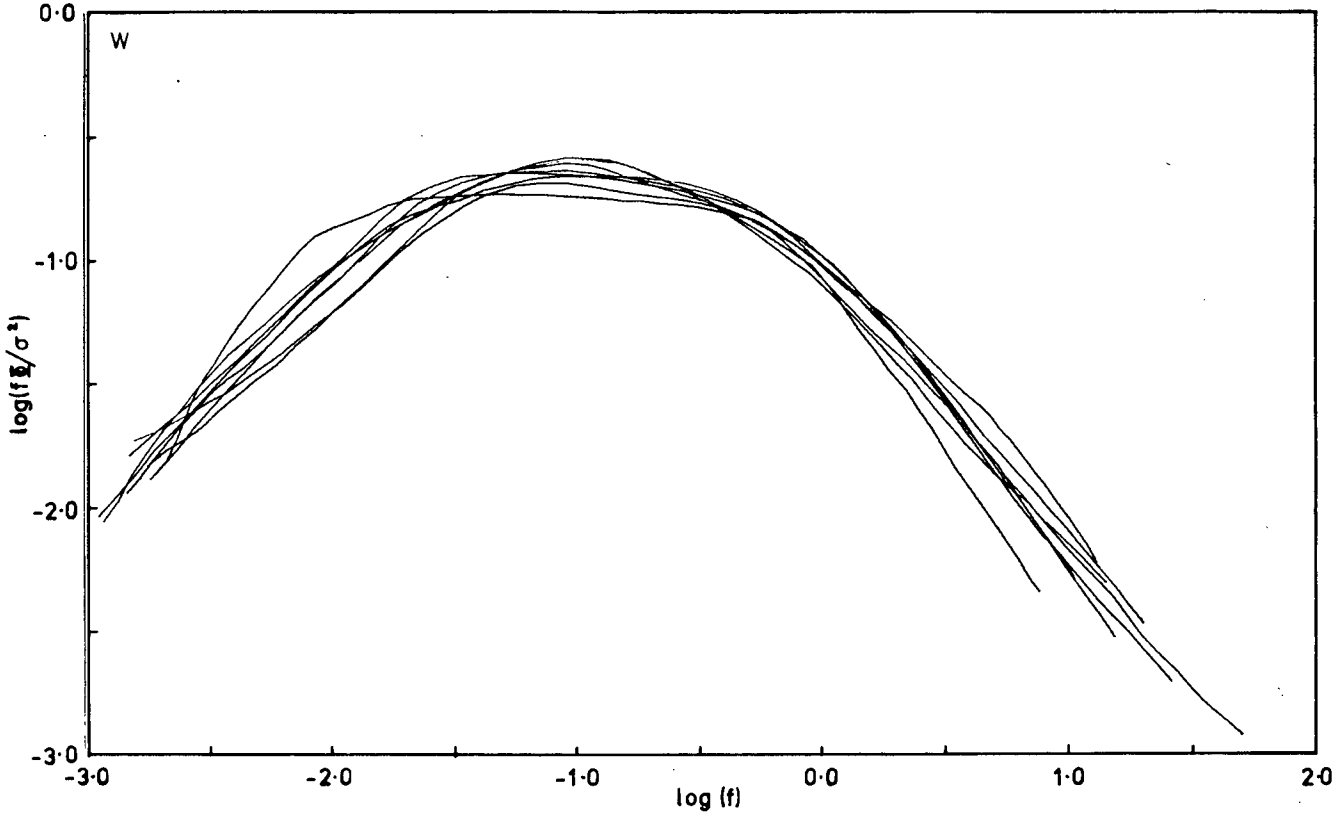

Figure F.2c: Construction of Composite Spectrum.

Vertical component.

G. Program to Compute Dispersion Function from Digitized Spectra

```
CCCCCCC INTEGRATE DISPERSION FUNCTION FROM DIGITIZED SPECTRUM
      DIMENSION F(100),Y(100),FN(100),FI(100),TI(100),A(3)
CCCCCCC READ HEADING CFF DIGITIZED SPECTRUM FILE
      READ(7,103)A(1),A(2),A(3)
 103  FORMAT(3A4)
      N=1
CCCCCCC READ DIGITIZED SPECTRAL CO-ORDINATES IN LOG SPACE
 66   READ(7,100,END=11)DX,DY
CCCCCCC CONVERT CO-ORCINATES TO LINEAR SPACE
      F(N)=10.0**DX
      Y(N)=(10.0**DY)/F(N)
      N=N+1
      GO TO 66
 11   N=N-1
CCCCCCC LOOP THROUGH TRAVEL TIME 0 TO 150 IN 3S
      DO 22 JT=1,51
      TI(JT)=FLOAT(JT-1)*3.0
CCCCCCC LOOP THROUGH SPECTRAL CO-ORDINATES
      DO 33 JK=1,N
      F1=TI(JT)*F(JK)*6.283185
      F2=SIN(F1)
      IF(F1.EQ.0.0)GO TO 55
      F3=F2/F1
      GO TO 33
 55   F3=1.0
CCCCCCC COMPUTE INTEGRAND
 33   FN(JK)=Y(JK)*F3*F3
CCCCCCC INTEGRATE FUNCTION
      FI(JT)=SQRT(QINT4P(F,FN,N,1,N))
 22   CONTINUE
CCCCCCC CHECK OUTPUT SPECTRAL INTEGRAL
      AINT=FI(1)
      WRITE(6,101)AINT
 101  FORMAT(1X,'      T*     F(T*)',3X,F7.5)
CCCCCCC OUTPUT TABLE AND PLOT F(T*)
      DO 44 JK=1,51
      FI(JK)=FI(JK)/AINT
      WRITE(6,102)TI(JK),FI(JK)
      TI(JK)=TI(JK)/25.0
 44   FI(JK)=FI(JK)*5.C
 102  FORMAT(2X,F6.0,3X,F6.4)
      CALL AXIS(0.0,0.0,'T*',-2,6.0,0.0,0.0,25.0)
      CALL AXIS(0.0,0.0,'F(T*)',+5,5.0,90.0,0.0,0.20)
      CALL LINE(TI,FI,51,+1)
      CALL SYMBOL(0.5,4.6,0.14,A,0.0,12)
      CALL PLOTND
      STOP
 100  FORMAT(2F9.3)
      END
```

H. Application of the Dispersion Functions

The dispersion functions given in Equations (4.1) and (4.2) may be used to estimate plume spread from basic meteorologic variables, and utilizing accepted relations between these variables. Three examples follow, relying to varying degrees on direct measurement.

Example 1.

If the mean wind speed and variances of the horizontal wind components are known from measurement, the plume width at a given height may be estimated as follows:

$$\overline{u} = 5.0 \text{ m s}^{-1}$$

$$\sigma_u = 0.50 \text{ m s}^{-1}$$

$$\sigma_v = 0.38 \text{ m s}^{-1}$$

$$z = 20.0 \text{ m}$$

At a travel time of 60s for example (amounting to a downwind distance of 300 m), the non-dimensional travel time is:

$$t^* = t\sigma_u/z = 1.50$$

The dispersion function (from Equation 4.1) is:

$$S_y = 0.57$$

so

$$\sigma_y = S_y t/\sigma_v$$

$$= 90 \text{ m}$$

Example 2.

The above example requires considerable measurement. In the absence of that degree of knowledge of atmospheric variables, a neutrally stratified atmosphere or one with high wind speed (> 10 m s^{-1}; Pasquill (1974))

may be quite easily treated, requiring knowledge of the mean wind speed and Counihan's (1975) equations. An estimate of the aerodynamic roughness length must be made on the basis of the surface type. This estimate may be based on Counihan's (1975) Figure 8, a mean wind speed of 10 m s^{-1} over surface type 3 gives the following results.

$$0.2 < z_o < 1.0 \text{ m, take } z_o = 0.6 \text{ m.}$$

From Counihan's (1975) Equation 4

$$\sigma_u = 2.28 \text{ m s}^{-1} \quad \text{for } z = 20 \text{ m}$$

and $\sigma_v = 1.71$ m s^{-1} from Counihan's (1975) Equation 3.

The values of $\overline{u}$, σ_u, σ_v and z can now be applied as in Example 1 to provide an estimate of σ_y (the result for t = 60 s is σ_y = 9.7 m).

Example 3.

In an unstable atmosphere, in the absence of measured wind variances, some estimate of the turbulent sensible heat flux must be available, either through direct measurement or parameterization. The former method is demanding in terms of instrumentation and operational requirements and the latter is at best rough with the currently available schemes.

Given a measured value of Q_H, a value for $u_*/\overline{u}$ may be estimated from Pasquill's (1974) Figures 6.3 and 6.4, using a value of z_o obtained as in example 1. Pasquill's (1974) Figure 6.5 may then be used to estimate the Monin-Obukhov length L. Panofsky et al.'s (1977) forms for σ_i/u_* as functions of z/L and z_i/L will provide estimates of σ_u and σ_v which will allow estimation of σ_y as in example 1. for a given wind speed.

I. Theodolite-Tracked, Balloon-Borne Temperature Soundings

Data from the theodolite sightings (altitude and azimuth) together with temperatures from the mini-sonde sensors (see Appendix B.2.6) were fed into a computer program based on the method of Thyer (1962). This program generated profiles of wind-speed, wind-direction and temperature and provided estimates of the height of the balloon at each sighting. The positions of the balloon as determined by this method are subject to errors related to the geometry of the tracking system and can be prohibitively large, as indicated by Schaefer and Doswell (1978) and Netterville and Djurfors (1979). These errors are inherent in the technique and can be minimized by ensuring that the apex angle of the theodolite-balloon-theodolite triangle does not become too small. This was not a problem in this study as the most useful information came from the sonde at altidues of less than 700 m which (with a 300 m base-line) was well within the region of acceptable errors. With each height determination, the program computes two forms of error estimate. One is based on the analysis of Schaefer and Doswell (1978) which gives an estimate of the maximum probable error in height from the tracking system geometry. The second error estimate is the length of the "short line" which is the shortest distance between the sighting lines from the two theodolites. This quantity is a measure of the overall consistency of the sighting. These two error estimates were used as guides in interpreting profiles from these soundings.

In order to produce detailed potential temperature profiles the temperature-time output of the radiosonde receiver was digitized at approximately 0.2 min intervals and those values fed into a computer program together with the theodolite-determined heights for the first

six minutes of that flight. This corresponds to approximately 1100 m of rise at the mean rise rate of 3.1 m s^{-1}. The temperature-time pairs were then converted to temperature-height pairs using linearly interpolated heights between the theodolite determined ones. The temperatures were then converted to potential temperature (adjusted for mean pressure changes as measured at Vancouver International Airport) and plotted as potential temperature profiles, examples of which are shown in Figures 6.2 and K.1.

The intensity of the inversion immediately above the mixed layer was extracted graphically from these profiles and used as input to the mixed layer depth model (see Sections 7.1 and 7.2). The temperature of the mixed layer was estimated from the approximately adiabatic portion of the profile and used for comparison with the model's prediction. The initial temperature of the mixed layer was determined by extending the early morning capping inversion profile down to the measured (by acoustic sounder) initial inversion height. This temperature was usually found to be in good agreement with the minimum morning temperature measured at the top of the tower. The use of these profiles in determining the subsidence rate is illustrated in Appendix K.

One of the required variables in the implementation of the mixed layer depth model is the mean wind speed in the mixed layer. Point estimates of this quantity are available from the position of the balloon at each pair of sightings. The theodolite data is analysed by a program which provides profiles of wind speed, from which reasonable estimates for the height-averaged mean may be drawn. The hourly mean wind speeds at the top of the tower are plotted against these mixed layer values on Figure I.1 which shows a strong relationship between the two. The linear regression equation being

$$\overline{u}_{tower} = -0.32 + 1.02\ \overline{u}_{balloon}$$

On the strength of this result, the model input is simply the hourly averaged mean wind speeds from the top of the tower.

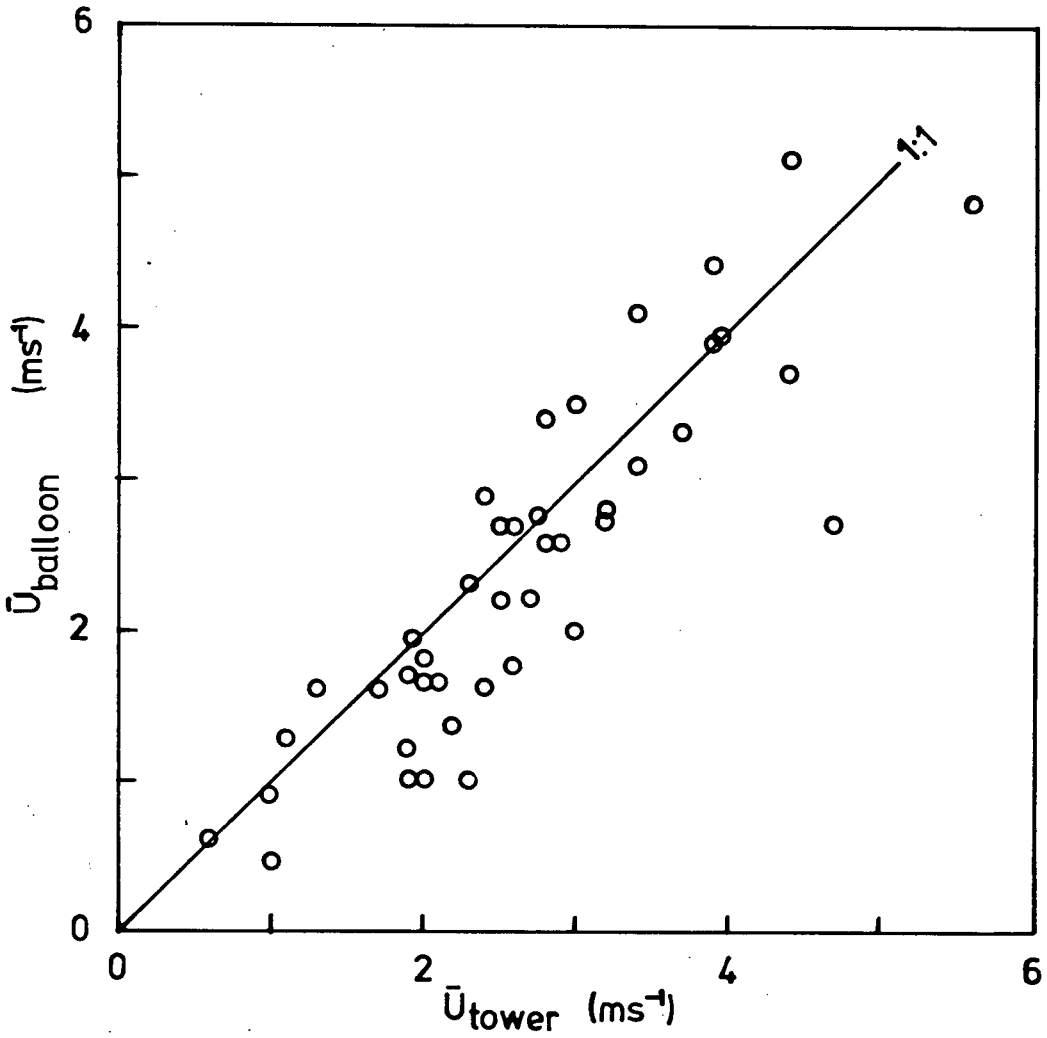

Figure I.1: Hourly mean wind speeds from the top of the tower and from the balloon sonde.

J. Comparison of Acoustic and Balloon Soundings

As well as providing valuable information about subsidence rates and inversion intensities the potential temperature profiles were used to indicate the position of the inversion base in relation to the wide and often diffuse band on the acoustic sounder trace. The potential temperature profiles generally showed clear discontinuities which were taken to be the inversion base (Coulter, 1979). This level was generally found to be within the elevated scattering band from the acoustic sounder. Figure J.1 shows a comparison of the inversion height as measured by the acoustic sounder and as determined from the potential temperature profiles. The diagonal line represents agreement. The data show no obvious trend and indicate that statistically the best estimate of inversion height will be given by the centre of the scattering band on the acoustic sounder record.

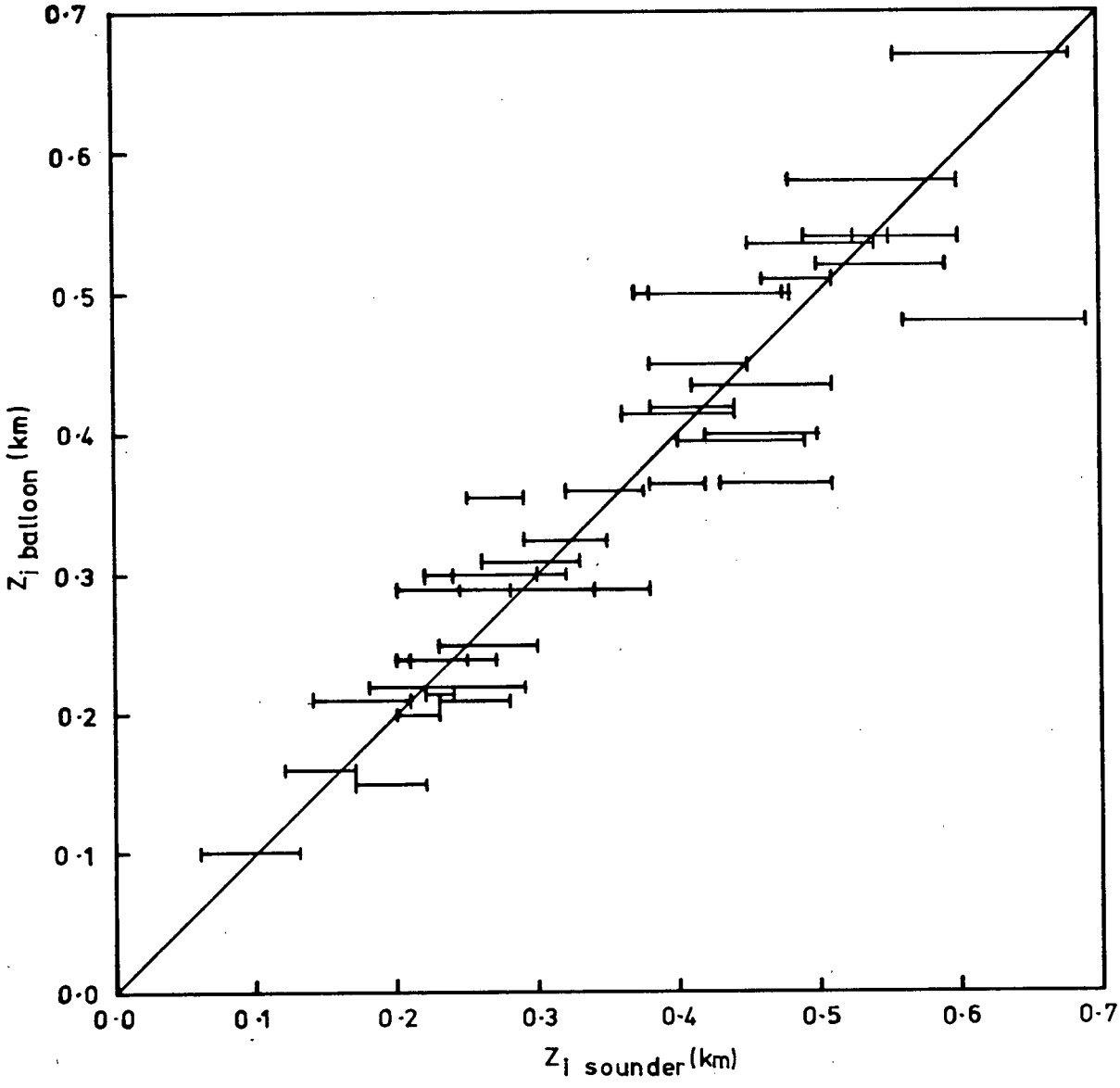

Figure J.1: Inversion height from acoustic sounder and potential temperature profile.

K. Subsidence Estimation from Potential Temperature Profiles

Estimates of the horizontal divergence (see Section 6.3.1) can be obtained by observing the subsidence of features in the potential temperature profiles above the inversion base. A pair of such profiles is shown in Figure K.1, where a "kink" in the potential profile is clearly defined in two soundings separated by 2 h, in this time the "kink" had subsided by 154 m. This thermal feature was clearly evident throughout that day (August 8th), exhibiting a slow downward movement.

Equation (6.12) is an exact form for the subsidence, followed by the successive approximations of (6.13) and (6.14). Representing these forms by the general function $w(\theta_o,\gamma,\alpha,\beta,z)$, we want to solve

$$\frac{dz}{dt} = w(\theta_o,\gamma,\alpha,\beta,z). \tag{K.1}$$

Clearly the first four arguments of w are unknown functions of time and the equation is insoluble. If we presume them to be approximately constant and replace them by their mean values from Figure K.1, then substitution of (6.13) for w renders (K.1) soluble. The use of the approximate form (6.13) is justified here since the conditions of the approximation are met (see Section 6.3.1).

$$\frac{dz}{dt} = -\beta z \frac{\theta_o b + 2\gamma(1 - \alpha)}{b(\theta_o + \gamma(1 - \alpha)z)}$$

Integrating this leads to:

$$\beta = \frac{b}{(\theta_o b + 2\gamma(1 - \alpha))(t_1 - t_2)} (\theta_o \ln(z_2/z_1) + \gamma(1 - \alpha)(z_2 - z_1)) \tag{K.2}$$

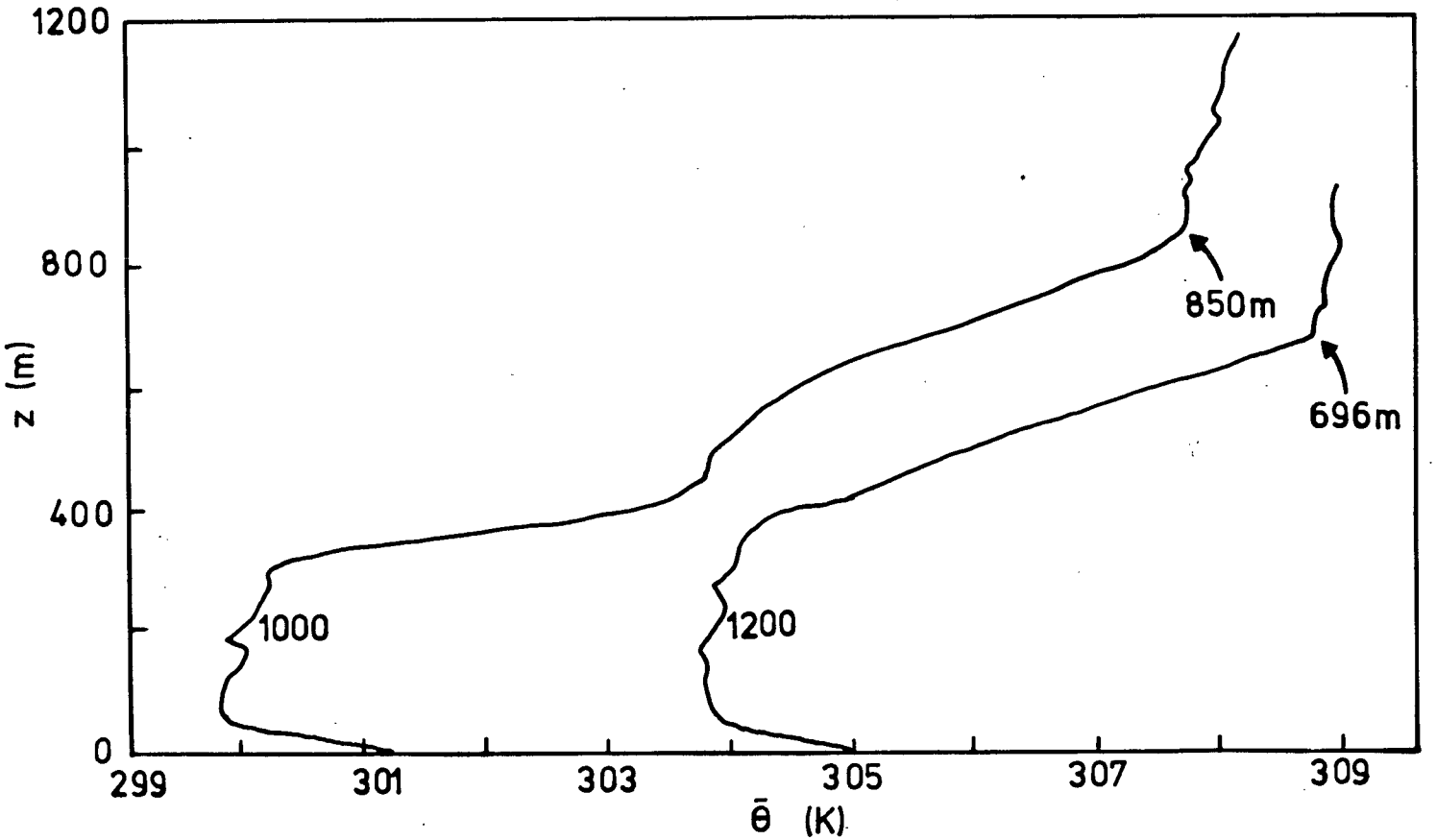

Figure K.1: Subsidence in potential temperature profiles on August 8th.

The subsiding "kink" is indicated by an arrow, in each case, with its height in metres. Relevant parameters are as follows -

Time	(LST)	1000	1200
z_{kink}	(m)	850	696
γ	(K m^{-1})	0.0176	0.0171
$\bar{\theta}$	(K)	300.1	303.1
z_i	(m)	315	370

Substituting the mean values of θ_0, γ and α and the values for z_1, z_2, t_1 and t_2 from Figure K.1 leads to:

$$\beta = 1.74 \times 10^{-5}\ s^{-1}\ ,$$

a typical value in this study.

If the second (and also justifiable) approximation (Equation 6.14) is taken, a similar analysis results in

$$\beta = 2.78 \times 10^{-5}\ s^{-1}\ .$$

Similar analyses were performed for as many pairs of flights as possible on each day on which the inversion height model was tested, a single constant value of β being input for the synoptic scale subsidence for each day.

L. Mixed Layer Depth Program and Sample Data

FORTRAN IV program to simulate inversion rise.

```
      DIMENSION QH(14),A(7),ZI(140),TH(140),DT(140),VP(3),TV(6)
      DIMENSION THE(14)
      DIMENSION T(140),S(2),GAM(14),UB(14),V(3),QHI(10),THV(6)
      COMMON A,P2,TIS,B
      EXTERNAL F
CCCCCCC BDY LAY SIM PIGGY , BACK PLOT , WITH SUBSIDENCE HTNG.
CCCCCCC READ BOUNDARY CONDITIONS AS HOURLY AVERAGED VALUES OF SENSIB
CCCCCCC LE HEAT FLUX, LAPSE RATE, MEAN WIND SPEED, MEAN WIND DIRECTI
CCCCCCC N, AND INITIAL INVERSION HEIGHT, MIXED LAYER TEMPERATURE, DA
CCCCCCC TE, TWO PARAMETERS, START TIME AND EXPONENT FOR MESO SCALE
CCCCCCC SUBSIDENCE, AND MEASURED TIME AND MEAN TEMPERATURE OF MIXED
CCCCCCC LAYER.
      READ(5,100)QI,(QH(I),I=1,14),QF,(GAM(I),I=1,14),(UB(I),I=1,14)
     1,(THE(I),I=1,14),ZIO,THO,B,S(1),S(2),P1,P2,ITS,FB,GO
     2,(TV(I),THV(I),I=1,6)
CCCCCCWRITE(6,103)S(1),S(2)
      C=0.20
      N=3
      REL=1.0E-10
      ABS=1.0E-10
      DTO=0.1
CCCCCCC LOOP THROUGH FOURTEEN HOURS
      DO 22 J=1,14
CCCCCCC INTERPOLATE QH AT TEN POINTS WITHIN THIS HOUR.
      DO 77 IK=1,10
      IF(J.EQ.1)GO TO 99
      Q1=QH(J-1)
      GO TO 55
 99   Q1=QI
 55   Q2=QH(J)
      IF(J.EQ.14)GO TO 44
      Q3=QH(J+1)
      GO TO 222
 44   Q3=QF
 222  IF(IK.GT.5)GO TO 88
      DQ=(Q2-Q1)/10.0
      QHI(IK)=Q1+DQ*FLOAT(IK+5)
      GO TO 77
 88   DQ=(Q3-Q2)/10.0
      QHI(IK)=Q2+DQ*FLOAT(IK-5)
 77   CONTINUE
CCCCCCC LOOP THROUGH TEN SIX MINUTE INTERVALS
      DO 11 K=1,10
      JK=10*(J-1)+K
      JK1=JK-1
      IF(QHI(K).LT.0.0.AND.J.EQ.1)GO TO 66
      IF(QHI(K).LT.0.0)GO TO 878
      IFLAG=1
CCCCCCC COMPUTE FETCH OF URBAN SURFACE FOR ELLIPTICAL CITY
      RS=7.00
      THES=0.3937
      IF(THE(J).LT.90.0) GO TO 901
```

```
      PHI=(THE(J)-90.0)*1.7453E-02
      GO TO 902
 901  PHI=(270.0+THE(J))*1.7453E-03
 902  CS=COS(PHI)**2
      SI=SIN(PHI)**2
      RP=SQRT(7056.0/(196.0*SI+36.0*CS))
      DX=1000.0*((RP*COS(PHI)+RS*COS(THES))**2
     ++(RP*SIN(PHI)+RS*SIN(THES))**2)**0.5
CCCCCCC SET COEFFICIENTS A1 TO A7
      A(1)=QHI(K)*(1.0+C)/1212.0
      A(2)=0.7171*SQRT(UB(J)*QHI(K)*P1*GAM(J)/(1212.0*DX))
      A(3)=C*QHI(K)/1212.0
      IF(JK.GE.ITS)GO TO 6
      A(4)=B
      GO TO 7
 6    A(4)=B*EXP(FB*0.1*FLOAT(JK-ITS))
 7    A(5)=SQRT(UB(J)*QHI(K)*(1.0+2.0*C)/(2424.0*GAM(J)*P1*DX))
      A(6)=GAM(J)*P1
      A(7)=B*GO
      TIS=360.0*FLOAT(JK)
      TI=0.0
      TF=360.0
CCCCCCC SET ARRAY VALUES OF INVERSION HEIGHT, MEAN TEMPERATURE AND
CCCCCCC TEMPERATURE STEP TO INITIAL OR COMPUTED VALUES.
      IF(JK1.GT.0)GO TO 67
      V(1)=THO
      V(2)=ZIO
      V(3)=DTO
      GO TO 1
 67   V(1)=TH(JK1)
      V(2)=ZI(JK1)
      V(3)=DT(JK1)
CCCCCCC COMPUTE DERIVATIVES FOR OUTPUT
      VP(2)=A(3)/V(3)-A(4)*V(2)-A(5)
      VP(1)=A(1)/V(2)-A(2)
      VP(3)=A(6)*VP(2)-VP(1)+A(7)*V(2)*EXP(B*TIS)
      WRITE(6,104)J,K,(V(I),I=1,3),(VP(I),I=1,3),(A(I),I=1,7)
CCCCCCC USE NUMERICAL SOLUTION OF DIFFERENTIAL EQUATIONS TO COMPUTE
CCCCCCC NEW VALUES OF THE THREE VARIABLES.
 1    CALL DE(F,N,V,TI,TF,REL,ABS,IFLAG)
      GO TO(3,4,1,1,1,3),IFLAG
 3    WRITE(6,101)J,K,IFLAG,TI,TF,REL,ABS,N
      GO TO 33
 4    TH(JK)=V(1)
      ZI(JK)=V(2)
      DT(JK)=V(3)
      GO TO 11
 66   DT(JK)=DTO
      ZI(JK)=ZIO
      TH(JK)=THO
 11   CONTINUE
 22   CONTINUE
CCCCCCC LOOP THROUGH ARRAYS FOR PLOTTING.
 878  DO 111 M=1,JK1
      THS=THO-2.0
      THF=THO+18.0
```

```
      T(M)=1.0+FLOAT(M)/20.0
      IF(TH(M).LT.THS)TH(M)=THS
      IF(TH(M).GT.THF)TH(M)=THF
      TH(M)=6.0+(TH(M)-THS)/10.0
  111 ZI(M)=1.0+ZI(M)/200.0
CCCCCCCALL DASHLN(.07,.07,.07,.07)
      CALL AXIS(1.0,1.0,'INVERSION HEIGHT (M)',20,5.,90.,0.,200.)
      CALL AXIS(1.0,1.0,'SOLAR TIME (H)',-14,7.0,0.0,5.0,2.0)
      CALL AXIS(1.0,6.0,'THETA (K)',9,2.,90.,THS,10.)
      CALL PLOT(1.0,8.0,+3)
      CALL PLOT(8.0,8.0,+2)
      CALL PLOT(8.0,1.0,+2)
      CALL PLOT(8.0,6.0,+3)
      CALL PLOT(1.0,6.0,+2)
CCCCCCC READ DIGITISED VALUES OF INVERSION HEIGHT FOR PLOTTING.
  444 READ(5,105,END=333)TD,ZD,NPEN
      TD=(TD-5.0)*0.5+1.0
      ZD=ZD/200.0+1.0
      CALL PLOT(TD,ZD,NPEN)
      GO TO 444
  333 CALL LINE(T,ZI,JK1,+1)
      I=0
  777 I=I+1
      IF(THV(I).EQ.0.0)GO TO 888
      TVT=(TV(I)-5.0)*0.5+1.0
      THT=6.0+(THV(I)-THS)/10.0
      CALL SYMBOL(TVT,THT,0.07,1,0.0,-1)
      GO TO 777
  888 CALL LINE(T,TH,JK1,+1)
      CALL SYMBOL(1.2,7.6,0.14,S,0.0,8)
      CALL PLOTND
  33  STOP
  100 FORMAT(10F6.1,/,6F6.1,/,3(10F6.1,/,4F6.1,/),2(1X,F5.1),1X,
     1E7.1,2A4,2(1X,F4.2),1X,I3,1X,F4.2,2X,F6.1,/,6(F6.2,F6.1))
  101 FORMAT(10X,2(I2,2X),'ERROR IN DE - CODE  ',I2,2(2X,F6.1)
     1,2(2X,E14.4),2X,I3)
  103 FORMAT(2X,'INVERSION RISE FOR  ',2A4)
  104 FORMAT(2(1X,I2),6X,2(1X,F6.1),1X,F6.3,3(1X,E14.7)
     1,/,7(1X,E14.7))
  105 FORMAT(2F9.3,I2)
      END
      SUBROUTINE F(TI,V,VP)
CCCCCCC ROUTINE FOR COMPUTING DERIVATIVES (CALLED BY DE).
      COMMON A,P2,TIS,B
      DIMENSION V(3),VP(3),A(7)
      VP(1)=A(1)/V(2)-A(2)
      VP(2)=A(3)/V(3)-A(4)*V(2)-A(5)
      VP(3)=A(6)*VP(2)-VP(1)+A(7)*V(2)*EXP(B*TIS)
      RETURN
      END
```

```
-26.7  24.3  67.4 104.6 170.9 170.4 210.3 213.7 147.7 239.2
369.3 261.8 161.0 113.7  10.8 -14.3
.0200 .0320 .0440 .0368 .0248 .0128 .0134 .0144 .0154 .0165
.0175 .0185 .0195 .0196
  1.4   2.4   2.6   2.8   2.4   2.6   2.6   2.7   3.3   4.9
  4.3   4.2   4.6   3.9
134.0 145.0 162.0 158.0 166.0 182.0 179.0 204.0 224.0 152.0
150.0 149.0 146.0 138.0
 35.0 290.0 5.2E-06 AUG  01 0.70 1.00  65 0.45  0.0124
 7.70 291.4 10.53 294.4 15.62 296.4
   5.081   45.841 3
   5.127   64.558 4
```

Sample input data for inversion rise simulation.